# Blasting Design Using Fracture Toughness and Image Analysis of the Bench Face and Muckpile

**Kwangmin Kim**

Thesis submitted to the Faculty of the Virginia Polytechnic Institute and State University in partial fulfillment of the requirements for the degree of

## Master of Science

In

## Mining and Minerals Engineering

Committee Members:

Dr. Erik C. Westman, Chair

Dr. Mario G. Karfakis

Dr. Tom Novak

**July 21, 2006**
**Blacksburg, Virginia**

**Keywords:** Fracture toughness, Blasting, Image analysis

# Blasting Design Using Fracture Toughness and Image Analysis of the Bench Face and Muckpile

**Kwangmin Kim**

## Abstract

Few studies of blasting exist because of difficulties in obtaining reliable fragmentation data or even obtaining consistent blasting results. Many researchers have attempted to predict blast fragmentation using the Kuz-Ram model, an empirical fragmentation model suggested by Cunningham.

The purpose of this study is to develop an empirical model to relate specific explosives energy ($E_{SE}$) to blasting fragmentation reduction ratio (RR) and rock fracture toughness ($K_{IC}$).

The reduction ratio was obtained by analyzing the bench face block size distribution and the muck fragment size distribution using image analysis. The fracture toughness was determined using the Edge Notched Disk Wedge Splitting test.

Blasting data from twelve (12) blasts at four (4) different quarries were analyzed. Based on this data set, an empirical relationship, $E_{SE}=11.7\ RR_{80}^{1.202}\ K_{IC}^{4.14}$ has been developed. Using this relationship, based on the predicted blasting energy input for a desired eighty-percent passing (P80) muckpile fragment size the burden and spacing may be determined.

# ACKNOWLEDGEMENT

First and foremost I would like to express my sincere appreciation to my advisor Dr. Erik C. Westman and co-advisor Dr. Mario G. Karfakis for their guidance, and encouragement. In spite of their busy schedule, their participation was precious. Their suggestion on this work was valuable and helpful. I would also like to thank to my committee member, Dr. Tom Novak.

My parents Youngduck Kim, and Guinam Bae, and my wife, Yundeok Kim, their support, trust, and sacrifice made a big portion of this thesis.

# TABLE OF CONTENTS

Page

# LIST OF FIGURES

# LIST OF TABLES

# Chapter 1 Introduction

## 1.1 Statement of the Problem

The United States National Materials Advisory Board estimates that improving the energy efficiency of comminution processes using a practical approach could result in energy savings of over twenty (20) billion kilowatt-hours per year. Practical savings in the comminution process, especially blasting, is one of the most important steps (Adel, 2004).

Few studies of blasting exist because of the difficulty in obtaining reliable fragmentation data, and getting consistent results is difficult. Furthermore, although blasting engineers differ with regards to desired results, all blasting designs rely on the experience of these engineers. Excessive fines or oversized fragments are examples of what to avoid. Blasting has historically been regarded as a stand-alone operation and is usually reported as a single cost in most analyses.

Blasting engineers widely use the Kuz-Ram model to predict the rock size distribution arising from blasting. Many researchers have attempted to predict blast fragmentation using the Kuz-Ram model, which is based on empirical studies of fragmentation.

The model has two primary parameters: the characteristic size, derived from blasting parameters using the model of Kuznetsov (Kuznetsov, 1973), and a uniformity index, based on geometric parameters of the drilling and blast design. The size distribution curve is determined by these two parameters. However, this original Kuz-Ram fragmentation model is limited in its application and erroneously assumes a fifty percent (50%) passing size as the average adjusted size in the Rosin-Rammler model (Spathis, 2004 and Chung & Katsabanis, 2000). In addition, even though the fracturing of rock, as well as of other materials, is usually due to tensile failure, no current blasting model considers tensile

strength. For example, the Kuz-Ram model considers the Uniaxial Compressive Strength (UCS) and the Young's Modulus (E).

**Figure 1.1 Blasting in Pittsboro**

In-situ block size is an important aspect of any blasting model and design because many pieces of blasted rock are released from the in-situ block, as shown in Figure 1.1. Currently in-situ block size is still obtained by manually estimating the bench face because there is no instrument for measuring a whole bench face to obtain easily and cheaply an in-situ block size.

## 1.2 Proposed Solution

The purpose of this study is to develop a new empirical model in order to obtain the proper burden and spacing for target fragment size, P80 (the desired eighty percent [80%] passing size) in the muckpile and to predict a size distribution curve from the muckpile after a bench blasting.

A blasting fragmentation model of the same form as the model proposed by Donovan's for energy prediction in the comminution is considered, the proposed model is as follow.

$$E_{SE} = a\,\mathrm{RR}^{b}\,\mathrm{K_{IC}}^{c}$$

Where:

- $E_{SE}$ is specific explosives energy (wh/ton).
- RR is the reduction ration based on % passing.
- $K_{IC}$ is Mode I fracture toughness value (Mpa*$m^{1/2}$).
- a,b, and c are constant.

The blasting reduction ratio (RR) is obtained by determining the in-situ block size on the bench face and the blasting muckpile fragment size using image analysis. The fracture toughness, $K_{IC}$, is determined using the Edge Notched Disk Wedge Splitting test (END) on samples prepared from post blast rock blocks.

# Chapter 2 Literature Review

The proposed equation, $E_{SE} = a\,\mathrm{RR}^{b}\,\mathrm{K_{IC}}^{c}$, is used to develop a new empirical blasting fragmentation model. To obtain the reduction ratio (RR) data, the bench face and the muckpile have been analyzed using an image analysis program. The fracture toughness, $K_{IC}$, represents the rock properties. In addition, blasting fragmentation prediction model, Kuz-Ram, is used for the application of this new empirical model. Thus, image analysis, fracture toughness and blasting fragmentation prediction models will be introduced in this chapter.

## 2.1 Image analysis

Image analysis on the bench face and muckpile was conducted to get the reduction ratio (RR).

### *The Reduction Ratio (RR) in blasting*

In a crusher, the concept of the reduction ratio, RR, is the feed size over the product size ratio, and the reduction ratio in blasting is very similar. The feed size is represented by the bench block size and the product size is represented by the muckpile fragment size. Figure 2.1 shows the reduction ratio in a crusher.

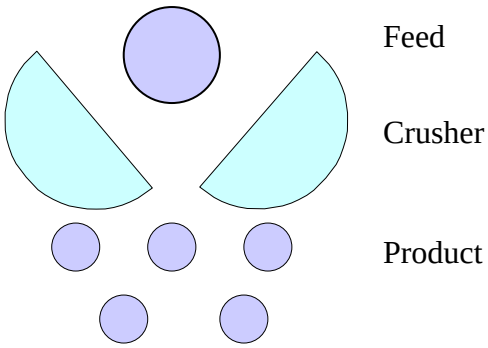


**Figure 2.1 The Reduction Ratio in a crusher**

For example, the new concept of $RR_{50}$ in blasting is shown in the following equation.

$$RR_{50} = \frac{F50}{P50}$$
$$= \frac{\text{50\% passing size from the bench face image analysis}}{\text{50\% passing size from the muckpile image analysis}}$$
$$= \frac{\text{The feed size before blasting}}{\text{The product size after blasting}}$$

Reduction factors for 20% and 80% passing can also be determined in the same way.

### 2.1.1 Image analysis programs

Recent fragmentation assessment techniques using image processing program allow rapid and accurate blast fragmentation size distribution assessments.

There are a number of different image-processing programs, and the following describes some of the commonly used programs.

***The IPACS system***

The IPACS has the software functions: grabbing scaling, image enhancing, grey level image segmentation, shape analysis (merging and splitting) and processing parameters. The host computer for this image system is an industrial PC, and this system is well suited for industrial purposes. Processing speed and accuracy are good, and the system is conducted automatically with a video input picture (Dahlhielm, 1996).

***TUCIPS system***

TUCIPS (Technical University Clausthal Image Processing System) has been developed to measure blast fragmentation at Technical University Clausthal (Germany). This system involves general algorithms of image processing and a specially created algorithm for

muckpile image analysis. There is just five percent (5%) deviation in the practical test with this program, so this system is suitable for practical use (Havermann and Vogt, 1996).

***FRAGSCAN***

FRAGSCAN measures the size distribution of blasted rock from the dumper or the conveyer belt due to camera and mathematic morphology techniques. The equipment is composed of a camera, an Image acquisition card, a control data card, a computer type PC, a light. Conversion from surface to volume distribution is possible by using a spherical model and the operating system is fully automatic. This tool provides reliable, consistent results for industrial usage because extensive experimentation has provided satisfying results (Schleifer and Tessier, 1996).

***WipFrag system***

Using digital image analysis of rock photographs and videotape images with granulometry system, grain size distribution may be obtained by WipFrag. Photographic images are digitized by using WipFrag from slides, prints or negatives, using a desktop copy stand. In order to overcome size limitations inherent with a single image, WipFrag has the function for zoom-merge analysis. Therefore, combined analysis of images taken at different scales of observation may be analyzed. In addition, Using Edge Detection Variables (EDV), fragment boundaries are analyzed efficiently, and manual editing can improve edge detection (Maerz, Palangio, and Franklin, 1996)

***SPLIT System***

SPLIT is operated from eight bit grayscale images of rock fragments, and was developed from the University of Arizona to figure out size distribution of rock fragment. There are two kinds of SPLIT programs; one is used on the conveyor belt and its automatic and continuous program, and the other is a manual program which uses the saved images. However, the same algorithm is used in both programs (Ozdemir, Kahriman, Karadogan, and Tuncer, 2003).

### 2.1.2 The errors associated with image processing systems

It is extremely hard to obtain accurate estimates of rock fragmentation after blasting. Following are the main reasons for error in using image analysis programs (Liu and Tran, 1996).

(1) Image analysis can only process what can be seen with the eye.
Image analysis programs cannot take into account the internal rock, so the sampling strategies should be carefully considered.

(2) Analyzed particle size can be over-divided or combined.
That means larger particles can be divided into smaller particles and smaller particles can be grouped into larger particles. This is a common problem in all image-processing programs. Therefore, manual editing is required.

(3) Fine particles can be underestimated especially, from a muckpile after blasting.
There is no good answer to avoid these problems. In order to reduce these errors, sampling strategies should be carefully selected and flexibility of system configurations as well as the change of materials is important.

When rock size uniformity is high and thickness of layer is low, the image-processing program is useful and efficient. However, if the uniformity of rock size is low and thickness of layer is significant, the user should be especially careful accepting the results of image analysis (Cunningham, 1996). Figure 2.2 shows an example of an analyzed muckpile image using the SPLIT system.

**Figure 2.2 Image of the muckpile and delineated image using the Split software**

## 2.2 Fracture toughness

Fracture toughness of rock is an important index property for comminution. Using this index, crushing equipment may be properly sized to meet specific needs without over sizing equipment and increasing capital equipment costs. To determine the index of fracture, toughness samples are loaded so that stress is concentrated on the tip of a crack.

The stress intensity factor for Mode I, $K_I$ is a measure of the stress field at a loaded crack tip with mode I type (Tada, Paris, and Irwin, 2000). When this value reaches a point of catastrophic growth, it is said to have reached $K_{IC}$. The value of $K_{IC}$ means Mode I fracture toughness and refers to an index of dissipated energy that was required to propagate a crack to a point of catastrophic growth (ISRM, 1998).

The value of $K_{IC}$ is affected by temperature, loading rate, and the thickness of the member, so the fracture toughness can be the property of the material.

The following laboratory tests may be conducted to determine the value of $K_{IC}$.

- Chevron Bend [(ISRM, 1998) and (Sun and Ouchterlony, 1986)]
- Short Rod [(ISRM, 1998) and (Sun and Ouchterlony, 1986)]
- Cracked Chevron Notched Brazilian Disc (Wang, 1998)

- Single Edge Notched Bend (Fenghui, 2000)
- Compact Tension (Sun and Ouchterlony, 1986)
- Semi Circular Bend (Chong and Kuruppu, 1984)
- Flattened Brazilian Disc Specimen (Wang and Wu, 2004)

The Chevron Notched Short Rod and Chevron Notched Round Bar in Bending was suggested as a fracture toughness test by the International Society of Rock Mechanics (ISRM).

These methods are all variants of the same technique. A sample is prepared to a certain specification and then has a notch cut into the sample. The sample is then loaded in such a way that a crack is propagated from the notch. From the load applied and the geometry of the sample $K_{IC}$ can be calculated. The main disadvantage to these methods of finding $K_{IC}$ is that they have very intense sample preparation procedures and the loading apparatus is complex. Another difficulty encountered with these methods is the means of measuring the dilatation of the notch prior to crack growth. Therefore, another method for fracture toughness testing of rocks is necessary and a relatively easier test, END test, has been proposed by Donovan and Karfakis (Donovan and Karfakis, 2004).

The relatively easier test proposed by Donovan uses an edge notched disk (END) sample loaded on a wedge of set geometry. The sample is loaded uniaxially until failure. The peak load and friction coefficient are used into following equation to determine the fracture toughness:

$$K_{IC} = 2 \cdot \sqrt{\frac{D}{2a}} \cdot \left( \frac{P_v}{2\tan\left(\frac{\alpha}{2}\right)} * \frac{1-\mu\tan\left(\frac{\alpha}{2}\right)}{1+\mu\cot\left(\frac{\alpha}{2}\right)} \right) \cdot \left( \frac{a}{0.355715(D-a)^{3/2}} + \frac{1}{0.966528(D-a)^{1/2}} \right) \cdot \frac{1}{t} \qquad \textbf{(2.1)}$$

Where:

$K_{IC}$ = The critical stress intensity factor ($MPa*m^{1/2}$)

$P_v$ = The applied peak load (N)

$\alpha$ = The wedge angle ($11^o$)

$\mu$ = Friction coefficient ($\tan\phi$)

a = The notch length (m)

D = Specimen diameter (m)

T = Thickness of disc (m)

A new fracture toughness test, the Edge Notched Disk Wedge Splitting test, was developed and verified to permit rapid and easy assessment of the fracture toughness of a rock.

In addition, Donovan's work has shown that fracture toughness is related more strongly to the specific comminution energy than any other material property tested. As a result, a method for predicting the specific comminution energy, $E_c$, required to reduce a rock particle to a given size based on fracture toughness, $K_{IC}$, was proposed (Donavan and Karfakis, 2004).

***Single Particle Breakage Testing***

Bearman and Donovan (Bearman, 1989 and Donovan, 2004) have shown that a strong correlation exists between the fracture toughness of a material and the power consumption of a laboratory crusher used to crush the material, indicating that fracture toughness may have practical application in the evaluation of blast fragmentation.

Single particle breakage test is to achieve crushing energy and product size distribution data regarding the rocks, and these data will be compared with the fracture toughness of those rocks. HECT system, the Allis-Chalmers High Energy Crushing Test, is used for single particle breakage tests. Using HECT system, crushing force and actuator displacement can be obtained as well as the net energy for rock crushing. Additionally, HECT can simulate

all crusher operating conditions, a wide range of crusher sets, speeds, and throws (Allis-Chalmers, 1985 and Donovan, 2003).

Using HECT system, Donovan applied this $K_{IC}$ value to the prediction of jaw crusher power consumption in 2003. From this application, there is a strong relationship between rock fracture toughness, $K_{IC}$ and specific comminution energy, $E_C$, and this correlation was used to achieve an empirical model for the jaw crusher power consumption prediction as the change of reduction ratio. As result, the predicted $E_C$ and actual $E_C$ were in agreement. The following is one of the Donovan's $E_C$ model.

$$E_c = \left[-0.511 + 0.511RR\right]K_{IC} \quad (1 \le RR < 1.5)$$

$$E_c = \left[0.215RR^{0.425}\right]K_{IC} \qquad (RR \ge 1.5) \qquad \left[kwh/t\right] \qquad \textbf{(2.2)}$$

Where, $E_C$ is the specific comminution energy given in terms of kilowatt-hours per metric ton, and reduction ratio (RR) is the particle size divided by the closed side set.

Because the relationship between Ec and $K_{IC}$ is based on only several rocks and two reduction ratios in Donovan's test, Equation 2.2 is limited. However, the results of Donovan's experiment indicate a strong and proportional relationship between fracture toughness and specific comminution energy. In addition, fracture toughness was shown to be related to specific comminution energy more strongly than any other material property tested, including tensile strength (Donovan, 2003).

Donovan's test shows the possibility that fracture toughness can be used for practical applications to predict blast fragmentation. In addition, $K_{IC}$ value can replace the other rock properties; uniaxial compressive strength (UCS) and young's modulus (E) which are used in Kuz-Ram, the empirical comminution energy prediction model in blasting.

## 2.3 Blasting fragmentation prediction

Assessment of the blast performance is critical for optimal blasting, and the size distribution of the blasted material is essential to determine the degree of fragmentation. However, fragmentation is influenced by both controllable and uncontrollable parameters: rock properties, the geometry of rock, and blasting patterns, and the optimal size distribution of the blasted material depends on the mining objective. Optimal blasting is a very complex and difficult issue. Furthermore, there is no method or equation which can predict the blast fragmentation exactly because of varying desired blasting fragmentation and numerous controlling parameters involved in the process.
Many researchers have recently developed models and computerized simulations. Following are some of the widely accepted models (Jimeno and Carcedo, 1995).

### 2.3.1 Kuz-Ram model

Kuz-Ram is the combination of Kuznetsov and Rosin-Rammler equation, and an empirical fragmentation model. Since its introduction by Cunningham, the Kuz-Ram model has been used by many mining engineers to predict rock fragmentation arising from blasting, and many researchers have attempted to improve the Kuz-Ram fragmentation prediction model (Cunningham, 1983 and 1987).

The model has two main factors;
The characteristic size ($X_C$): It was derived by the Kuznetsov model (Kuznetsov, 1973).
The uniformity index (N): It is based on geometric parameters of the drilling and blast design.

The size distribution of the muckpile rock after blasting is determined by these two main factors. However, this original Kuz-Ram fragmentation model has the limitation of application and a high margin of error (Spathis, 2004).

***The mean size of the fragments formed by blasted rock***

The distribution function, an analytical representation of the fragment size composition of blasted rock, has been suggested by Rosin-Rammler model (Lilly, 1986), (Chung and Katsabanis, 2000), and (Kuznetsov, 1973).

$$\Phi_{(X)} = 1 - R_{(x)} = 1 - \exp\left[-\left(\frac{x}{x_0}\right)^N\right] \quad \textbf{(2.3)}$$

Where:

$\Phi_{(X)}$ is the distribution function (the total relative volume of fraction not longer than x).

$X_0$ is the Characteristic Size.

N is the Uniformity Index.

$R_{(x)}$ is the fraction of material retained on screen.

Using the Rosin-Rammler equation, the formula for the mean fragment size was suggested with given rock volume and needed explosives by Kuznetsov (Kuznetsov, 1973).

$$< X >= A\left(\frac{V_0}{Q}\right)^{4/5} Q^{1/6} \quad \textbf{(2.4)}$$

Where:

<X> is the mean fragment diameter (cm).

$V_0$ is the volume of blasted rock per hole ($m^3$).

Q is the weight of explosives of TNT equivalent explosives per hole (kg).

A is rock factor:

A=7 The medium hard rocks, f =8~10.

A=10 The hard but highly fissured rocks, f=10~14.

A=13 Very hard and weakly fissured rocks, f=12~16.

f is the Protodyakonov factor.

An equivalent quantity of any explosives, $Q_e$ related to TNT is calculated by Equation 2.5 because TNT is not currently used in blasting as a standard explosive (Clark, 1987).

$$Q = Q_e\left(\frac{E_e}{1090}\right) \quad \textbf{(2.5)}$$

Where:

$E_e$ is the absolute weight strength of the explosives (cal/g).

The factor 1090 is the absolute weight strength of TNT.

***Cunningham***

Cunningham used the Rosin-Rammler model for blasting analysis (Equation 2.3). If the characteristic size ($X_0$) and the uniformity index (N) are known, then the size distribution will be obtained from Equation 2.3, Cunningham suggested following formula for determining uniformity exponent (Cunningham, 1987).

$$N = \left(2.2 - 14\frac{B}{D}\right)\left(1 + \frac{S/B}{2}\right)^{0.5}\left(1 - \frac{W}{B}\right)\left(\frac{|L_B - L_C|}{L_B + L_C} + 0.1\right)^{0.1}\frac{L}{H} \times (1.1 \text{ or } 1.0) \quad \textbf{(2.6)}$$

Where:

D is the hole diameter **(**mm)

B is the burden (m)

W is the standard deviation of drilling accuracy (m)

S is the spacing (m)

$L_B$ in the bottom charge length (m)

$L_C$ is the column charge length (m)

L is the total charge length (m)

H is the Bench height (m)

The factor “1.1 or 1.0” means that if a staggered drilling pattern is employed, then ‘N’ will be increased by 10% (1.1).

Usually ‘N’ varies between 0.8 and 2.2. High values indicate uniform sizing, but low values indicate non-uniform sizing, high proportion of fines and the oversize. Therefore, ‘N’ higher values and a staggered pattern is preferred for uniform sizing.

If the burden of hole diameter is decreased, drilling accuracy is increased, the charge length of bench height is increased, and spacing of burden is increased, then the uniformity index is increased (Cunningham, 1983). This relationship may be derived by Equation 2.6.

In addition, the characteristic size, $X_C$ was suggested by adjusting Rosin-Rammler (Equation 2.3).

$$R = Exp\left( -\left( \frac{X}{X_C} \right)^N \right)$$

If X is the average size ( $\overline{X}$ ), then the value of R is 0.5 (50% passing) as following;

$$0.5 = Exp\left( -\left( \frac{X}{X_C} \right)^N \right)$$

Thus,
$$X_C = \frac{\overline{X}}{(0.693)^{1/N}} \qquad \textbf{(2.7)}$$

Cunningham suggested the Kuz-Ram model as demonstrate in Equation 2.7. The effect of the uniformity index and the characteristic size on fragmentation distribution is such that the characteristic size fixes the specific size in the size distribution curve, and the uniformity index determines the shape of size distribution curves by having this characteristic size.

***Limitation of the Kuz-Ram***

Cunningham assumed that the fifty percent (50%) passing size as the average size during adjusting Rosin-Rammler model in Equation 2.7. The fifty percent (50%) passing size is not the same as the average size of the fragments in the muckpile (Spathis, 2004).

Therefore, Equation 2.7 is modified by simply using the fifty percent (50%) passing size ($X_{50}$) instead of the average size ($\overline{X}$).

$$X_C = \frac{X_{50}}{(0.693)^{1/N}} \quad \textbf{(2.8)}$$

In addition, the Kuz-Ram model has limits; the S/B ratio should not exceed two (2), initiation and timing should be arranged to avoid misfires and cut-offs, the calculated relative weight strength should be closed with yielded explosives energy, and the jointing of the ground should be assessed carefully.

Kuz-Ram model is merely focused on the prediction of size distribution after blasting in the muckpile. However, blasting engineers want to know the proper blasting pattern for optimal blasting at any given blasting site and situation. Therefore, more practical usage of Kuz-Ram model will be examined in this study using empirical specific explosives energy prediction model.

### 2.3.2 Larsson's model

In 1973, Larsson has proposed the equation for K50, 50% passing size. Namely, assessment of blast fragmentation, 50% passing size, is predicted by using the model. The Equation 2.9 shows that model (Jimeno and Carcedo, 1995).

$$K_{50} = S' \times e^{(0.58*\ln B - 0.145*\ln(S/B) - 1.18*\ln(CE/c) - 0.82)} \quad \textbf{(2.9)}$$

Where:

B is the Burden (m)

S is the Spacing (m)

CE is the Specific charge (kg/m$^3$)

C is the Rock constant

S’ is the Blastability constant

The blastability constant, S’ considers the rock structure and heterogeneity.

S’ = 0.60 Very jointed and fissured rock

S’ = 0.50 Normal rock with hair cracks

S’ = 0.45 Relatively homogeneous rock

S’ = 0.40 Homogeneous rock

The rock constant, C, has a similar concept with the powder factor, and usually has a value between 0.3 and 0.5 kg/m$^3$.

### 2.3.3 The SVEDEFO (Swedish Detonic Research Foundation) model

SVEDEFO adds terms about the effect of bench height and stemming length from Larson’s model. Following is the SVEDEFO model (Jimeno and Carcedo, 1995).

$$K_{50} = S' \times \left[ 1 + 4.67 \left( \frac{T}{L} \right)^{2.5} \right] \times e^{0.29 \ln B^2 \sqrt{\frac{s}{1.25}} - 1.18 \ln \left[ \frac{CE}{c} \right]^{-0.82}} \qquad \textbf{(2.10)}$$

Where:

B is the Burden (m).

S is the Spacing (m).

CE is the Specific charge (kg/m$^3$).

C is the Rock constant.

S’ is the Blastability constant.

T is the stemming length (m).

L is the depth of blast hole (m).

Although the exact prediction of the blast fragmentation is not possible, three of the widely accepted blasting fragmentation prediction models were introduced in this chapter.

The purpose of this study is to develop a new empirical model. However, Kuz-Ram model will be incorporated in the development of the empirical blasting model. Since the Kuz-Ram model allows the prediction of the blasting fragmentation size distribution.

# Chapter 3 Experiment

Experimental data were collected from four quarries, two in South Korea and two in the United States. The “Bosung” and “Sanyang” quarry are located in Ul-san and Jin-hae, South Korea respectively, and the “Pittsboro” and “Boxley” quarry are located in North Carolina and Virginia, USA. From these four quarries, data from twelve blasts were obtained. For each quarry blast, image sampling and analysis were conducted to obtain the data for the reduction ratio from the bench face and the muckpile. Fracture toughness, $K_{IC}$, was obtained by using the END test on samples prepared from rock blocks.

## 3.1 Image Sampling and Analysis From a Quarry Blast

Figure 3.1 shows the importance of determining in-situ block size in the blasting. Many blocks on the bench face are just released from in-situ block by the blasting energy.

**Figure 3.1 The released rock from in-situ block of the bench in Warrenton,VA**

Although an in-situ block size is an important factor in the blasting model, the in-situ block size has typically been estimated by observation of rock mass and structural mapping analysis both manually and partially.

**Figure 3.2 The bench face image in Pittsboro**

As seen in Figure 3.2, in practice it is impossible to measure the entire bench face to obtain the in-situ block size manually because the bench face is both too high and too dangerous to measure. Therefore, SPLIT was used to measure the whole bench face structure and to obtain the in-situ block size in this research.

### 3.1.1 Image Sampling

Important issues in image sampling are: the location of the image, the image angle from the surface of the muckpile, and the scale of the image. In order to obtain good images, which are both capable of being analyzed and representative of the entire rock assemblage, sampling strategies must be carefully considered.

The location of image taking is important, and there are two sampling methods, random and systematic. Both methods are complex and must be considered the purpose of the investigation. Another consideration is the angle of the surface being photographed. Ideally, the surface should be perpendicular to the camera lens.

Consistent sampling from image to image is the main strategy in this research and one of the most important factors in the sampling strategy. Analyzed data show large variations from image to image, but as a whole, the data demonstrate consistency. In a muckpile after blasting, merely remaining consistent in sampling may not be sufficient to show the real size distribution. This strategy saves time in sampling and is convenient for the blasting engineer to make a site-specific model for quarry blasting.

***The Image Sampling on a Bench Face***

To consider the whole bench face, the in-situ block size on a bench face will be obtained by using SPLIT program.

A digital camera was used to get the image of the bench face, which will be used in SPLIT. The maximum size image that can be processed using SPLIT is 1680*1400 pixels, so the maximum size image needs to be considered during sampling images because image editing may be required in SPLIT, and a larger image may not be opened in SPLIT without such editing.

**Figure 3.3 The bench face image from Bosung quarry**

Image samples were obtained during charging explosives after drilling for blasting. Approximately five to seven (5-7) pictures were taken at each blasting, and three to five (3-5) appropriate pictures for analyzing in SPLIT were chosen. Figure 3.3 is an example of image sample. An article of known dimensions, a scale material, must be in the picture in order to provide scale. A white plate was used as a scale material on the bench face. The same scale material must be used from image to image for analyzing all pictures in SPLIT regarding each blasting. Also, the number of scale materials should be the same from image to image for analysis. Typically, only one scale material was used for the bench face image analysis in this research.

***The Image Sampling From a Muckpile After Blasting***

Fragmentation assessment can be achieved by analyzing scaled photographs taken of the muckpile. The digital camera should be held such that the long axis of the photograph is vertical. The image should be taken with the camera lens perpendicular to the muckpile surface (JKMRC, 1996).

**Figure 3.4 The muckpile image from Bosung quarry**

To provide scale in the photograph, a tennis ball was used. If the slope of a pile needs to be shown, then two scale materials can be used as shown in Figure 3.4. These materials should

neither be placed randomly on the muckpile nor in a horizontal line across the muckpile. In addition, the same number of scale materials should be used from sample to sample in the same blasting site to analyze together in SPLIT.

As previously mentioned, the maximum image size is 1680*1400 pixels. If the size is too large to be analyzed in SPLIT, then image editing is required.
A more representative sample may be obtained by photographing the material being loaded into a truck or as a truckload is being dumped because the outside surface of a muckpile before digging cannot represent the material within the pile. That means obtaining images of the entire exposed surface of the pile to avoid biased results, however it takes longer to acquire these images.

The main focus of sampling of muckpile images in this research is consistency rather than representation. Therefore, the image samples after blasting were obtained directly from the muckpile and five to seven images of the muckpile were captured and analyzed at each blasting. To show as much of the muckpile as possible, each image sample was obtained at the different part of a muckpile and overlapping images were avoided.

Safety is tantamount during sampling images from a muckpile. Scale material was thrown to the dangerous site and the zoom function of a digital camera was used for sampling purposes. It is especially dangerous near the bench face after blasting.

### 3.1.2 Image Analysis Using SPLIT

SPLIT, image analysis program, will be used for analyzing a bench face and a muckpile. The block structure of bench in a quarry before blasting may be obtained by analyzing the bench face, and the result of blasting will be estimated by using SPLIT on the muckpile.

***Imgae analysis on a bench face***

Consistency is the primary focus in the initial trial of the image analysis program used on the bench face to obtain information regarding the in-situ block size.

Following is the important and specific setting at the step of Editing and Compute Size in SPLIT for analyzing the bench face.

1. Only the scale material should be edited.
2. Zero percent (0%) of percent fines adjustment.
3. Rosin-Rammler was used for fines distribution.

Bench face images were not edited much in this study. Only the scale material and the other parts of image except the bench face were edited. Therefore, the part of the bench face image was not edited except for the actual scale material. If the bench face image is edited, then the editing image is not sufficient because the crack on the bench face is often very difficult to see. Although non-edited images analysis cannot reflect the real size distribution of the block on the bench faces and contains errors, non-edited images revealed more consistent analysis result than edited ones.

On the bench face, the fines are not considered because the bench face image analysis is for obtaining information regarding the in-situ block size. Therefore the setting for fines adjustment is zero percent (0%).

For the prediction of fines in SPLIT, there are three options - Schuhmann, Rosin-Rammler, and best-fit. Any prediction model may be used, but the same model should be used from image to image. The Rosin-Rammler model was chosen for this research.

At the step of Graphs and Outputs, this setting depends on the user. The setting of graphing is “Cumulative”, and size axis and percent axis is “Linear” in this research. Figure 3.5 shows the bench face image analysis in SPLIT.

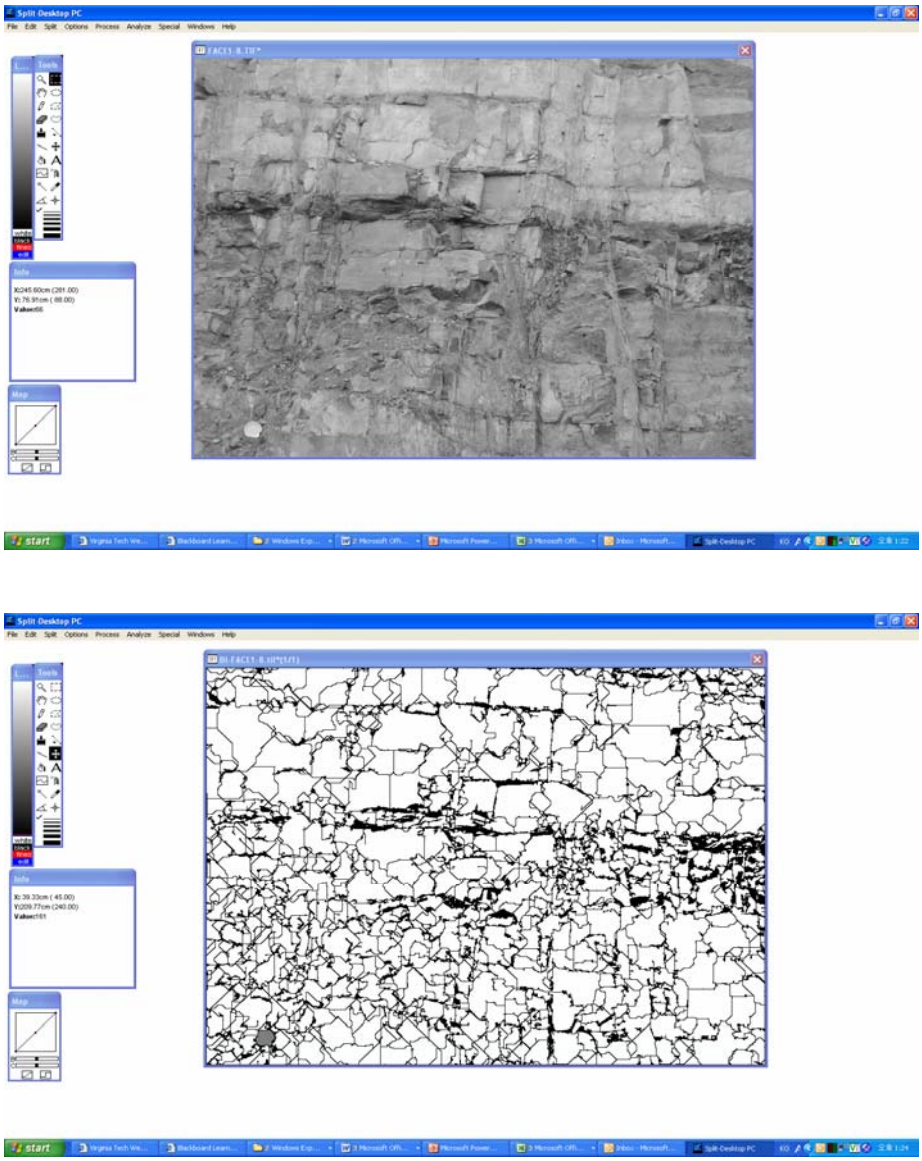

**Figure 3.5 The analyzed bench face image of Bosung quarry in SPLIT**

***Image Analysis on a Muckpile***

At the step of Editing and Compute Size in SPLIT, the important settings are as follows.

1. Fifty (50%) of percent fines adjustment (Medium).
2. Rosin-Rammler was used for fines distribution.

Usually one or two scale materials were used on the muckpile. If the angle of muckpile surface needs to be considered then two scale materials were used. Of course, the number of scale materials depends on the sampling situation.

Muckpile image analysis has the following limitations regarding fines estimation, so the percent fines adjustment was set to “Medium.” The percent fines adjustment percentage may be changed to twenty (20%), forty (40%), or sixty percent (60%), but the percentage should be consistent from image to image. In this research, fifty percent (50%) was chosen as the percent fines adjustment because this is the usual setting for muckpile image analysis in SPLIT. Figure 3.6 shows the muckpile image and analyzed image in SPLIT.

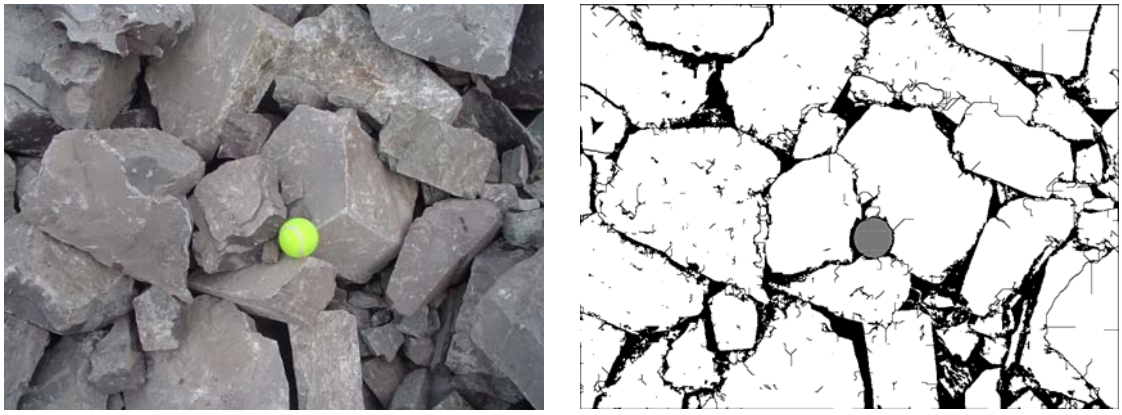

**Figure 3.6 The muckpile image and analyzed image in SPLIT**

In addition, Rosin-Rammler model was used for prediction of fines. Users may choose the prediction model. The situation is the same with the bench face image analysis. Consistency of the model choice should be kept from image to image.

The setting of graphing is “Cumulative”, and size axis and percent axis is “Linear” at the step of Graphs and Outputs in this research. This setting also depends on the user(s).

***The Size Distribution Curves from a Bench face and a Muckpile***

As the result of image analysis, two kinds of cumulative size distribution curve were obtained from a bench face and a muckpile at each location.

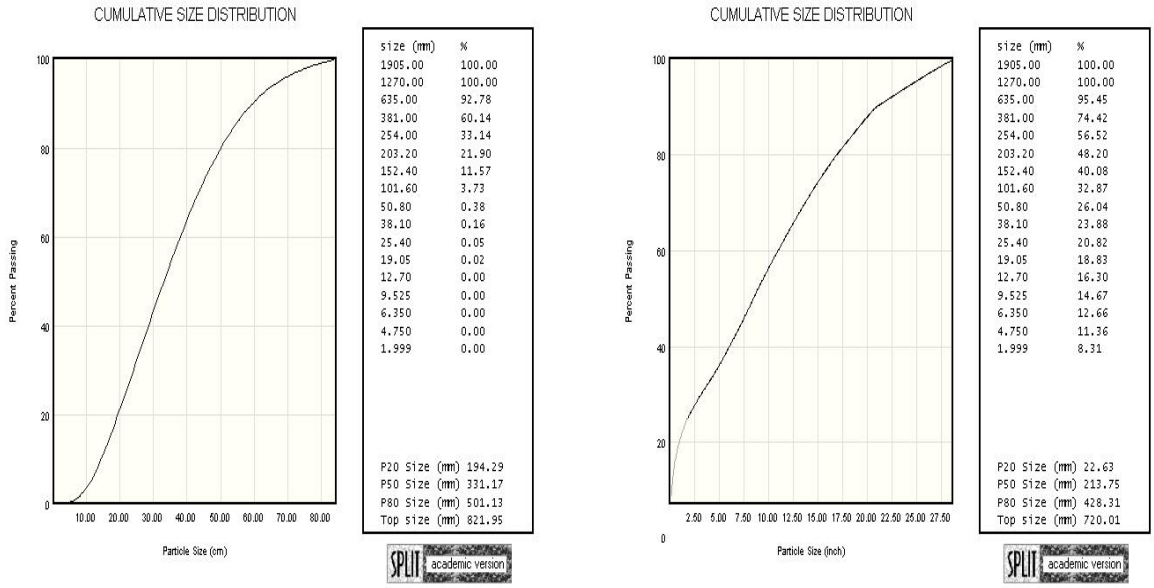


**Figure 3.7 The size distribution curves from the bench face (left) and muckpile (right)**

Figure 3.7 shows size distribution curves. The left chart represents the result of the bench face image analysis, and the right chart is the result of the muckpile image analysis.

From these size distribution curves, the data in Table 3.1 were obtained. These data are analyzed, and will be used for making an empirical equation model. The unit in the table is represented in millimeters. Prefix “F” and “P” before the % passing sizes represent bench face and muckpile respectively.

**Table 3.1 The data from the size distribution curve of the bench face and muckpile**

| | F20 | F50 | F80 | P20 | P50 | P80 |
|---|---|---|---|---|---|---|
| **Bosung1** | **165** | **410** | **810** | **46** | **255** | **493** |
| **Bosung2** | **245** | **586** | **937** | **23** | **214** | **428** |
| **Bosung3** | **196** | **420** | **821** | **91** | **226** | **431** |
| **Bosung4** | **158** | **285** | **467** | **72** | **209** | **335** |
| **Bosung5** | **178** | **330** | **551** | **93** | **252** | **499** |
| **Pittsboro** | **158** | **281** | **483** | **40** | **100** | **187** |
| **Boxley** | **514** | **929** | **1512** | **69** | **161** | **304** |
| **Sanyang1** | **102** | **192** | **334** | **55** | **179** | **350** |
| **Sanyang2** | **102** | **196** | **382** | **88** | **192** | **290** |
| **Sanyang3** | **114** | **211** | **360** | **24** | **89** | **199** |
| **Sanyang4** | **50** | **91** | **149** | **21** | **82** | **163** |
| **Sanyang5** | **81** | **164** | **309** | **31** | **144** | **265** |

F20, F50, and F80 in Table 3.1 are from the size distribution curve of a bench face. F20 means the twenty percent (20%) passing size in the size distribution curve of a bench face, and F50 and F80 are the same as F20.

P20, P50, and P80 are similar with F20, F50, and F80. These are twenty (20%), fifty (50%), and eighty percent (80%) passing size in the size distribution curve of the muckpile.

***F50 and the Mean In-situ Block Size***

The reason for the bench face analysis using SPLIT is to obtain information about the block size. In Pitttsboro blasting, the mean in-situ block size was measured manually, and the size is 0.2 meters. In Table 3.2, the scale of F50 (or F20) and the mean in-situ block size is similar. Although more research will be needed, it shows the possibility that F50 may be used as a new index of mean in-situ block size. In addition, reasonable results of data analysis were shown with these data in Chapter 4.

**Table 3.2 The data from the bench face, and the manually measured block size in Pittsboro**

| Location | F20 | F50 | F80 | Mean in-situ block |
|---|---|---|---|---|
| **Pittsboro** | **158** | **281** | **483** | **200** |

### 3.2 Calculation of $K_{IC}$

Standardized experimental testing has not been developed to determine the fracture toughness of rock. The critical value of stress intensity factor, $K_{IC}$, may be determined experimentally in different ways. Most methods involve intense sample preparation and are then loaded under very specific conditions.

Donovan proposed a relatively easier test (Donovan and Karfakis, 2004). This test uses an edge notched disk (END) sample loaded on a wedge of set geometry. The sample is then loaded uniaxially until failure.

The wedging device used in END test consists of hardened steel. The wedge angle ($\alpha$) is $11^{o}$. The experimental set-up is shown in Figure 3.8.

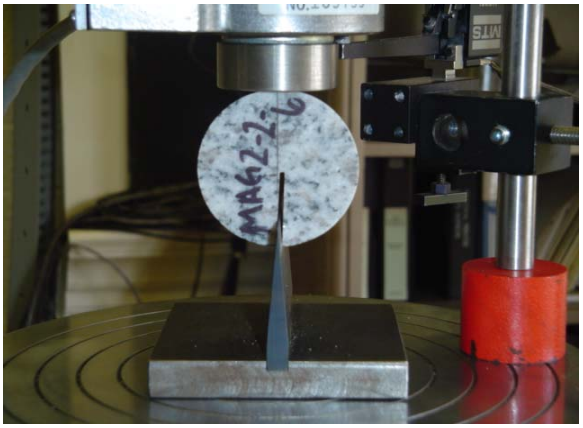

**Figure 3.8 Test set-up for END wedge test**

The experimental set-up is shown in Figure 3.8, and using MTS 810, the axial force is applied with 8996N load cell. The obtained data (load, load-line displacement) is saved in a PC. Loading rate of 0.003mm/sec for the load line displacement was used for the test (Donovan, 2003). The peak load, $P_V$ is recorded for $K_{IC}$ calculation using Equation 3.1.

$$K_{IC} = 2 \cdot \sqrt{\frac{D}{2a}} \cdot \left( \frac{P_v}{2\tan\left(\frac{\alpha}{2}\right)} * \frac{1-\mu\tan\left(\frac{\alpha}{2}\right)}{1+\mu\cot\left(\frac{\alpha}{2}\right)} \right) \cdot \left( \frac{a}{0.355715(D-a)^{3/2}} + \frac{1}{0.966528(D-a)^{1/2}} \right) \cdot \frac{1}{t} \quad \textbf{(3.1)}$$

Where: $P_v$ = the applied peak load

$\alpha$ = the wedge angle

$\mu$ = friction coefficient

a = the notch length

D = specimen diameter

The peak load and friction coefficient are used in Equation 3.1 to determine the fracture toughness.

The sample properties and geometric values used in this study were taken from experiments. The angle of wedge is eleven degrees ($11^o$). A tilt test was used to determine friction coefficient ($\mu$) on hardened steel. The sliding angle is $\phi$ and $\tan\phi$ is equal to $\mu$. The friction coefficients for the four quarry rocks are given in Table 3.3.

**Table 3.3 Values of $\phi$ and $\mu$ of four quarries rock**

| **Friction Coefficient ($\mu$)** | | |
|---|---|---|
| **Rock Type** | **$\phi$ (degree)** | **$\mu$** |
| **Pittsboro** | **$24.0 \pm 1.11$** | **0.445** |
| **Boxley** | **$24.8 \pm 3.03$** | **0.462** |
| **Bosung** | **$30.1 \pm 2.14$** | **0.580** |
| **Sanyang** | **$27.2 \pm 1.67$** | **0.514** |

Table 3.4 shows mode I fracture toughness, tensile strength, and specific gravity values for the rocks in the four quarries.

**Table 3.4 Fracture toughness, $K_{IC}$, Tensile strength, $\sigma_t$, and Specific Gravity**

| Location | $K_{IC}$(MPa*m^0.5) | $\sigma_t$ (MPa) | Specific Gravity (t/m$^3$) |
|---|---|---|---|
| **Pittsboro** | **1.539 ± 0.100** | **16.94 ± 1.92** | **2.69 ± 0.06** |
| **Boxley** | **1.724 ± 0.193** | **17.45 ± 2.57** | **2.73 ± 0.01** |
| **Bosung** | **1.889 ± 0.398** | **22.48 ± 4.70** | **2.58 ± 0.05** |
| **Sanyang** | **1.230 ± 0.216** | **14.72 ± 1.23** | **2.49 ± 0.07** |

### 3.3 Blasting specific explosives energy

Specific energy for fragmentation is the explosive or mechanical energy required to fragment a unit of volume or mass of rock (Rustan, 1998). The Specific Explosives Energy ($E_{SE}$) in this research represents the blasting energy required to fragment a unit of mass of rock. Therefore the unit is "wh/tonne". This value is affected by a blasting pattern (explosives amount, bench height, burden, spacing, hole diameter, rock specific gravity, and the type of explosives), consequently $E_{SE}$ can be assumed to represent the blasting pattern and can be determined using Equation 3.2.

$$E_{SE} = \frac{\text{Explosives Energy per hole(wh)}}{\text{Height} \times \text{Burden} \times \text{Spacing} \times \text{S.G.(ton)}} \quad \textbf{(3.2)}$$

Explosives energy per hole is affected by the diameter of the hole, bench height, and type of explosives. The explosives amount per hole was estimated as the average explosives amount per hole in this research.

Powder factor is the quantity of explosives used per unit of rock blasted (Kg/ton or Kg/m$^3$). An accurate prediction of powder factor in blasting is needed for optimal blasting to reduce operation costs (drilling, blasting, loading, haulage and crushing). Powder factor is one of the most important tools used to design the blasts (Jimeno and Carcedo, 1995). Since $E_{SE}$ is conceptually same with powder factor, $E_{SE}$ prediction will be evaluated for optimal blasting

pattern by using an empirical equation model in this study. Blasting pattern for Pittsboro and Specific Explosives Energy ($E_{SE}$) are tabulated in Table 3.5.

**Table 3.5 Blasting pattern and $E_{SE}$ in Pittsboro blasting**

| Blasting pattern and $E_{SE}$ | Pittsboro | Unit |
|---|---|---|
| Bench Height | 19.8 | m |
| Burden | 4.57 | m |
| Spacing | 4.57 | m |
| Rock Specific Gravity | 2.69 | t/m^3 |
| Hole diameter | 165 | mm |
| Explosives | Hydromite4400 | |
| Explosives amount per hole | 429 | kg |
| Explosives energy per gram | 863 | Kcal/Kg |
| Explosives energy per hole | 431 | Kwh |
| Specific Explosives Energy (Ese) | 387 | wh/tonne |

## 3.4 The Main Issues in SPLIT for the Research (Norton, B., 2005)

There are various issues in the use of SPLIT. The concepts, P50, fines, the fines percent adjustment in a muckpile, and the size of images, were considered as described below.

### *An Average Size and P50 in SPLIT*

The P50 is not necessarily the average size, but is fifty-percent (50%) passing size by weight. That means the P50 is not the mean size in terms of dimension. It is the mean size by weight. Half of the volume or weight is less than this size particle. It is assumed the particles have all the same density, so the terms of volume and weight can be used interchangeably.

### *Larger or Smaller Image*

When the muckpile was evaluated, the smaller image would definitely be more efficient because it is smaller and closer to the size of the material. A larger image would be less

efficient as it takes longer to edit. However, a larger image provides more particles for the sample, so there is a tradeoff. When the bench face was evaluated, the small and large images showed similar results of image analysis. Once again, the main focus is keeping scale consistent from image to image.

***Fines***

Smaller particles are hidden under the larger particles and are not visible. The resolution of the image is such that the software can only measure down to a certain point. Therefore the empirical model, either Rosin-Rammler or Schumann, below the point of the size distribution curve, predicts the size distribution. The curve color is a little changed at that point from that at which the size distribution is predicted by the empirical model in SPLIT.

***The Selection of the Fines Percent Adjustment in a Muckpile***

The key is not to change the setting from sample to sample. The default setting is fifty percent (50%) and this is what many people use ninety-nine percent (99%) of the time when analyzing muckpile images. This is because we do not have sieve results and we want to be able to compare curves knowing the same setting was used to generate them. The evaluation of images from a blast muckpile is particularly difficult due to its size, depth and internal variations.

To obtain information of the in-situ block size on the bench face, the default setting is zero percent (0%) because fines analysis on the bench face are not needed for this study, and the key is keeping the setting consistent from image to image.

# Chapter 4 – Data Analysis

Donovan has developed a model to predict the specific comminution energy, $E_C$, in jaw crushers using the HECT system. Following is one of the Donovan's models (Donovan and Karfakis, 2004).

$$E_c = \left[-0.511 + 0.511RR\right]K_{IC} \quad (1 \le RR < 1.5)$$

$$E_c = \left[0.215RR^{0.425}\right]K_{IC} \qquad (RR \ge 1.5) \qquad \left[kwh/t\right]$$

The unit of $E_c$ is kilowatt-hours per metric ton and reduction ratio is defined as the particle size divided by the closed side set of a jaw crusher.

Conceptually $E_{SE}$ and Donovan's $E_C$ are similar with each other. Thus, the prediction model, $E_{SE} = a\,\mathrm{RR}^{b}\,\mathrm{K_{IC}}^{c}$, is assumed, and data analysis is performed using this proposed equation.

For the assessment of rock blasting, four factors should be considered (Cunningham, 1987) and (JKMRC, 1996).

(1) Rock density

(2) Mechanical strength (UCS)

(3) Elastic properties (Young's modulus)

(4) Structure (In-situ block size)

Mechanical strength is related with the Uniaxial Compressive Strength (UCS), and UCS has been used as mechanical strength in usual blasting model. However, the Uniaxial Tensile Strength (UTS), measured by the Brazilian test, has a better correlation with rock fracturing. Especially, fracture toughness has a strong relationship with the tensile strength of rock, and further, a good correlation with energy consumption for rock fragmentation in a crusher (Donovan, 2003). Thus, the rock properties, mechanical strength and elastic

modulus, will be replaced by the $K_{IC}$, fracture toughness, in the empirical blasting model in this study.

Assumed energy prediction equation form contains following meanings:

- $E_{SE}$ is affected by a blasting pattern (Bench height, burden, spacing, hole diameter, and explosives amount) and rock density, so $E_{SE}$ will represent a blasting pattern in the model.
- RR reflects both whole benches face structure (In-situ block size, F) and the desired fragment size (P) after blasting.
- $K_{IC}$ represents rock properties for prediction of explosives energy consumption.

Therefore, assumed equation form contains the necessary factors for assessment of rock fragmentation and includes target fragment size, P80.

### 4.1 The Equation Model

Table 4.1 summarizes the blasting and rock property data from twelve blasts in the four quarries. The bench face and the muckpile information are represented by “F” and “P” respectively. The data in Table 4.1 is analyzed using the proposed equation, $E_{SE} = a\,\mathrm{RR}^{b}\,\mathrm{K_{IC}}^{c}$.

**Table 4.1 The obtained data of blasting**

| | $E_{SE}$ | $K_{IC}$ | F20 | F50 | F80 | P20 | P50 | P80 | $RR_{20}$ | $RR_{50}$ | $RR_{80}$ |
|---|---|---|---|---|---|---|---|---|---|---|---|
| **Bosung1** | **103** | **1.539** | **165** | **410** | **810** | **46** | **255** | **493** | **3.6** | **1.6** | **1.6** |
| **Bosung2** | **103** | **1.539** | **245** | **586** | **937** | **23** | **214** | **428** | **10.8** | **2.7** | **2.2** |
| **Bosung3** | **107** | **1.539** | **196** | **420** | **821** | **91** | **226** | **431** | **2.2** | **1.9** | **1.9** |
| **Bosung4** | **107** | **1.539** | **158** | **285** | **467** | **72** | **209** | **335** | **2.2** | **1.4** | **1.4** |
| **Bosung5** | **110** | **1.539** | **178** | **330** | **551** | **93** | **252** | **499** | **1.9** | **1.3** | **1.1** |
| **Pittsboro** | **387** | **1.724** | **158** | **281** | **483** | **40** | **100** | **187** | **4.0** | **2.8** | **2.6** |
| **Boxley** | **268** | **1.230** | **514** | **929** | **1512** | **69** | **161** | **304** | **7.4** | **5.8** | **5.0** |
| **Sanyang1** | **268** | **1.889** | **102** | **192** | **334** | **55** | **179** | **350** | **1.8** | **1.1** | **1.0** |
| **Sanyang2** | **292** | **1.889** | **102** | **196** | **382** | **88** | **192** | **290** | **1.2** | **1.0** | **1.3** |
| **Sanyang3** | **336** | **1.889** | **114** | **211** | **360** | **24** | **89** | **199** | **4.8** | **2.4** | **1.8** |
| **Sanyang4** | **222** | **1.889** | **50** | **91** | **149** | **21** | **82** | **163** | **2.4** | **1.1** | **0.9** |
| **Sanyang5** | **210** | **1.889** | **81** | **164** | **309** | **31** | **144** | **265** | **2.6** | **1.1** | **1.2** |

### 4.1.1 Specific Explosives Energy, $K_{IC}$ and $RR_{80}$

Following data in the table shows that $E_{SE}$ is correlated with $RR_{80}$ and $K_{IC}$ value.

**Table 4.2 $E_{SE}$ with given $K_{IC}$ and $RR_{80}$**

| Location | $E_{SE}$(Wh/tonne) | $K_{IC}$(Mpa*$m^{1/2}$) | $RR_{80}$ |
|---|---|---|---|
| **Bosung1** | **103** | **1.539** | **1.6** |
| **Bosung2** | **103** | **1.539** | **2.2** |
| **Bosung3** | **107** | **1.539** | **1.9** |
| **Bosung4** | **107** | **1.539** | **1.4** |
| **Bosung5** | **110** | **1.539** | **1.1** |
| **Pittsboro** | **387** | **1.724** | **2.6** |
| **Boxley** | **268** | **1.230** | **5.0** |
| **Sanyang2** | **292** | **1.889** | **1.3** |
| **Sanyang3** | **336** | **1.889** | **1.8** |
| **Sanyang5** | **210** | **1.889** | **1.2** |

In Bosung and Sanyang quarries, each blasting location was close to the other, so the rock property, $K_{IC}$ value was assumed to be the same within the same quarry blasting in this study. Therefore, although END test was just conducted for $K_{IC}$ value from Bosung1 and Sanyang1 blasting, the other blasted rock in Sanyang and Bosung were assumed as the same with Bosung1 and Sanyang1 at each.

There is the reduction ratio for 80% passing for blast 1 and 4 at the Sanyang quarry, but consequently the data was omitted from the analysis. The reason is that although explosives energy was given, breakage was not realized and the entire blasting energy was consumed to release the block on the bench.

In Table 4.2, regression analysis in EXCEL and SAS was fit to the proposed model, and both programs gave the same result.

$$E_{SE} = 11.7\ RR_{80}^{1.202}\ K_{IC}^{4.14} \qquad \textbf{(4.1)}$$

Where:

$E_{SE}$ is specific explosives energy (wh/ton).

$RR_{80}$ is the reduction ratio based on 80% passing.

$K_{IC}$ is the Mode I fracture toughness of rock.

Figure 4.1 shows the accuracy between predicted specific explosives energy using Equation 4.1 and actual specific explosives energy with the given $RR_{80}$ and $K_{IC}$

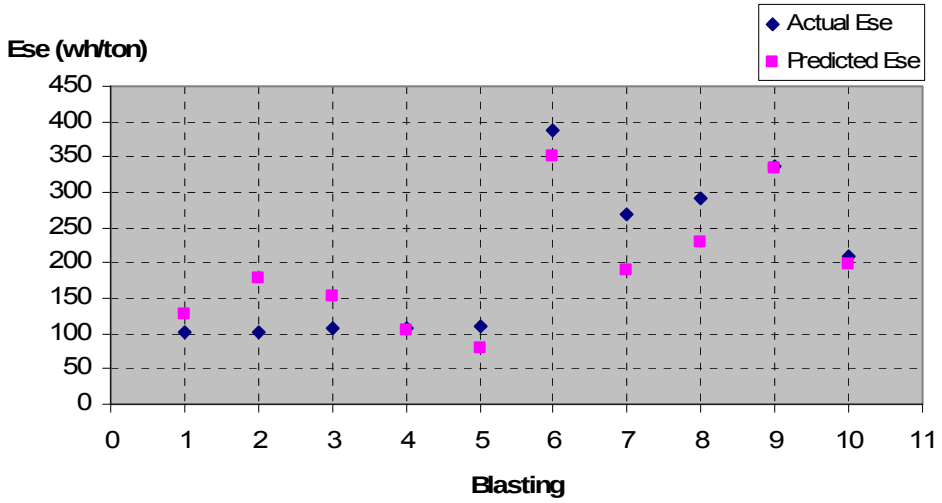


**Figure 4.1 The accuracy between predicted $E_{SE}$ and $E_{SE}$ with given $RR_{80}$ and $K_{IC}$**

Since there are just ten (10) blasting data, statistically there is not enough data to make the equation model. However, predicted $E_{SE}$ is in agreement with $E_{SE}$ as seen in Figure 4.1. The plot of Equation 4.1 with respect to $K_{IC}$ is shown in Figure 4.2.

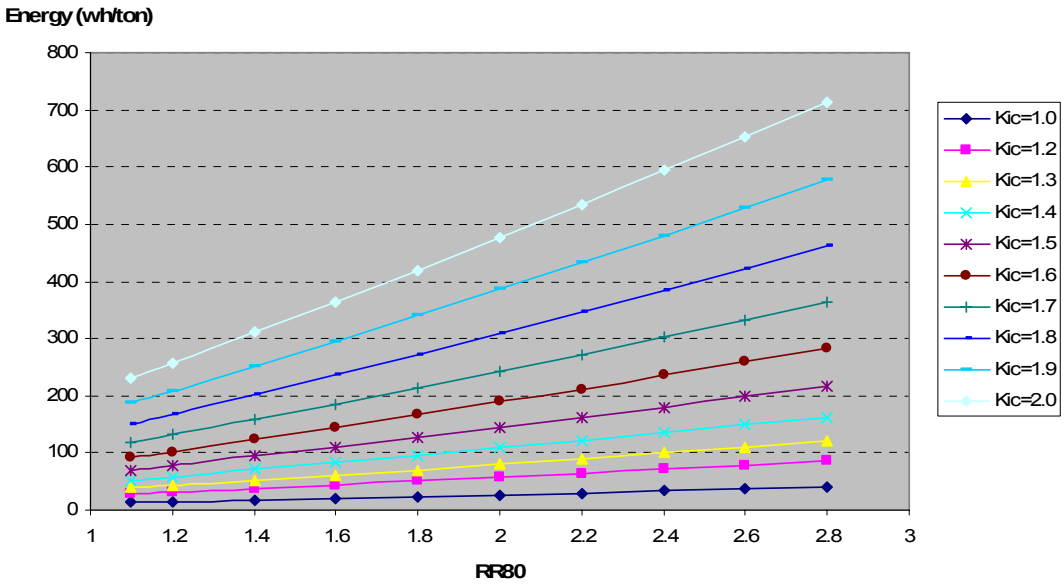


**Figure 4.2 Predicted $E_{SE}$ for $RR_{80}$ and given $K_{IC}$**

Figure 4.2 means that:

- $E_{SE}$ and $RR_{80}$ are in proportion. That means larger $RR_{80}$ needs more specific explosives energy to fragment.
- $E_{SE}$ and $K_{IC}$ are also in proportion, thus the rock having larger $K_{IC}$ is required more specific explosives energy for breakage.

Larger RR means more breakage, and the rock having larger $K_{IC}$ is harder to fragment. Therefore, these relationships based on Equation 4.1 are reasonable.

***$RR_{50}$ and $RR_{80}$***

It is interesting that $RR_{50}$ and $RR_{80}$ have similar values in Table 4.2. Therefore, the relationship among $E_{SE}$, $K_{IC}$ and $RR_{50}$ is similar with $RR_{80}$'s. Figure 4.3 shows the similarity between $RR_{50}$ and $RR_{80}$.

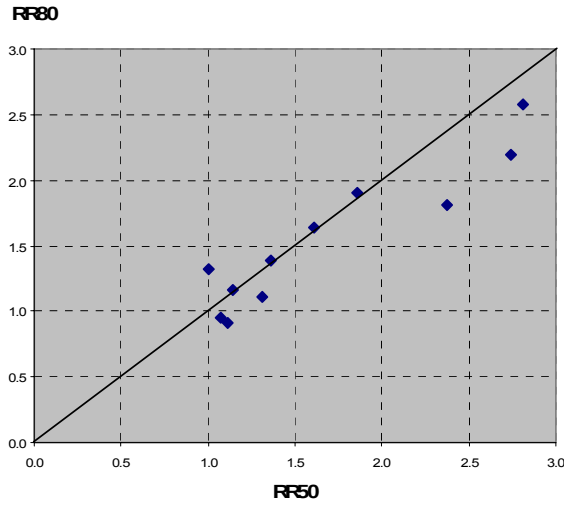


**Figure 4.3 $RR_{50}$ and $RR_{80}$**

The equation is also similar with Equation 4.1, which is about $RR_{80}$.

$$E_{SE} = 15.0\ RR_{50}^{0.86}\ K_{IC}^{4.02} \qquad \textbf{(4.2)}$$

Thus, the relationship between $E_{SE}$ and $RR_{50}$ is in proportion, and the relationship between $E_{SE}$ and $K_{IC}$ is also in proportion. That means more explosives energy is required for more breakage (larger $RR_{50}$) and harder rock (larger $K_{IC}$).

### 4.1.2 Specific Explosives Energy, $K_{IC}$ and $RR_{20}$

Table 4.3 shows the data for analyzing the relationship between $RR_{20}$ and $E_{SE}$ with given rock fracture toughness, $K_{IC}$.

**Table 4.3 $E_{SE}$ with given $K_{IC}$ and $RR_{20}$**

| Location | $E_{SE}$(Wh/tonne) | $K_{IC}$(Mpa*$m^{1/2}$) | $RR_{20}$ |
|---|---|---|---|
| **Bosung1** | **103** | **1.539** | **3.6** |
| **Bosung2** | **103** | **1.539** | **10.8** |
| **Bosung3** | **107** | **1.539** | **2.2** |
| **Bosung4** | **107** | **1.539** | **2.2** |
| **Bosung5** | **110** | **1.539** | **1.9** |
| **Pittsboro** | **387** | **1.724** | **4.0** |
| **Boxley** | **268** | **1.230** | **7.4** |
| **Sanyang1** | **268** | **1.889** | **1.8** |
| **Sanyang2** | **292** | **1.889** | **1.2** |
| **Sanyang3** | **336** | **1.889** | **4.8** |
| **Sanyang4** | **222** | **1.889** | **2.4** |
| **Sanyang5** | **210** | **1.889** | **2.6** |

Using regression of EXCEL and SAS program, data analysis has been tried, and the equation was obtained.

$$E_{SE}=49.0\ RR_{20}^{0.20}\ K_{IC}^{2.19} \qquad \textbf{(4.3)}$$

Where:

- RR20 is the reduction ratio based on 20% passing.

However, the relationship was not in good agreement as seen in Figure 4.4, and the points of the accuracy graph were just scattered.

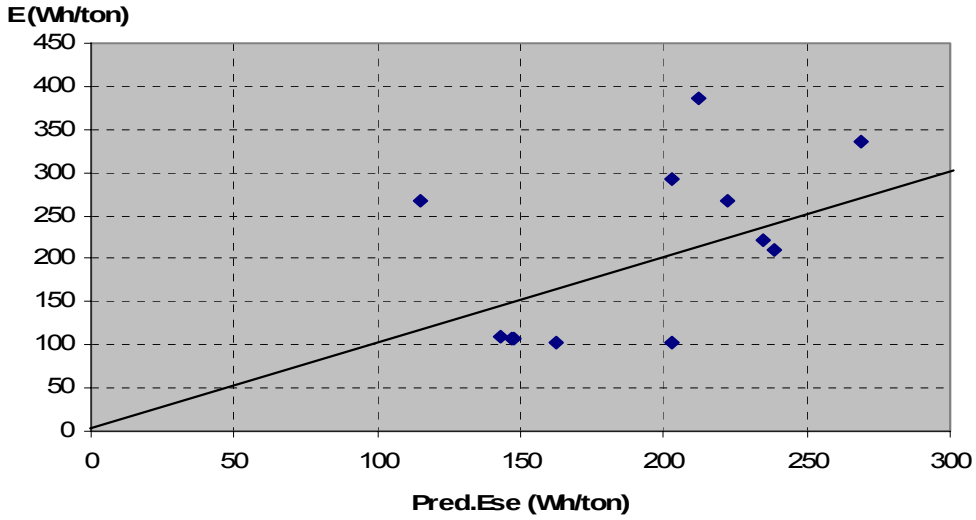


**Figure 4.4 Accuracy between predicted $E_{SE}$ and $E_{SE}$ with given $RR_{20}$ and $K_{IC}$**

The reason is that:

- SPLIT, image analysis program has the limitation of estimating fines in the muckpile. Usually P20 is near fines size in the distribution curve of muckpile image analysis.
- Muckpile image sampling has just done from the surface of a muckpile. However, as seen in Figure 4.5 upper part rock of the muckpile is just liberated from the bench, and the lower part rock is broken (JKMRC, 1996).

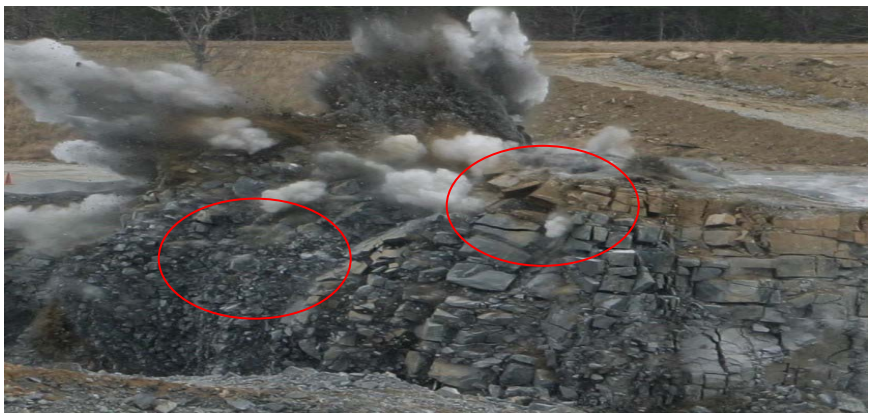

**Figure 4.5 Liberated versus broken rock in the Pittsboro blast (JKMRC, 1996)**

The lower part of the muckpile should be investigated to determine fines or small sizes of rock distribution in the muckpile. Thus, a sieving test is needed to analyze $RR_{20}$ or P20 in the muckpile, or image sampling may be done from a hauling truck, although it will take considerable time.

- Blasting data are too short to investigate the real relationship and to determine some models.

The sampling method and analysis tool in these blastings is not good enough to obtain fines in this research.

Although predicted $E_{SE}$ is not in agreement with given $RR_{20}$ and $K_{IC}$, the result is reasonable because there is the limitation of SPLIT usage and image sampling method in this research. The disagreement of relationships among $RR_{20}$, $K_{IC}$, and $E_{SE}$ is rather reasonable.

### 4.1.3 P50 and P80

The two factors, P50 and P80 are in proportion as the change of uniformity index, N from Rosin-Rammler model.

$$P50 = \left(\frac{\ln 0.5}{\ln 0.8}\right)^{1/N} P80 \qquad \textbf{(4.4)}$$

Where:

P50: 50 % passing size from the size distribution curve in a muckpile after blasting

P80: 80% passing size from the size distribution curve in a muckpile after blasting

N: The Uniformity index from Kuznetsov (Kuznetsov, 1973)

The Equation 4.4 can be derived from the following Rosin-Rammler equation.

$$R = e^{-(\frac{x}{x_C})^n}$$

Where:

R is the fraction of material retained on screen

X is the screen size

$X_C$ is characteristic size, constant

N is uniformity index, constant

Thus, P50 is $0.5 = e^{-(\frac{P50}{x_C})^n}$ , and P80 is $0.8 = e^{-(\frac{P80}{x_C})^n}$ in Rosin-Rammler model.

If natural logarithm is used in the both above equations, then both equations will be as following:

$$\ln 0.5 = - (P50/X_C)^N \quad \text{and} \quad \ln 0.8 = - (P80/X_C)^N$$

Thus,
$$\frac{\ln 0.5}{\ln 0.8} = \frac{-(P50/X_C)^N}{-(P80/X_C)^N}$$

Then,
$$P50 = \left(\frac{\ln 0.5}{\ln 0.8}\right)^{1/N} P80$$

Cunningham suggested Equation 4.5 to determine uniformity index as following (Cunningham, 1983 and 1987).

$$N = \left(2.2 - 14\frac{B}{D}\right)\left(1 + \frac{S/B}{2}\right)^{0.5}\left(1 - \frac{W}{B}\right)\left(\frac{|L_B - L_C|}{L_B + L_C} + 0.1\right)^{0.1} \frac{L}{H} \times (1.1 \text{ or } 1.0) \qquad \textbf{(4.5)}$$

Where:

D is the hole diameter in mm,

B is the burden in m,

W is the standard deviation of drilling accuracy in m,

S is the spacing in m,

$L_B$ in the bottom charge length in m,

$L_C$ is the column charge length in m,

L is the total charge length in m,

H is the Bench height in m.

If a staggered blasting pattern was employed, then the uniformity index will be increased by ten percent (10%).

In the quarry blasting with similar bench height and hole diameter, the change of total charge length, L, and the standard deviation of drilling accuracy, W, is limited.

Therefore, the range of $(\log 0.5/\log 0.8)^{1/N}$ is just (+/-) 0.1 as (+/-) 2 meters change burden and spacing with the same bench height and hole diameter in the blasting pattern from Equation 4.4 and 4.5.

Derived Equation 4.4 shows that the relationship between P50 and P80 will be in proportion in quarries blasting which have the similar bench height and hole diameter.

Bosung (1,2,3,4) and Sanyang blasting (4,5) have similar bench height, 11m, and hole diameter, 76mm. Table 4.4 is the blasting data of P50 and P80 in Bosung and Sanyang quarry.

**Table 4.4 P50 and P80 in Bosung and Sanyang**

| Location | P50(mm) | P80(mm) |
|---|---|---|
| **Bosung 1** | **255** | **493** |
| **Bosung 2** | **214** | **428** |
| **Bosung 3** | **226** | **431** |
| **Bosung 4** | **209** | **335** |
| **Sanyang 4** | **82** | **163** |
| **Sanyang 5** | **144** | **265** |

The data of “P50 and P80” from Table 4.4 was analyzed using EXCEL regression, and the following relationship was obtained.

$$P50=0.5P80 \quad \textbf{(4.6)}$$

Where:

P50: 50 % passing size from the size distribution curve in a muckpile after blasting

P80: 80% passing size from the size distribution curve in a muckpile after blasting

Figure 4.6 shows the accuracy of predicted P50 using Equation 4.6.

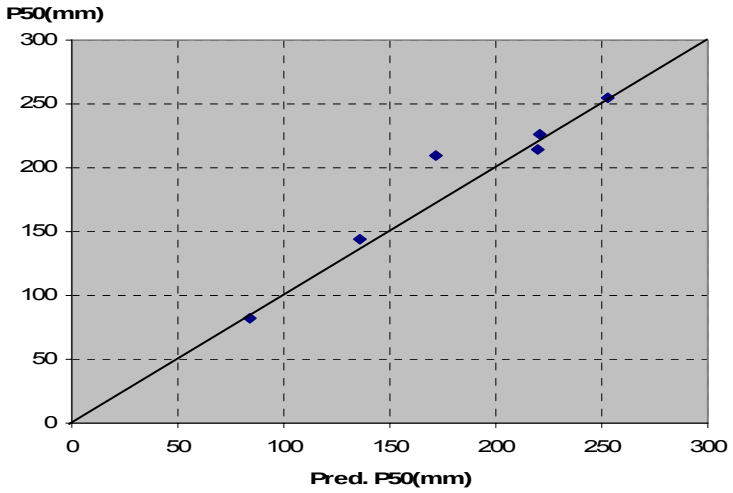


**Figure 4.6 The accuracy between predicted P50 and P50**

If there is the same bench height and hole diameter at the blasting sites, then P50 may be predicted with P80 from blasting to blasting. Although data is insufficient to determine the actual relationship between P50 and P80, there should be a proportional relationship between P50 and P80 in blasting with the same bench height and hole diameter because it is both theoretically and practically reasonable.

Again, to make a site-specific empirical blasting model, this relationship between P50 and P80 is useful because the bench height and hole diameter is usually similar or the same within each quarry.

# Chapter 5 Discussion of Results

## 5.1 Improvements Revealed by the Research

1. SPLIT was used successfully to examine the bench face.
Using SPLIT on the bench face was effective and produced reasonably consistent results. F50 in SPLIT on the bench face can be a new index as the mean in-situ block size. Actually, the manually measured mean in-situ block size and F50 in SPLIT on the bench face share the similar scale in the Pittsboro quarry.

2. The Kuz-Ram model was adapted as a practical means for predicting size distribution in the muckpile.

In the Kuz-Ram model, the average size of rock in the muckpile and the size distribution curve were predicted using given factors in the blasting site. However, in this research, because the products (P80) were what we wanted, the desired P80 was taken for granted, and P50 predicted by the empirical model; proper burden and spacing were predicted by using the empirical model with the given blasting factors. In addition, the size distribution curve in the muckpile was predicted with P50 and proper burden & spacing based on the given factors. P80, the eighty percent (80%) passing size, was assumed to be the optimum size desired by most model users and the representative size of the muckpile.

3. An attempt was made to use Mode I fracture toughness as the rock property in the blasting model instead of UCS (Uniaxial Compressive Strength) and E (Young's modulus) in Kuz-Ram.

Although tensile strength has a strong correlation with rock breakage, only UCS and E are used in Kuz-Ram. In our study Mode I fracture toughness was used in the blasting model because tensile strength has strong relationship with $K_{IC}$.

Mode I is the most commonly encountered mode of crack deformation in rock blasting applications. However, although the relationship between $K_{IC}$ and the size distribution of blasting result could be determined, the data was insufficient to figure out the correlation. Additional sieving tests seemed reasonable and justifiable. In addition we discovered that $K_{IC}$ may especially correlate with fines and the small size of rock in the muckpile's whole size distribution. However, further research is needed regarding these issues because the data is insufficient to make a final determination and an image analysis program has the disadvantage of underestimation of fines in the muckpile.

4. Although this model is not specific to any blasting area because of the shortage of blasting data, it may be adapted by blasting engineers to particular mines for the purpose of making a site-specific model.

The empirical model was derived step by step as follows:

- Collect blasting image data (the bench face and the muckpile image) and rock sample after blasting.
- Conduct the END test with sampled rock.
- Analyze collected data using image analysis.
- Conduct regression using SAS or EXCEL with suggested equation form.
- Adjust the empirical equations for specific blasting sites.
- Use this adjusted empirical equation model in the simulation model based on Visual Basic. NET program.

Thus, it would seem that an organized blasting design with the desired consistent result, P80, may be possible.

## 5.2 The Bench Face Structure and the Blasting Design for Desired Consistent Results

Optimized blasting in mining is a complex issue because the entire detailed process must be considered. Optimized blasting is different at each blasting site because there are different crushers, drilling machines, hauling machines, and bench height considerations. However, whether or not blasting is optimized, organized blasting for consistent results based on a simple and flexible blasting model will greatly reduce energy waste.

If there is a given bench height and diameter of the drilling hole at the blasting site, then burden and spacing are two of the most important factors in the blasting model because these factors are easy to manipulate, whereas other factors are more difficult to control. Therefore, application of the model has been focused on obtaining proper burden and spacing to obtain the desired blasting result by using the site-specific blasting equation model consistently.

To obtain consistent blasting results, one of the greatest obstacles in a given blasting site is accurate determination of changes in the bench face structure. Although the rock properties, bench height, and hole diameter are the same from blasting to blasting in a given blasting site, the bench face structure is almost always changed during each blasting.

In this research, the change of bench face structure was measured easily and quickly using the image-processing program. As with the change of the bench face structure (size ‘F’), the burden and spacing in a blasting pattern were likewise adjusted for each blasting site.

## 5.3 P80 for the Optimal Blasting in a Quarry (Kojovic, 2006)

Practically, for a typical quarry, waste is below 0.005m, the desired final product size ranging from 0.005 to 0.025m. That means everything above 0.025m has to be reduced. This is typically done via blasting followed by multi-stage crushing. The amount of

blasting will clearly impact the amount of crushing required, so the trick is to find the optimum level of blasting to maximize the yield of 0.005~0.025m product, at the lowest overall cost (of drilling, blasting, and crushing, including the cost of energy, liners and maintenance). Too much blasting can lead to too many fines, which may well reduce the amount of crushing required at the expense of lowering the overall yield. Too little initial crushing might require more crushing later in the process, which means more electrical energy and more wear and tear on the equipment, with the result that costs go up once again. Ideally, each quarry will maintain an optimum balance between the blasting and crushing required to achieve the best possible outcome. Because rock conditions will dictate what these balances should be, it is not enough to target just one size (P80). However, in practice, targeting a P80 of 0.2m in the blast might be great in terms of the reduced crushing requirements, but the blast would have to be too energetic, resulting in too much waste, that is to say, anything less than 0.005m. We are therefore looking for the best balance to achieve the optimum yield and lowest overall cost. To consider blasting as an isolated process is to ignore the possible negative impact downstream.

P80 may be just a convenient yardstick on the level of coarseness in the blasting model, but the predicted size distribution curve was obtained by using P80, resulting in proper burden and spacing in the research model. Thus, a closed design for optimization in a quarry process may be obtained by manipulating the blasting design (burden, spacing, and desired P80) in the model. In the mine to mill optimization project (Virginia Tech and JKMRC 2004~2006), the optimized blasting came up with a P80 range of 0.2~0.3m. This range may be used as the P80 size for optimized blasting in a usual quarry.

### 5.4 Generalized Blasting Model

A generalized blasting model is difficult to devise because rock properties and bench face structure vary greatly, and obtaining blasting data is both expensive and time-consuming. Actually, a generalized model may be unattainable because every blasting model must be

adjusted for the given blasting site. With this in mind, in constructing the present model just twenty or thirty pieces of blasting data were used per given blasting site. This model may be more powerful and efficient than any other blasting model within a given blasting site. Using the method described in this thesis, will assist blasting engineers in achieving more efficient blasting in their quarries and provide a much-needed reduction in the amounts of energy used in the mining process.

### 5.5 Application for the Simulation Model

Using the obtained empirical equation models and adjusted Kuz-Ram model, the simulation program can be made with Visual Basic.NET program.

Although the following simulation program is not truly sufficient for definitive conclusion, this practical trial will be useful for making a site-specific blasting model simulation for blasting engineers.

1. Given Factors in the model
*Blasting pattern
- **H,D :** Bench height(m)/ Hole diameter(mm)
- **Ex. :** Explosives amount (Kg, per hole)
- **L :** Charge length (m)
- **W :** Drill accuracy Standard Deviation(m)

*Rock properties
- **SG :** Rock Specific Gravity (tonne/$m^3$)
- **$K_{IC}$** : Fracture toughness (Mpa*$m^{0.5}$)

*The block structure on the bench face
- **F80 :** The in-situ block size (m)

*The goal of the blasting
- **P80** : Wanted P80 in the muckpile size distribution (m)

↓

2. The empirical model from the data analysis using regression
- $E_{SE} = 11.7\ RR_{80}^{1.202}\ K_{IC}^{4.14}$
- $P50 = 0.5\ P80$ → **P50**

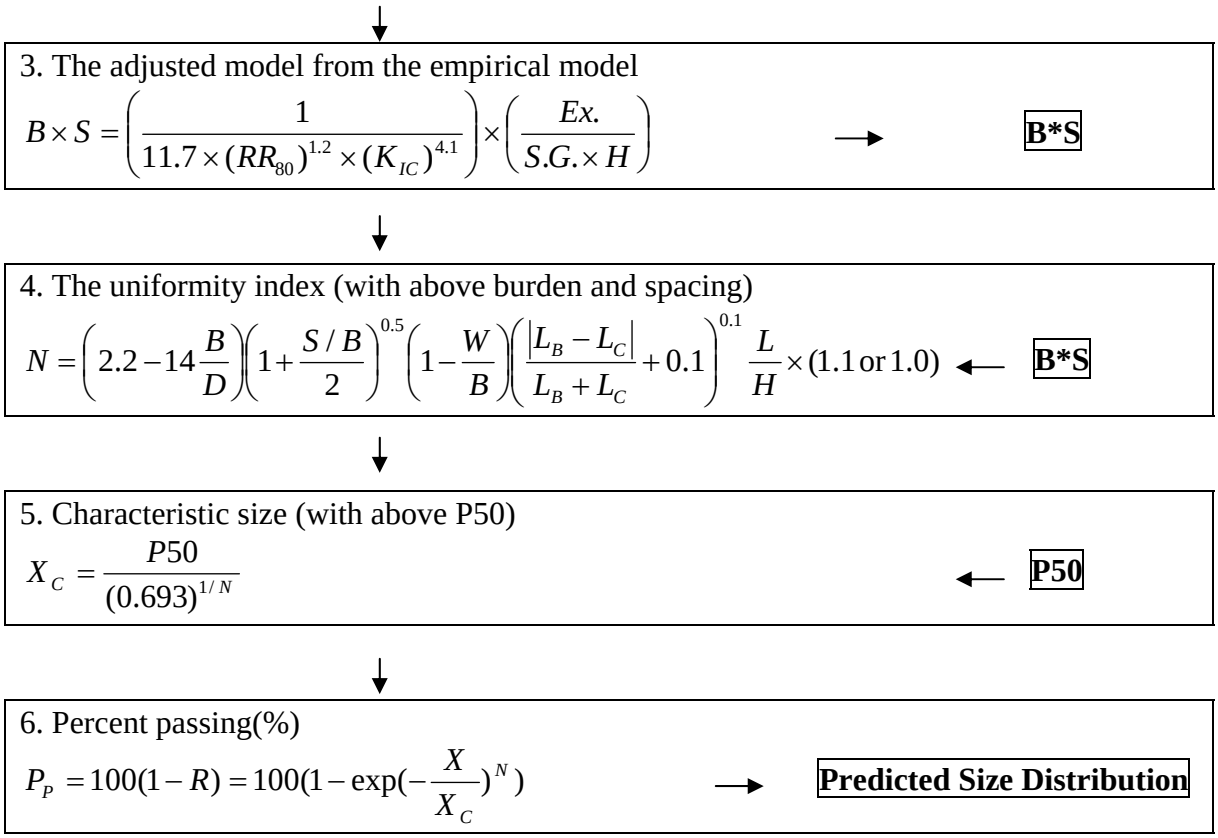


The previous flow chart shows the mechanism of the following simulation program in Figure 5.1. Using this mechanism, the following simulation can be made.

The suggested application is to obtain the proper burden and spacing with given hole diameter, bench height, explosives amount, and the kind of explosives as the change of the rock and the bench structure.

Above used equation in second blank of the flow chart, $E_{SE} = 11.7\ RR_{80}^{1.202}\ K_{IC}^{4.14}$ was obtained from 10 blasting data analysis, but another equation, (P50) = 0.5 (P80) is just from 6 blasting data analysis, both models were derived from the different number of blasting data. However, the above application is just for showing how to make the model practical using an empirical equation model. In addition, especially, the given factors (explosives

amount, charge length, and the kind of explosives) were based on the previously experienced blasting patterns in a given blasting site.

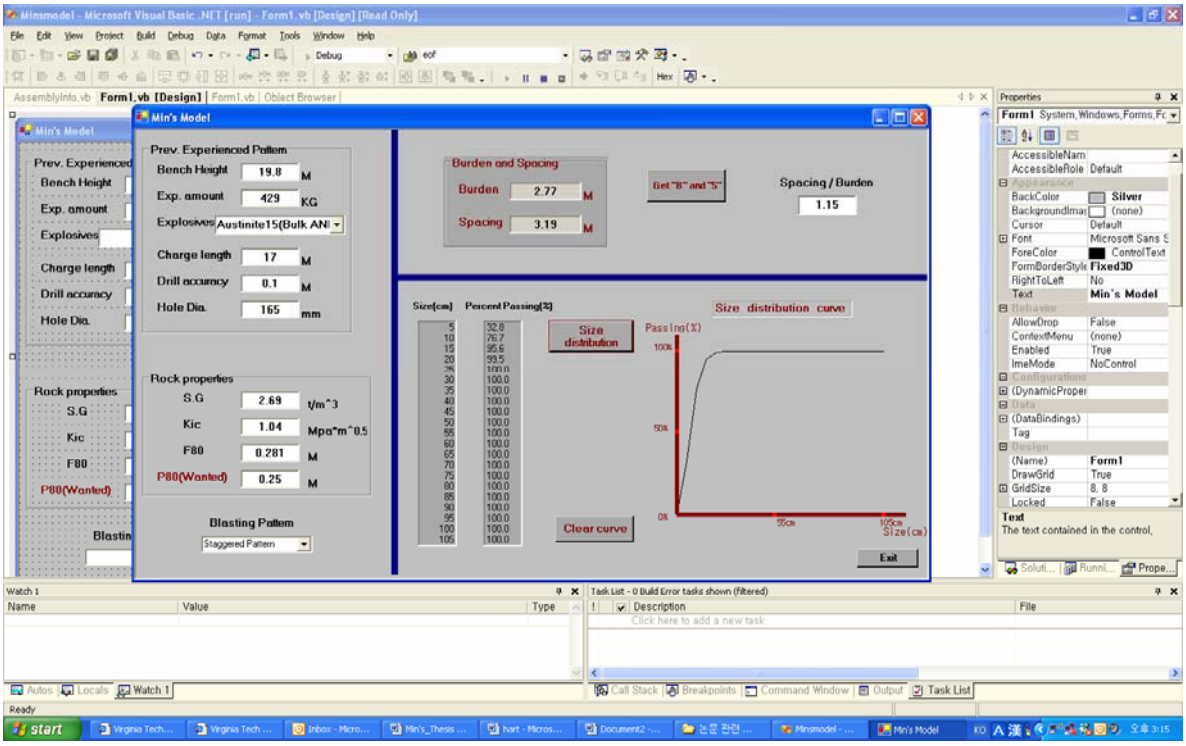


**Figure 5.1 Simulation using Visual Basic. Net Program**

The above simulation model contains the whole necessary factors for assessment of rock fragmentation (rock density, mechanical strength, elastic properties, and structure) and includes target fragment size, P80.

Using the above simulation program, proper burden and spacing may be predicted for desired P80 in the muckpile. In addition, predicted size distribution curve will be obtained using adjusted Kuz-Ram model.

Thus, proper burden and spacing may be changed and adjusted for desired size distribution in the muckpile.

# Chapter 6 Conclusion and Future Work

## 6.1 Research Summary

The following sequence was followed in the research:

1. Collect blasting image data and rock sample.

Bench face image sampling was conducted before blasting, and muckpile image sampling was done after blasting. For sampling images of the bench face and the muckpile, same scale materials were used from image to image. In addition, the angle between the bench face and the camera was kept perpendicular, and rock sampling was conducted after blasting. The most important factor for sampling image is consistency.

2. Conduct the END test with sampled rock.

Using suggested END test by Donovan (2003), the mode I fracture toughness value, $K_{IC}$ could be obtained easily and quickly. The obtained $K_{IC}$ value is as follows:

**Table 6.1 Fracture toughness, $K_{IC}$, and Tensile strength, $\sigma_t$**

| Location | $K_{IC}$(MPa*m^0.5) | $\sigma_t$ (MPa) |
|---|---|---|
| **Bosung** | **1.539 ± 0.100** | **16.94 ± 1.92** |
| **Sanyang** | **1.724 ± 0.193** | **17.45 ± 2.57** |
| **Pittsboro** | **1.889 ± 0.398** | **22.48 ± 4.70** |
| **Boxley** | **1.230 ± 0.216** | **14.72 ± 1.23** |

3. Analyze collected data using image analysis, SPLIT.

The setting in SPLIT depends on the users, but there should also be consistency from image to image analysis. Following is the summarized data from image analysis of the bench face and the muckpile, and specific explosives energy from each blasting pattern.

**Table 6.2 Blasting data from image analysis, END test, and the blasting pattern**

| | $E_{SE}$ | $K_{IC}$ | F20 | F50 | F80 | P20 | P50 | P80 | $RR_{20}$ | $RR_{50}$ | $RR_{80}$ |
|---|---|---|---|---|---|---|---|---|---|---|---|
| **Bosung1** | **103** | **1.539** | **165** | **410** | **810** | **46** | **255** | **493** | **3.6** | **1.6** | **1.6** |
| **Bosung2** | **103** | **1.539** | **245** | **586** | **937** | **23** | **214** | **428** | **10.8** | **2.7** | **2.2** |
| **Bosung3** | **107** | **1.539** | **196** | **420** | **821** | **91** | **226** | **431** | **2.2** | **1.9** | **1.9** |
| **Bosung4** | **107** | **1.539** | **158** | **285** | **467** | **72** | **209** | **335** | **2.2** | **1.4** | **1.4** |
| **Bosung5** | **110** | **1.539** | **178** | **330** | **551** | **93** | **252** | **499** | **1.9** | **1.3** | **1.1** |
| **Pittsboro** | **387** | **1.724** | **158** | **281** | **483** | **40** | **100** | **187** | **4.0** | **2.8** | **2.6** |
| **Boxley** | **268** | **1.230** | **514** | **929** | **1512** | **69** | **161** | **304** | **7.4** | **5.8** | **5.0** |
| **Sanyang1** | **268** | **1.889** | **102** | **192** | **334** | **55** | **179** | **350** | **1.8** | **1.1** | **1.0** |
| **Sanyang2** | **292** | **1.889** | **102** | **196** | **382** | **88** | **192** | **290** | **1.2** | **1.0** | **1.3** |
| **Sanyang3** | **336** | **1.889** | **114** | **211** | **360** | **24** | **89** | **199** | **4.8** | **2.4** | **1.8** |
| **Sanyang4** | **222** | **1.889** | **50** | **91** | **149** | **21** | **82** | **163** | **2.4** | **1.1** | **0.9** |
| **Sanyang5** | **210** | **1.889** | **81** | **164** | **309** | **31** | **144** | **265** | **2.6** | **1.1** | **1.2** |

4. Conduct regression using SAS or EXCEL with suggested equation form.

Using the assumed equation form to predict the specific explosives energy, regression was examined using SAS and EXCEL and the same constants were obtained. Actually, there were about 80 kinds of analysis trials, from which the following results were selected.

$$E_{SE} = 11.7\ RR_{80}^{1.202}\ K_{IC}^{4.14}$$

$$E_{SE} = 15.0\ RR_{50}^{0.86}\ K_{IC}^{4.02}$$

$$E_{SE} = 49.0\ RR_{20}^{0.20}\ K_{IC}^{2.19}$$

Where:

$E_{SE}$ is specific explosives energy (wh/ton).

$RR_{80}$ is the reduction ratio based on 80% passing.

F80 is 80% passing size from the bench face image analysis (mm).

P80 is 80% passing size from the muckpile image analysis (mm).

$RR_{20}$ and $RR_{50}$ are same as $RR_{80}$.

F50 is 50% passing size from the bench face image analysis (mm).

$K_{IC}$ is the Mode I fracture toughness of rock ($MPa*m^{1/2}$).

In addition, the relationship between P50 and P80 was derived from the Rosin-Rammler model.

$$P50 = \left( \frac{\ln 0.5}{\ln 0.8} \right)^{1/N} P80$$

$$P50 = 0.5\ (P80)$$

5. Use the empirically obtained equation models for making the site-specific blasting model. In this research, the following two equation models were selected for this application.

$$E_{SE} = 11.7\ RR_{80}^{1.202}\ K_{IC}^{4.14}$$
$$P50 = 0.5\ (P80)$$

6. Make the simulation model based on Visual Basic.NET program.

For convenience of usage, the language program VB.NET was used and a simulation program was created. With this simulation program, proper burden and spacing can be predicted for the target fragment size, P80, and P50 is predicted automatically. In addition, the size distribution is predicted for the given blasting factors. Using this predicted size distribution in reverse allowed us to adjust burden and spacing and target size, P80, in the muckpile to achieve the desired size distribution.

For an example of the program usage,

1. At the given site, a blasting engineer wants to have the specific target fragment size, P80, in the muckpile which is based on previous blasting data analysis at this site.
2. The rock properties and the bench face structure are totally different at each blast, but the bench height and hole diameter are usually the same at each blast within the given blasting site. Therefore, the blasting engineer uses the same blasting pattern (hole diameter, boring depth, explosives, and explosives amount) except burden and spacing at each blast.
3. The blasting engineer conducts END wedge splitting test to obtain $K_{IC}$, and uses the image analysis program on the bench face to obtain the in-situ block size information.

4. The equation models, obtained by the current research, are used to get the proper burden and spacing for the target fragment size, P80, in the muckpile.

Using this program, it is important to note that the blasting parameters, with the exception of burden and spacing, are set equal to those used previously at the site.

### 6.2 Conclusion

Two main ideas were combined in this study. First, the whole bench face structure information may be obtained by using an image-processing program, and this information can be used for the blasting model. Secondly, mode I fracture toughness, $K_{IC}$, can be used to represent the rock properties in the blasting energy prediction model.

In the research, these two ideas were investigated to determine whether these ideas are practical. The largest drawback in this investigation was the small amount of blasting data. To create a new empirical blasting model and to test the new ideas in this blasting model, twelve pieces of blasting data from four quarries was not enough.

However, if we consider that obtaining blasting data requires much time and expense, the data, although insufficient, may be used to determine certain possibilities.

Basically, if we consider the concept of RR, $E_{SE}$, and $K_{IC}$, in the blasting energy prediction model, then the following relationships are reasonable and may be hypothesized:
- $E_{SE}$ and RR will be in proportion.
- $E_{SE}$ and $K_{IC}$ will also be in proportion.
- The in-situ block size, F and $E_{SE}$ will be in inverse proportion because of leaking energy of the explosives.

There follow the main empirical equation models obtained from the blasting data analyzed in this research:

$$E_{SE} = 11.7\ (RR_{80})^{1.202}\ K_{IC}^{4.14}$$

$$P50 = 0.5\ (P80)$$

The above equations were not generalized because of the lack of data. However, the research results are consistently reasonable, especially the findings (1) that $E_{SE}$ and $K_{IC}$ with given $RR_{80}$ are in proportion and (2) that $E_{SE}$ and RR are in proportion with given $K_{IC}$, and (3) that P50 and P80 are in proportion within a given bench height and hole diameter.

Using SPLIT on the bench face to get in-situ block sizes (F) was the first challenge. At each image, the result of the SPLIT analysis reveals significant variability, but it also demonstrated consistency on the whole, and it is a reasonable challenge because the equation model is reasonable based on data analysis. Furthermore, in a blasting model, the actual properties of the rock may be replaced by the rock fracture toughness, $K_{IC}$ to predict the energy consumed in blasting.

Thus, although blasting data is insufficient to determine a model and verify any conclusion, the above hypotheses are supported by twelve (12) blasting data analyses, and are both reasonable theoretically and practical. The data shows at least the possibility that the proposed ideas are valid.

***Application***

Burden and spacing are two of the most important factors in the blasting model because these factors are easy to manipulate, whereas other factors are harder to control with given bench height and hole diameters. Therefore, application of the model focused on getting the proper burden, spacing for target fragment size, and, further, size distribution prediction of the muckpile after blasting.

Using the above equation models, proper burden and spacing for the desired target fragment size was obtained. The following equation is adjusted to show this:

$$B \times S = \left( \frac{1}{11.7 \times (RR_{80})^{1.202} \times (K_{IC})^{4.14}} \right) \times \left( \frac{Ex.}{S.G. \times H} \right)$$

In the above equation, $RR_{80}$ is F80/P80. Thus the desired target fragment size, P80 was considered, and F80 was obtained from the bench face image analysis. In addition, rock property, $K_{IC}$, and the amount of explosives per given bench height were considered in this equation. Size distribution using Kuz-Ram was predicted given this burden and spacing automatically in the simulation program.

This simulation program is not generalized because of the shortage of data, but it is a site-specific model program. Although it will take time and effort to determine, this kind of site-specific model program may be more powerful than the generalized blasting fragmentation prediction program, within a given blasting site, due to variable rock properties and structure in the site.

Following are the characteristics of the described simulation program in this research.
- Mode I fracture toughness was used as rock property for blasting energy prediction.
- Changed bench face structure was measured easily and quickly by SPLIT at each blasting.
- Proper burden and spacing was obtained for the target fragment size, P80, in each given blasting site, not just for the prediction of rock fragmentation, but for practical reasons appreciated by blasting engineers.

The author hopes to show in the future uses to which the obtained empirical equation models might be put, so the research is not completed. The suggested simulation program merely demonstrates the capability of the obtained empirical blasting equation models to obtain proper burden, spacing, and size distribution predictions after blasting.

## 6.3 Limitation in the Research and Future work

***Muckpile image Sampling***

In the muckpile image sampling, although the main sampling strategy in this research is consistency and this method is not time consuming, the findings are statistically inadequate accurately to represent the muckpile. To have better muckpile image samples to characterize the entire muckpile, obtaining images from the hauling truck is better, but this will add to the amount of time needed to perform the sampling.

***DATA***

In this research, there are initially three (3) givens in the empirical blasting model:

1. The use of $K_{IC}$ in the blasting model.
2. The use of conceptually new factors, $E_{SE}$ and RR.
3. The use of SPLIT for getting the in-situ block size of a bench face.

However, the empirical model consisted of just twelve (12) blasting data. More blasting data is needed to verify the findings regarding blasting energy prediction and to suggest additional aspects of the new empirical blasting model.

***P80***

To obtain consistent blasting results, the author chose the target fragment size, P80. However, this one size, P80, alone is not enough to represent the blasting result. The muckpile should be considered in its entirety to estimate size distribution.

However, finding P80 in the muckpile image analysis may be related with optimal blasting results. In a usual quarry blasting, if P80 is between 0.2~0.3m, then it would be excellent. However, the result ultimately depends on the situation present in each quarry, i.e., each quarry's particular variables. Additional research is needed to demonstrate this to the fullest extent.

***P50 and P80***

In the Rosin-Rammler model, the relationship between P50 and P80 is in proportion, as follows:

$$P50 = \left( \frac{\ln 0.5}{\ln 0.8} \right)^{1/N} P80$$

As the change of uniformity index, N, P50 is in proportion with P80. The empirical equation model of P50 and P80 is also in proportion to the Rosin-Rammler model. Therefore, the empirical model derived from the collected blasting data may be used in the research model. Further research using larger amounts of blasting data is required to resolve this issue and determine a generalized equation.

***P20 and Fines***

P20 in the size distribution of the muckpile was used to determine the relationship between rock properties and fines. However, this trial failed because in general the image processing system underestimates fines, and the available data is insufficient to provide a firm conclusion. As a result, obtaining good data about fines is not possible using available image processing systems. To resolve this issue, a sieving test of the muckpile must be done after blasting, and more investigation is needed.

**References**


Adel, G., Kojovic, T., Thornton, D. (2004) Mine-to-Mill Optimization of Aggregate Production-Annual report *Department of Mining and Mineral Engineering,Virginia Tech and JKTech-JKMRC Commercial Division, The University of Queensland.*

Adel, G. (2004) Abstract of Project "Mine-to-Mill Optimization of Aggregate Production" *Department of Mining and Mineral Engineering, Virginia Tech.*

Allis-Chalmers. (1985) Allis-Chalmers High Energy Crushing Test System User Manual. Version 1.0

Bearman, R.A., Pine, R.J., and Wills, B.A. (1989) Use of fracture toughness testing in character the comminution potential of rock. *Proceedings of MMIj/IMM Joint Symposium, Kyoto, 161~170*

Chong, K.P. and Kuruppu, M.D. (1984) New Specimen for Fracture Toughness Determination of Rock and Other Materials, *International Journal of Fracture*, Vol. 26, pp. R59-R62.

Chung, S. H. & Katsabanis, P.D. (2000) Fragmentation prediction using improved engineering formulae. *International Journal of Blasting and Fragmentatioin.*

Clark, G. B. (1987) Principles of Rock Fragmentation *John Wiley and Sons, New York, Chichester, Brisbane, Toronto, Singapore.*

Cunningham, C. (1983) The Kuz-Ram Model for the Prediction of Fragmentation from Blasting, *Proceedings of the international Symposium on Rock Fragmentation and Blasting, Lulea, Sweden.*

Cunningham, C. (1987) Fragmentation Estimations and the Kuz-Ram Model – Four years on, *Proceedings of the second international Symposium on Rock Fragmentation and Blasting, Keystone, Colorado.*

Cunningham, C. (1996) Optical fragmentation assessment - A techanical challenge *Proceeding Measurement of Blast Fragmentation, Balkema, Rotterdam*

Dahlhielm, S. (1996) Industrial applications of image analysis – The IPACS system *Proceeding Measurement of Blast Fragmentation, Balkema, Rotterdam*

Donovan, J. G. (2003) Fracture Toughness Based Models for the Prediction of power consumption, product size, and capacity of jaw crushers *Doctor of philosophy dissertation, Mining and Mineral Engineering, Virginia Tech, Blacksburg*

Donovan, J. G. and Karfakis, M. G. (2004) A Fracture Toughness Based Models for the Prediction of jaw crusher power consumption *American Rock Mechanics Association,* Vol. 04-545

Donovan, J. G. and Karfakis, M. G. (2004) Adaptation of a simple wedge test for the rapid determination of Mode I fracture toughness and the assessment of relative fracture resistance, *International Journal of Rock Mechanics & Mining Sciences,* Vol. 41, pp. 695 – 701.

Dowling, N.E. (1999) Mechanical behavior of materials – engineering methods for deformation, fracture, and fatigue *Upper Saddle River, NJ: Prentice-Hall*

Fenghui, W. (2000) Prediction of intrinsic fracture toughness for brittle materials from the apparent toughness of notched-crack specimen, *Journal of Materials Science*, Vol. 35, pp. 2543-2546.

Girdner,K.K., Kemeny, J.M., Srikant, A.& Mcgill, R. (1996) The split system for analyzing the size distribution of fragmented rock *Proceeding Measurement of Blast Fragmentation, Balkema, Rotterdam.*

Gregory, R.D. (1979) The edge-cracked circular disc under symmetric pin loading *Math Proc. Camb Phil Soc*

Havermann, T., Vogt W. (1996) TUCIPS- A system for the estimation of fragmentation after production blasts *Proceeding Measurement of Blast Fragmentation, Balkema, Rotterdam*

Isida, M., Imai, R., Tsuru, H. (1979) Symmetric plane problems of arbitrarily shaped plates with an edge crack *Trans Japan Soc. Mech. Eng.*

ISRM (1998) Suggested Methods for Determining the Fracture Toughness of Rocks, (coordinator F. Ouchterlony), *International Journal of Rock Mechanics & Geomechanics Abstracts*, Vol. 25, pp. 73-96.

Jimeno, C. L., Jimeno E. L., Carcedo, F. J. A. (1995) Drilling and Blasting of rocks *Balkema, Rotterdam,Brookfield*

JKMRC (1996) Open Pit Blast Design: analysis and optimization *The University of Queensland.*

Kemeny, J., Mofya, E., Kaunda, R. and Lever, P. (2002) Improvements in Blast Fragmentation Models using digital image processing *Proceedings Fragblast Vol.6,* No.3-4, pp. 311-320

Kojovic, Toni (2006) Private communication with an expert in JKMRC

Kuznetsov, V.M. (1973) The mean Diameter of the Fragments Formed by Blasting Rock, *Soviet Min. Sci.*.

Lilly, P.A. (1986) An empirical method of assessing rock mass blastability *Proceeding Large Open Pit Mining Conference*, pp. 89~92.

Lim, I. L., Johnston, I. W., Choi, S. K., Boland, J. N. (1994) Fracture testing of a Soft Rock With Semicircular Specimens Under Three Point Bending *International Journal of Rock Mechanics, Mining Sciences, and Geomechanics* Vol. 31, pp.185~197

Liu, Q., Tran, H. (1996) Comparing system- Validation of Fragscan, Wipfrag and Split *Balkema, Rotterdam*

Maerz N. H. (1996) Image sampling techniques and requirements for automated image analysis of rock fragmentation *Proceeding Measurement of Blast Fragmentation, Balkema, Rotterdam*

Maerz, N. H., Palangio, T. C., Franklin, J. A. (1996) WipFrag image based granulometry system *Proceeding Measurement of Blast Fragmentation, Balkema, Rotterdam*

Murakami, Y. (1987) Stress intensity factors handbook. *Pergamon Press*

Norton, B (2005) Private communication with an expert in SPLIT engineering

Ozdemir, K., Kahriman, A., Karadogan, A., and Tuncer, G. (2003) Blasting Fragmentation Assessment and control using the split digital image analysis system *International Conference on Earth Sciences and Electronics.*

Rustan, Agne (1998) Rock Blasting Terms and Symbols *A.A. Balkema, Rotterdam, Brookfield*

Schleifer, J., Tessier, B. (1996) FRAGSCAN: A tool to measure fragmentation of blasted rock *Proceeding Measurement of Blast Fragmentation, Balkema, Rotterdam*

Schmidt, R.A. (1980) A microcrack model and its significance to hydraulic fracturing and fracture toughness testing *Proceedings of the 21$^{st}$ US Symposium on Rock Mechanics*, pp.581~590

Schmidt, R.A and Rossmantihm, H.P (1983) Basics of Rock Fracture Mechanics, *Rock Fracture Mechanics*

Spathis, A.T. (2004) A Correction relating to the Analysis of the Original Kuz-Ram Model, *Fragblast,* Vol.8, No 4, pp 201-205.

SPLIT Engineering LLC(2001) Split-desktop software manual

Sun, Z. and Ouchterlony, F. (1986) Fracture toughness of stripa granite cores, *International Journal of Rock Mechanics & Geomechanics Abstracts*, Vol. 23, pp. 399-409.

Tada, H., Paris, P.C. and Irwin, G. R. (2000) The Stress Analysis of Cracks Handbook, *ASME Press, New York.*

Tada, H., Paris, P.C., and Irwin, G.R. (2000) The Stress Analysis of Cracks Handbook *ASME Press, New York*

Wang, Q.Z. (1998) Stress Intensity Factors of the ISRM Suggested CCNBD Specimen Used for Mode-I Fracture Toughness Determination, *International Journal of Rock Mechanics & Mining Sciences,* Vol. 35, pp. 977-982.

Wang, Q.Z. and Wu, L.Z. (2004) The flattened Brazilian disc specimen used for determining elastic modulus, tensile strength, and fracture toughness of brittle rocks: Experimental results, *International Journal of Rock Mechanics & Mining Sciences*, Vol. 41, No. 3.

# APPENDIX A -

## Image Analysis of the Bench Face

**Figure A.1 Bosung1, the bench face image**

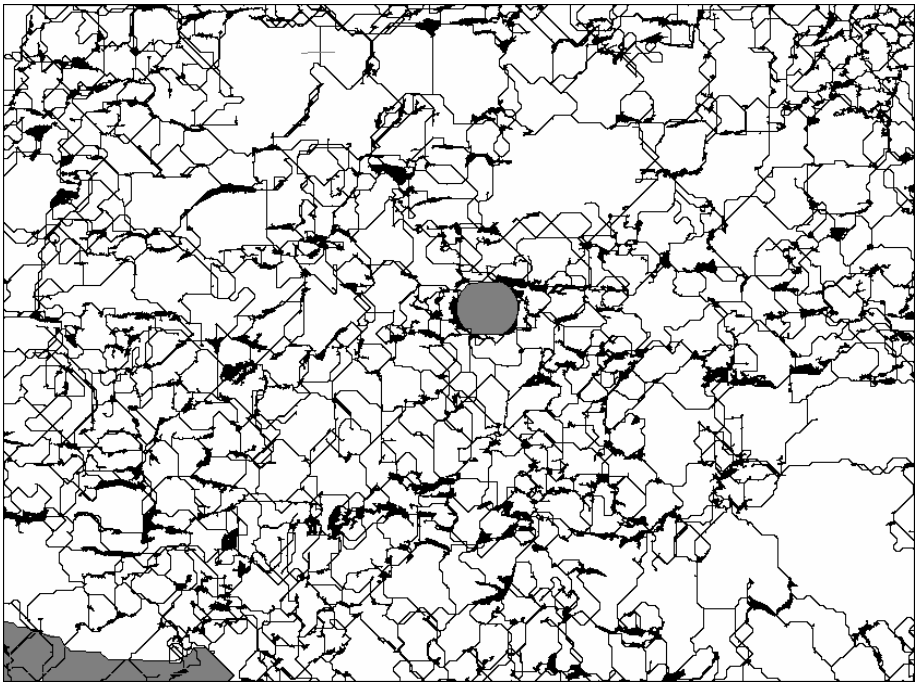

**Figure A.2 Bosung1, the analyzed image**

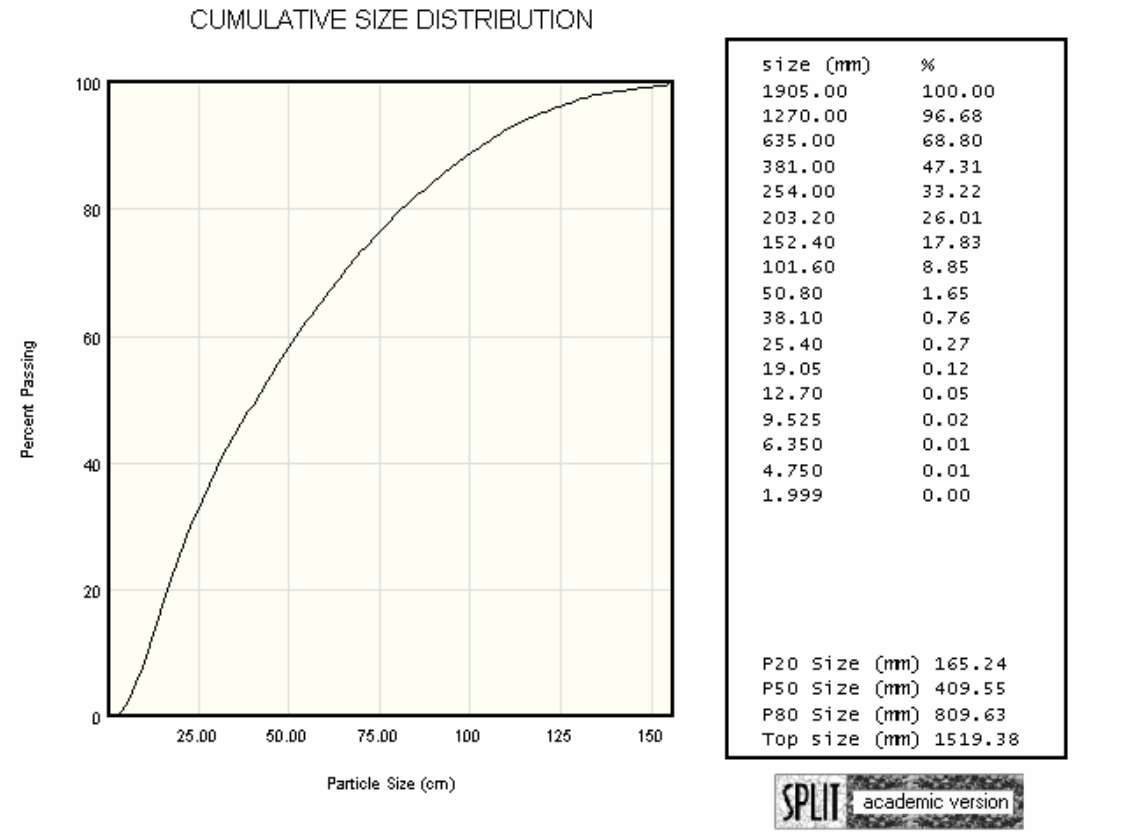


**Figure A.3 Bosung1, the size distribution of the bench face**

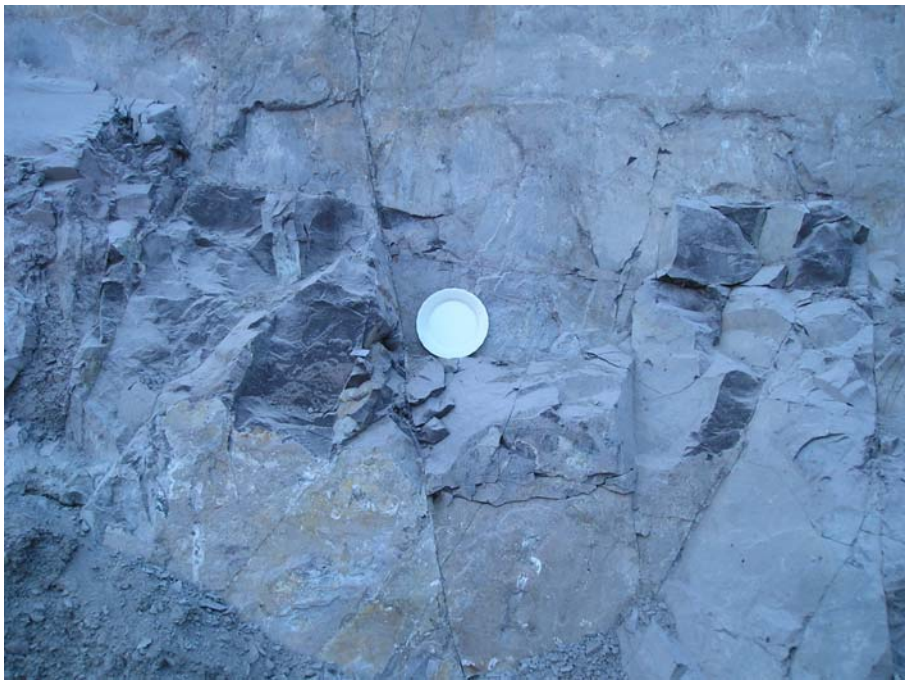

**Figure A.4 Bosung2, the bench face image**

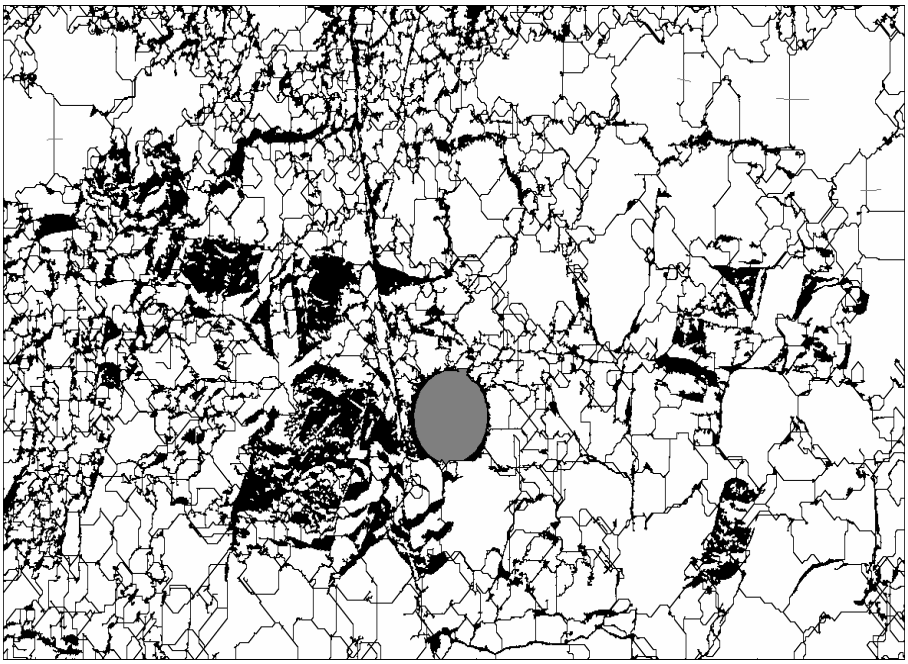

**Figure A.5 Bosung2, the analyzed image**

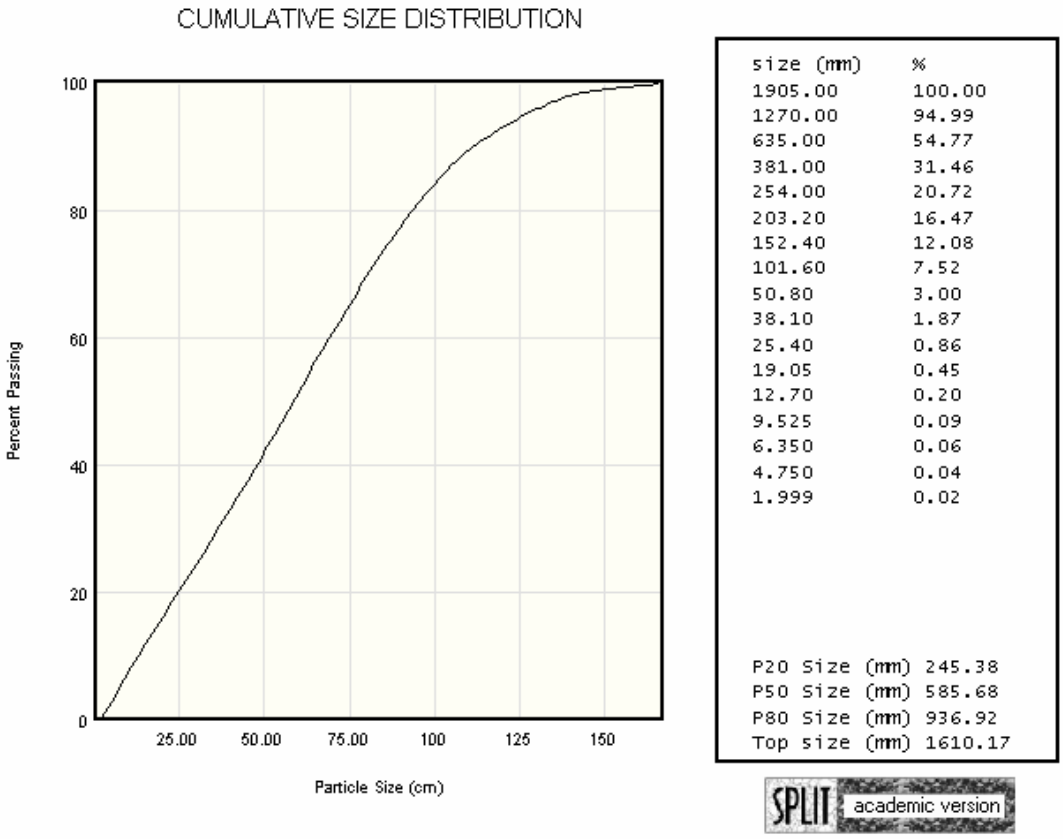


**Figure A.6 Bosung2, the size distribution of the bench face**

**Figure A.7 Bosung3, the bench face image**

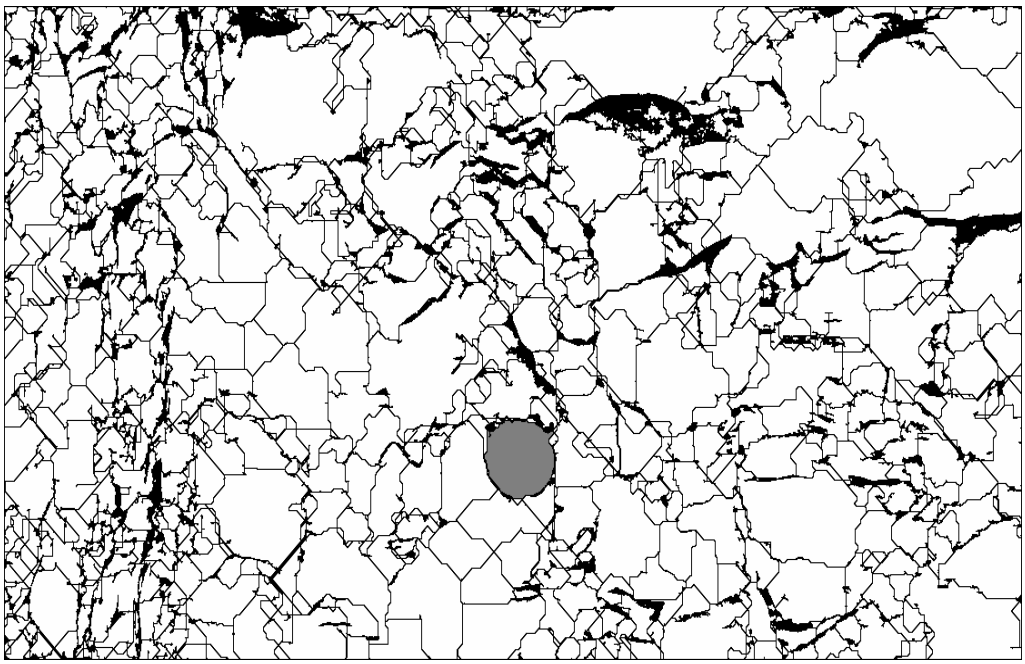

**Figure A.8 Bosung3, the analyzed image**

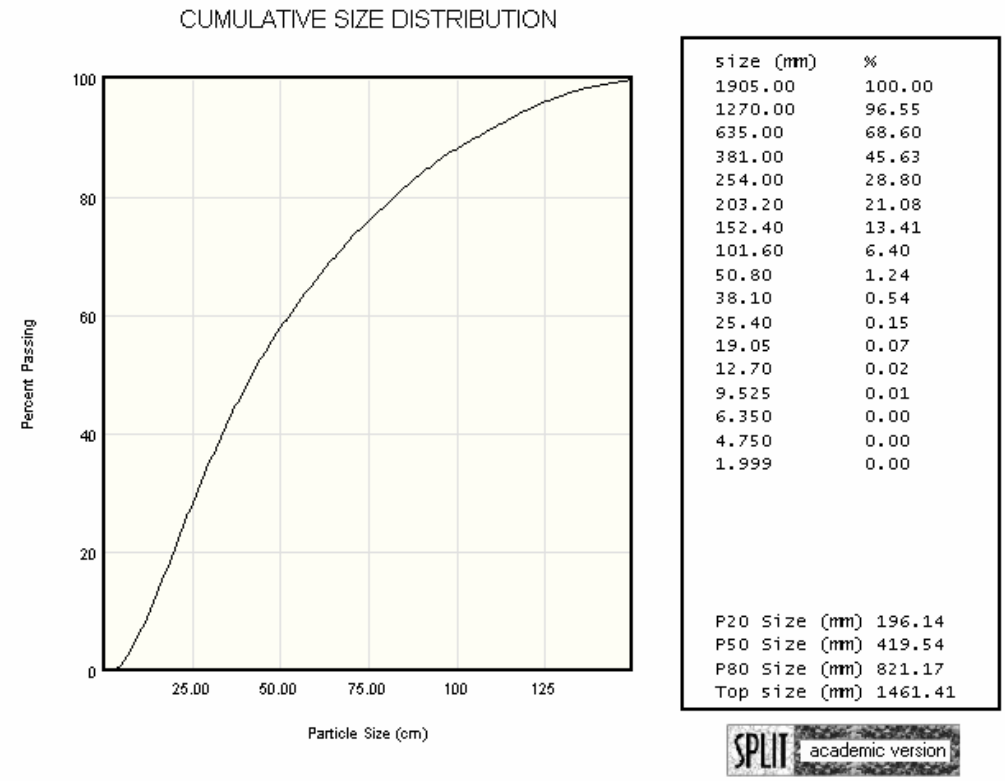


**Figure A.9 Bosung3, the size distribution of the bench face**

**Figure A.10 Bosung4, the bench face image**

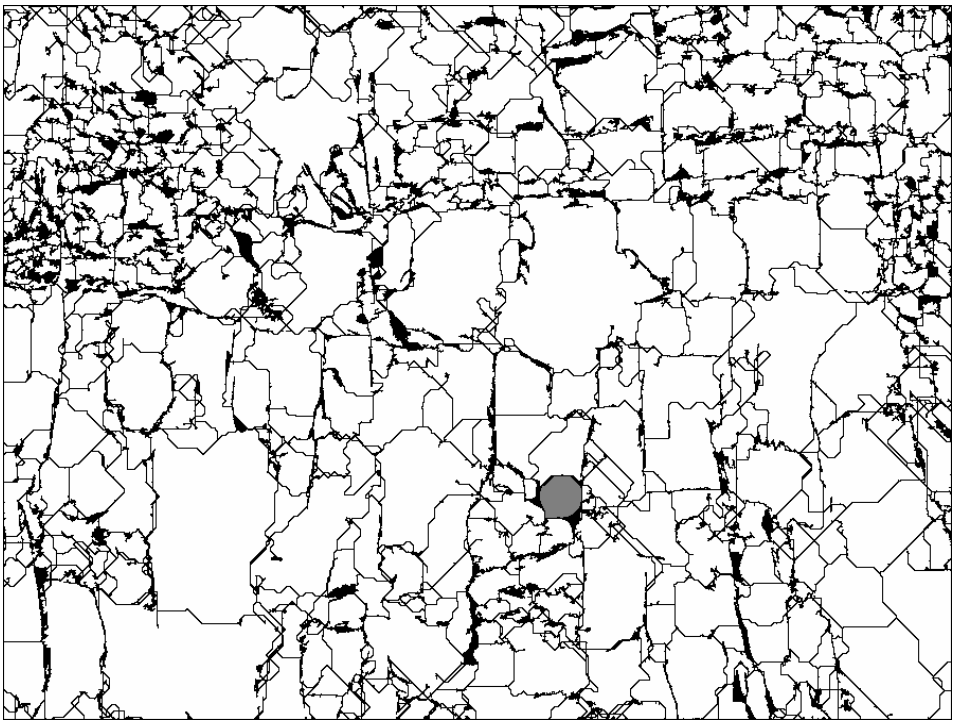

**Figure A.11 Bosung4, the analyzed image**

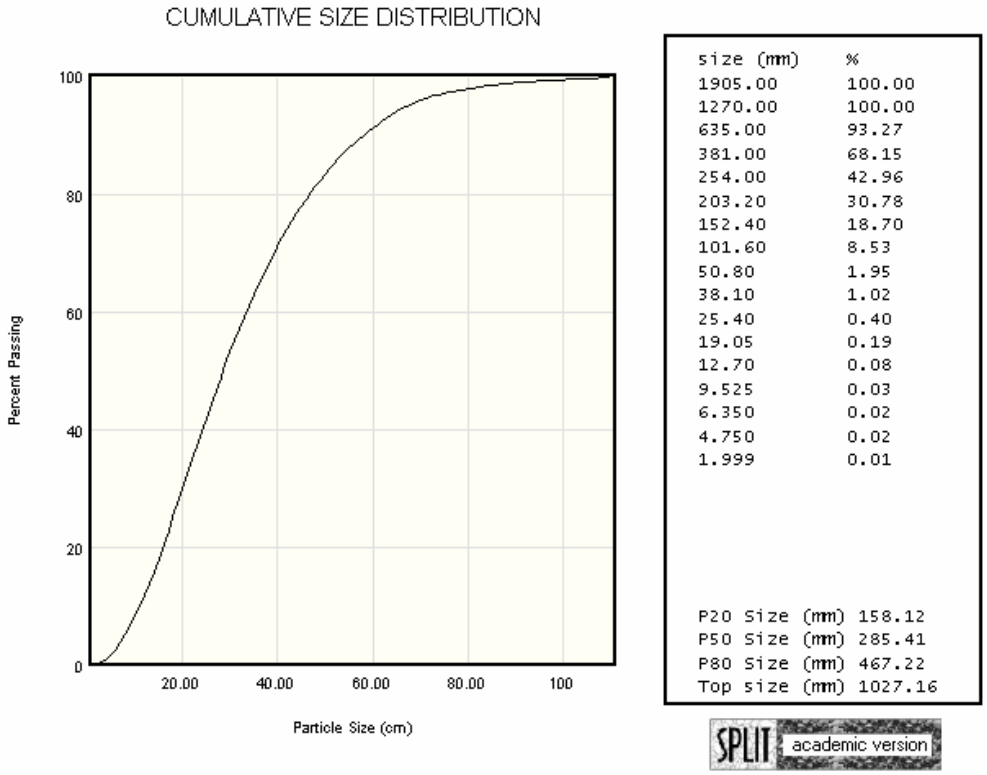


**Figure A.12 Bosung4, the size distribution of the bench face**

**Figure A.13 Bosung5, the bench face image**

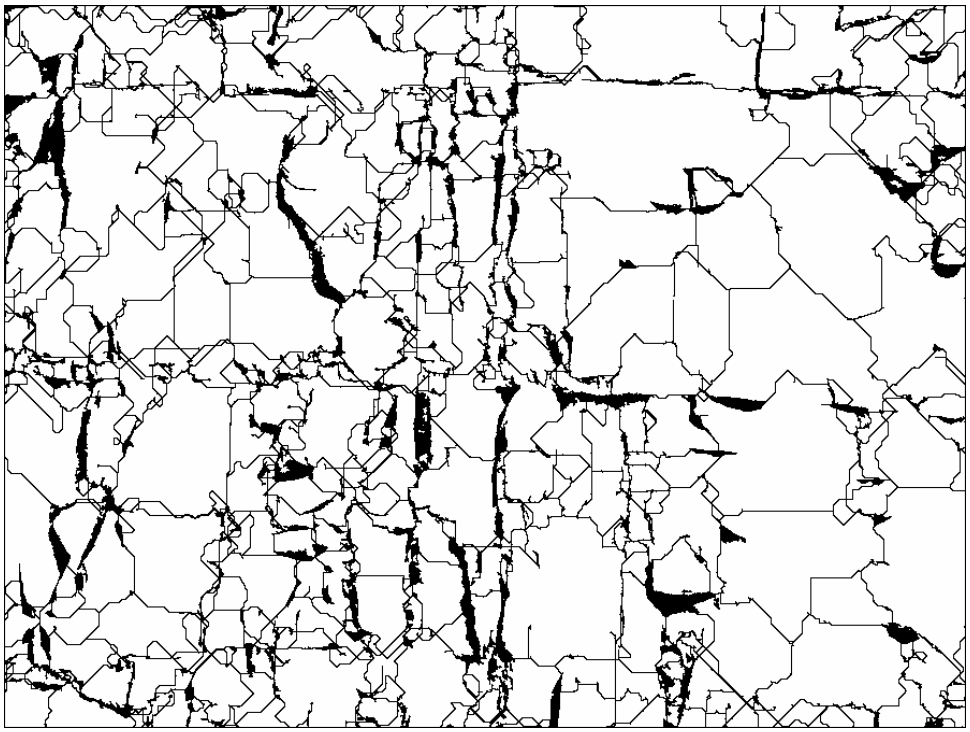

**Figure A.14 Bosung5, the analyzed image**

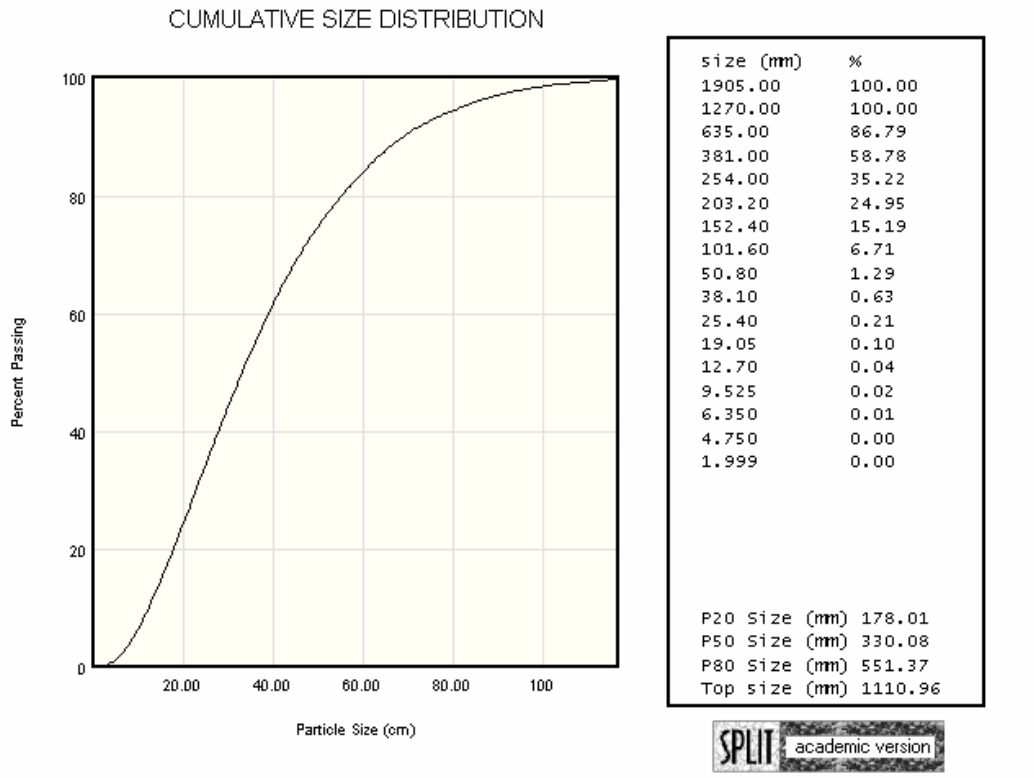


**Figure A.15 Bosung5, the size distribution of the bench face**

**Figure A.16 Pittsboro, the bench face image**

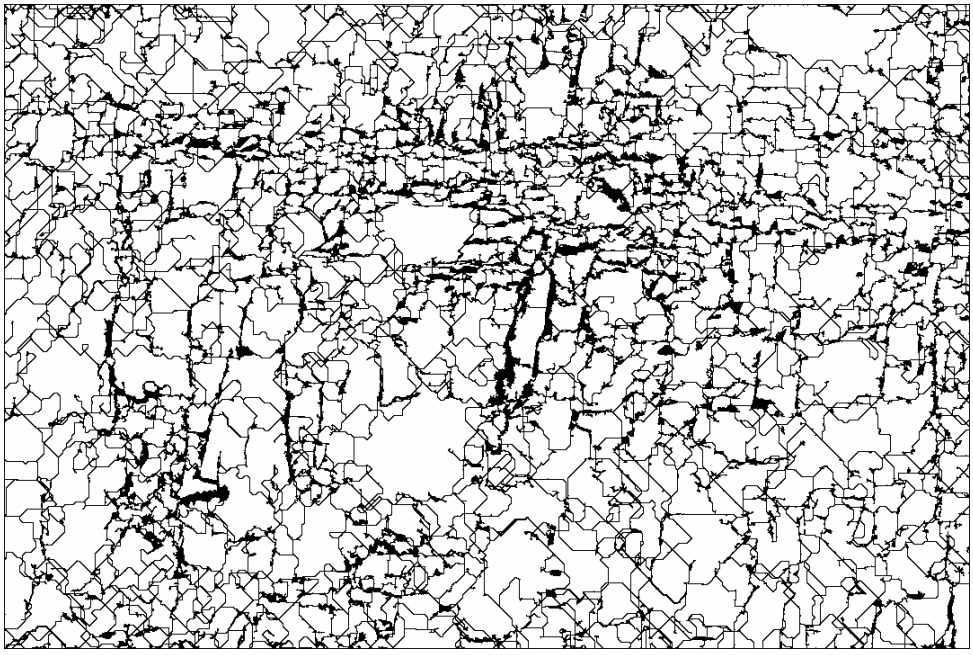

**Figure A.17 Pittsboro, the analyzed image**

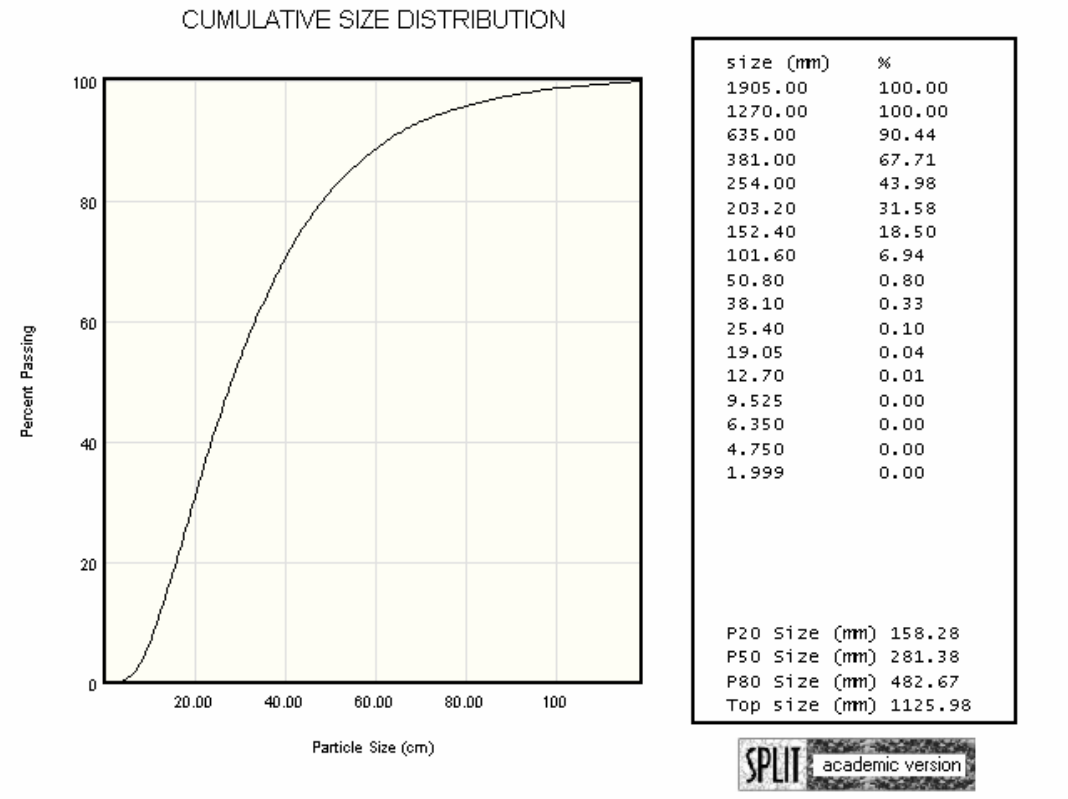


**Figure A.18 Pittsboro, the size distribution of the bench face**

**Figure A.19 Boxley, the bench face image**

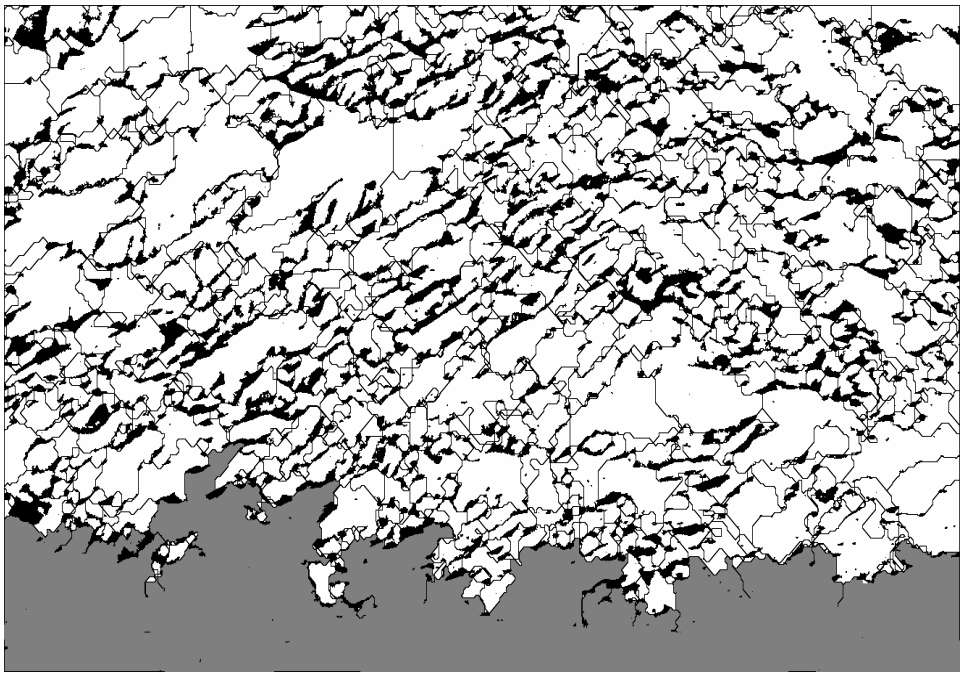

**Figure A.20 Boxley, the analyzed image**

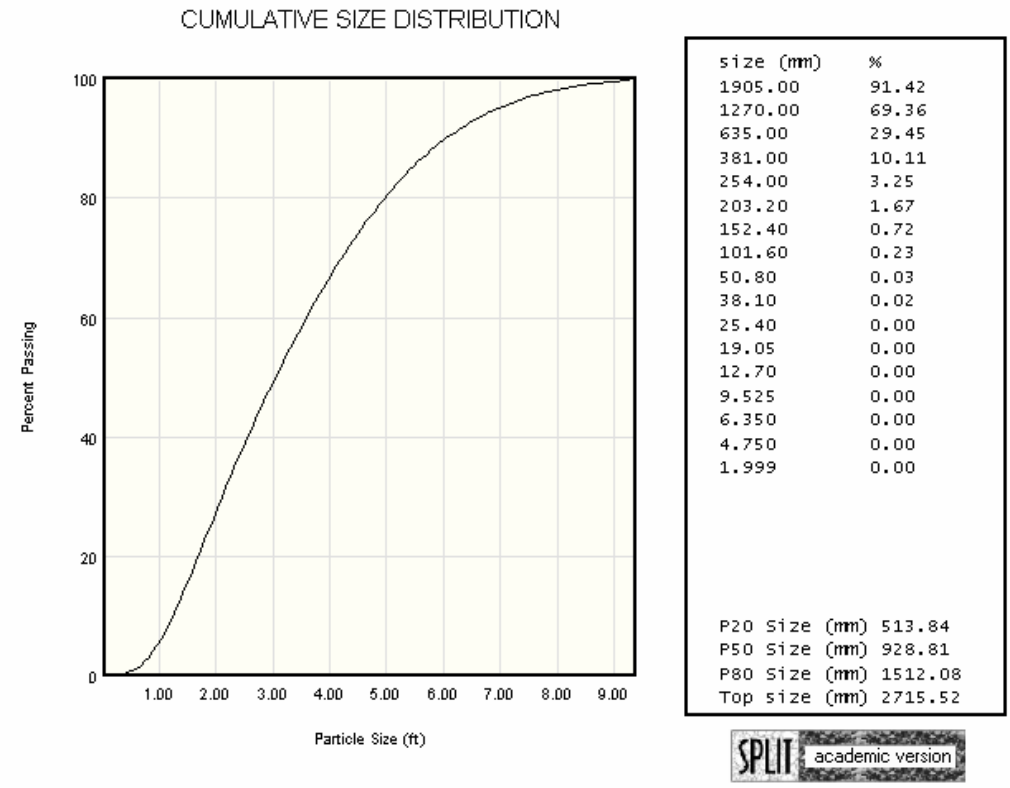


**Figure A.21 Boxley, the size distribution of the bench face**

**Figure A.22 Sanyang1, the bench face image**

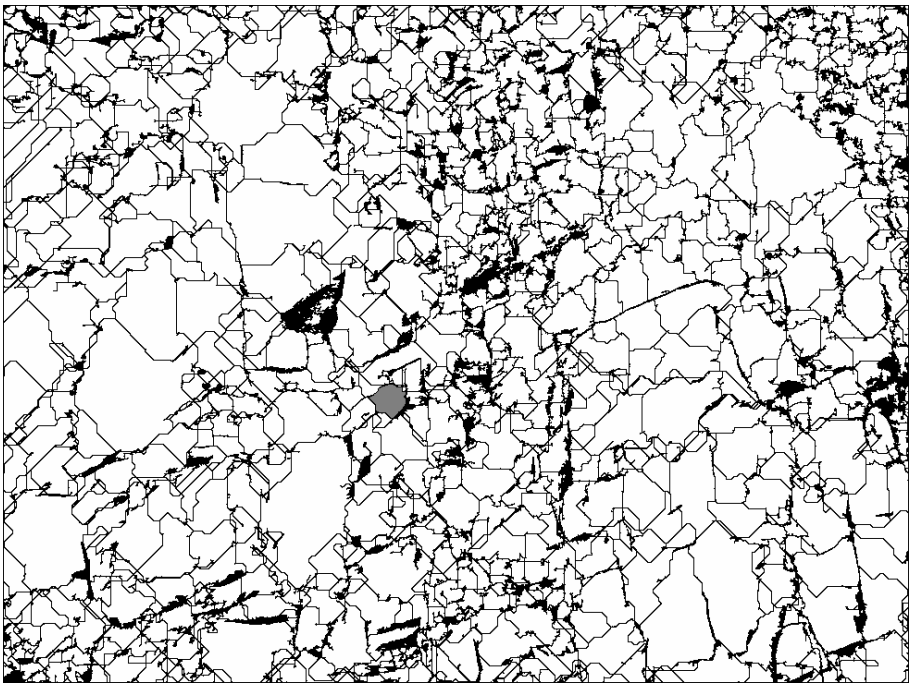

**Figure A.23 Sanyang1, the analyzed image**

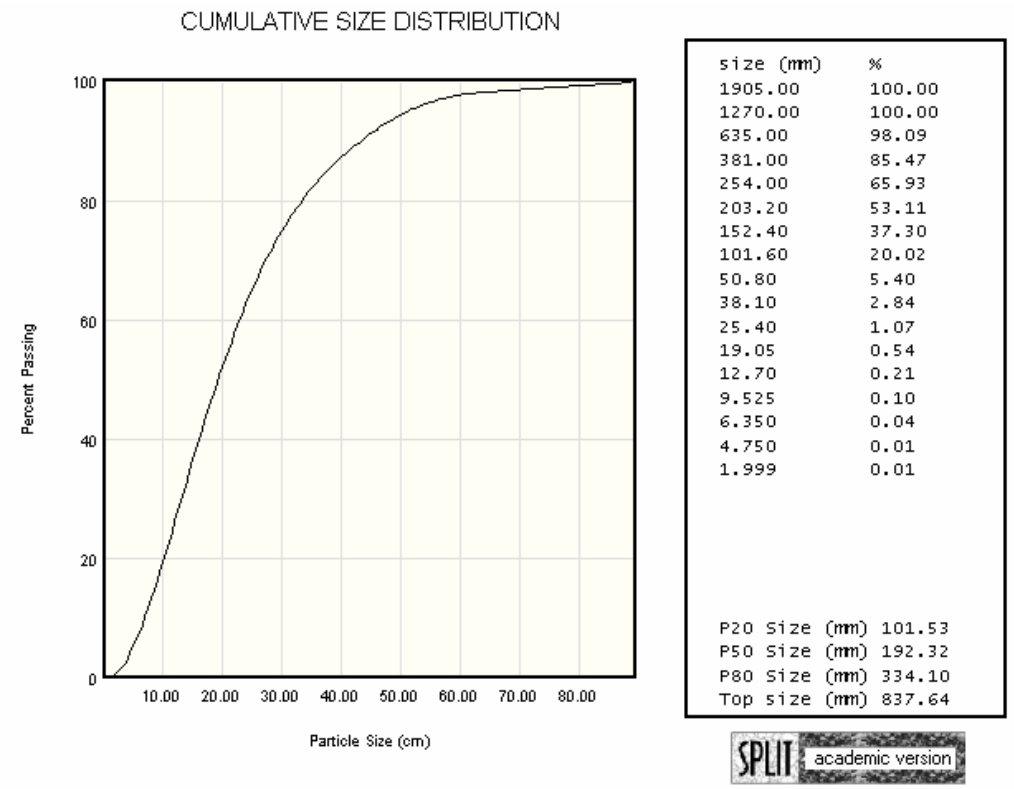


**Figure A.24 Sanyang1, the size distribution of the bench face**

**Figure A.25 Sanyang2, the bench face image**

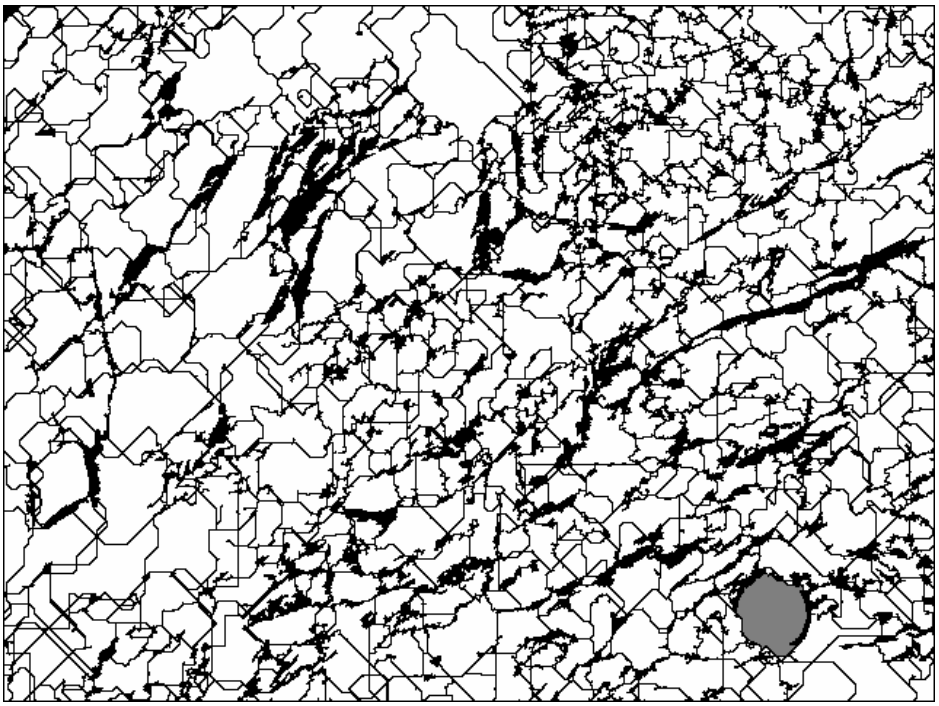

**Figure A.26 Sanyang2, the analyzed image**

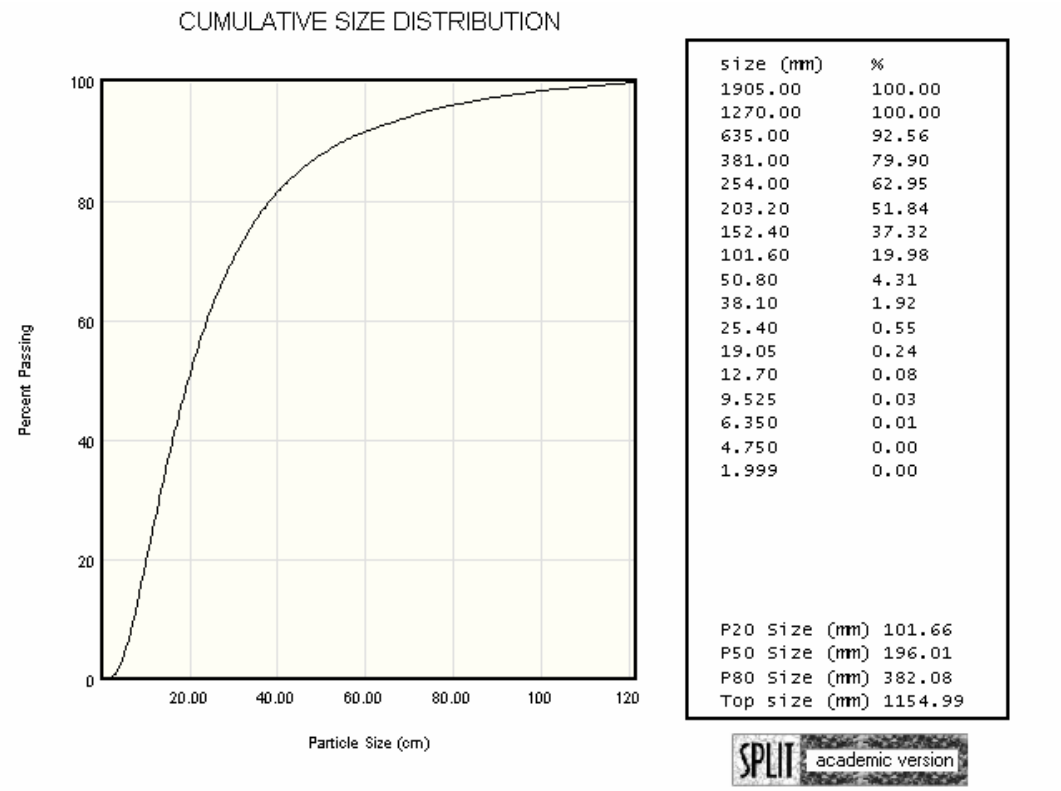


**Figure A.27 Sanyang2, the size distribution of the bench face**

**Figure A.28 Sanyang3, the bench face image**

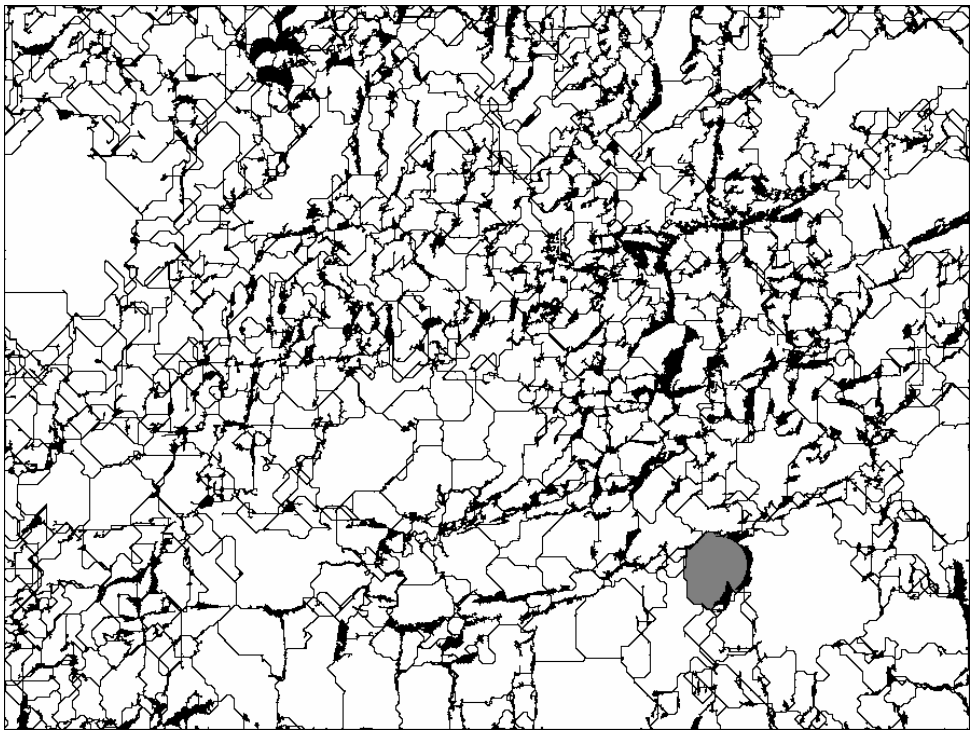

**Figure A.29 Sanyang3, the analyzed image**

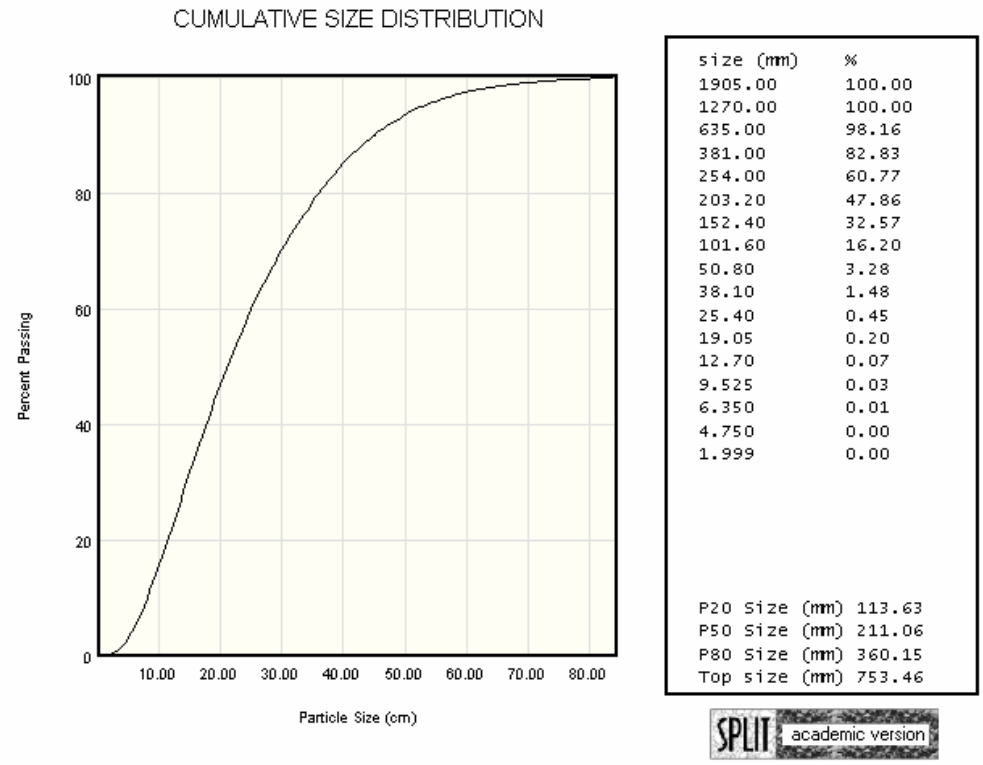


**Figure A.30 Sanyang3, the size distribution of the bench face**

**Figure A.31 Sanyang4, the bench face image**

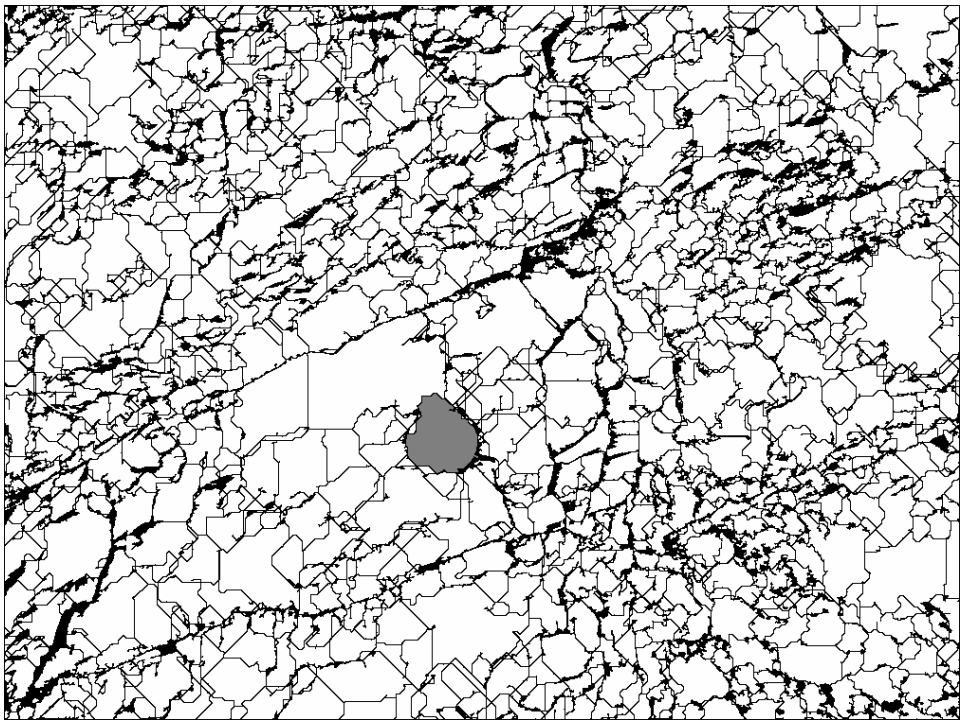

**Figure A.32 Sanyang4, the analyzed image**

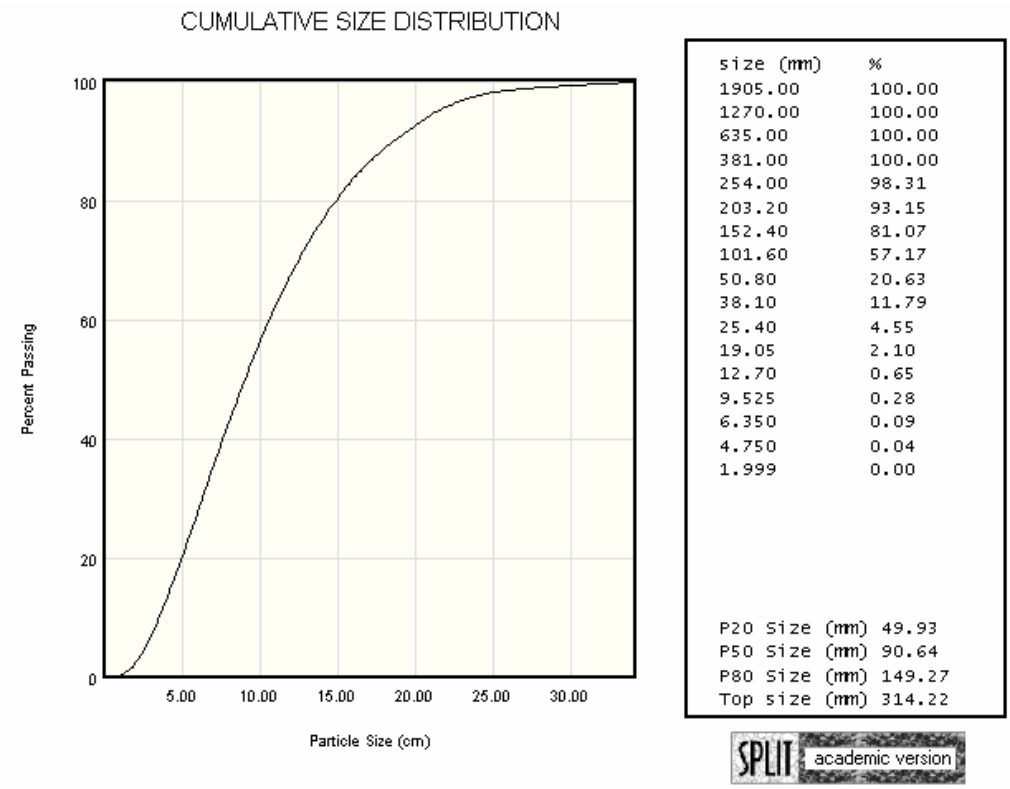


**Figure A.33 Sanyang4, the size distribution of the bench face**

**Figure A.34 Sanyang5, the bench face image**

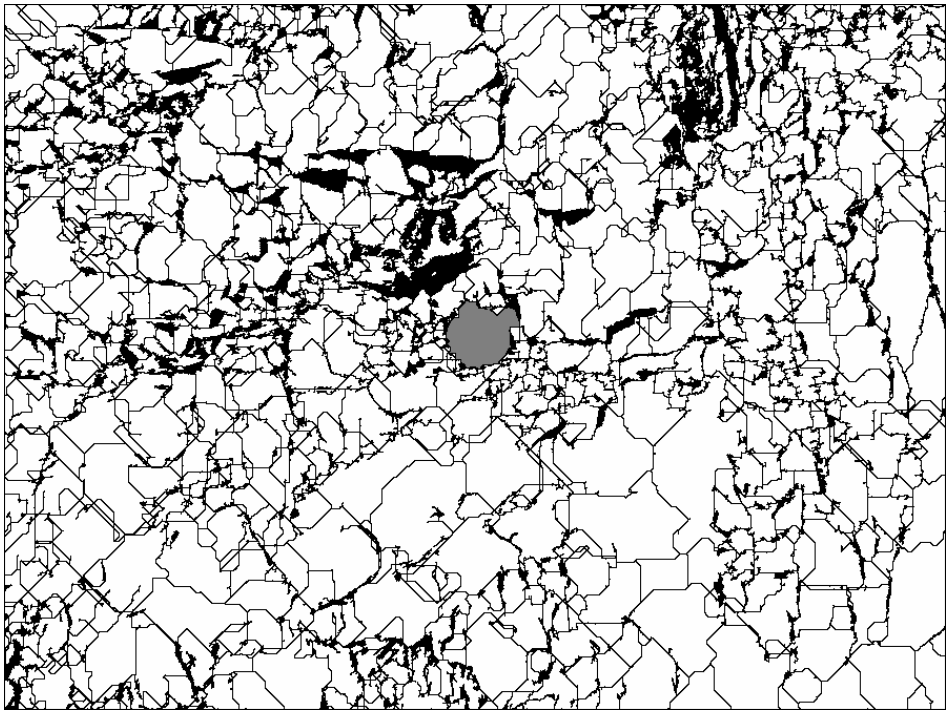

**Figure A.35 Sanyang5, the analyzed image**

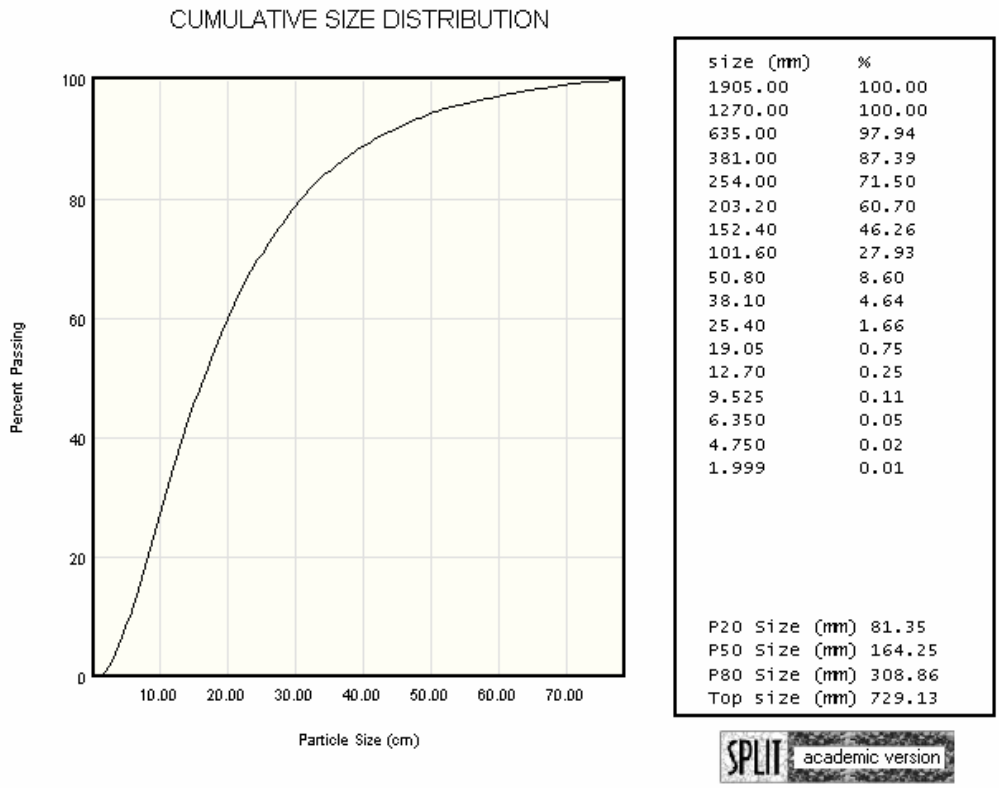


**Figure A.36 Sanyang5, the size distribution of the bench face**

# APPENDIX B -

## Image Analysis of the Muckpile

**Figure B.1 Bosung1, the muckpile image**

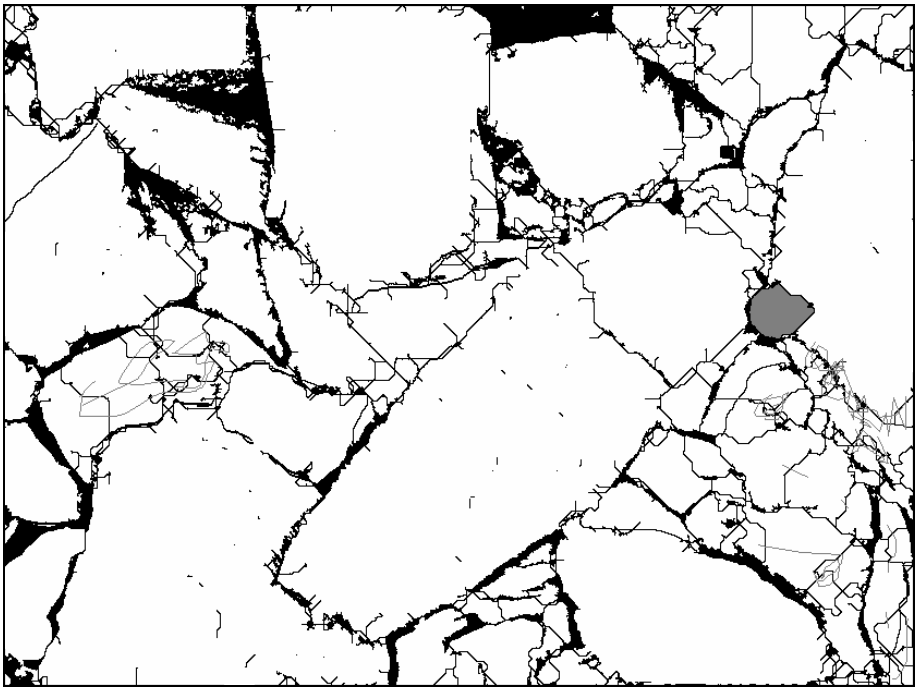

**Figure B.2 Bosung1, the analyzed image**

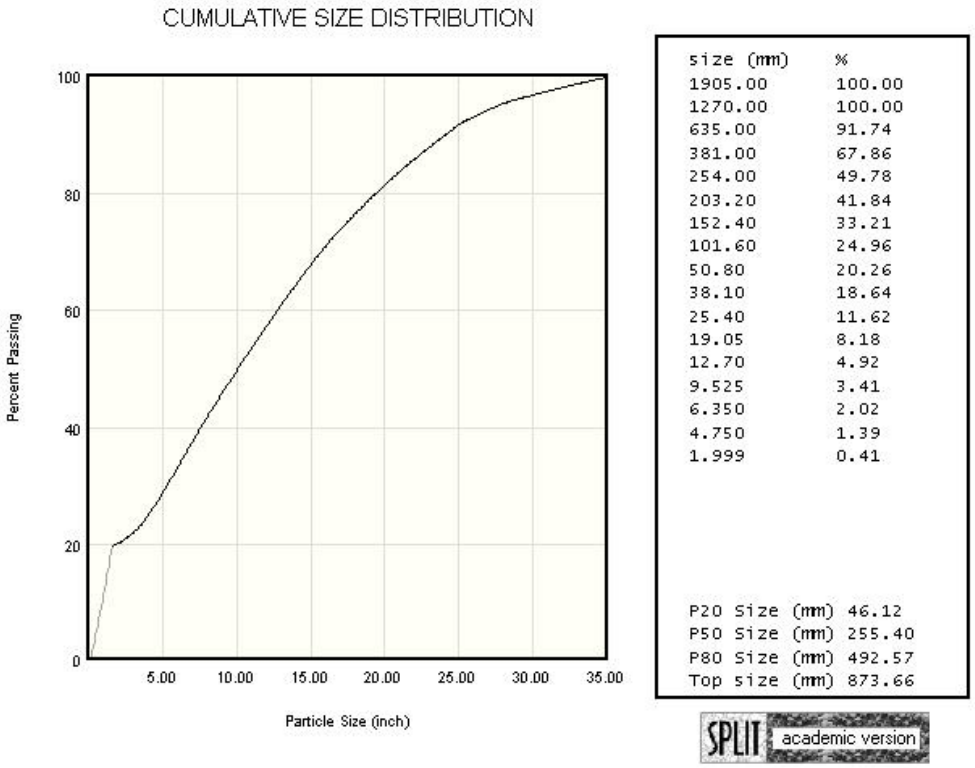


**Figure B.3 Bosung1, the size distribution of the muckpile**

**Figure B.4 Bosung2, the muckpile image**

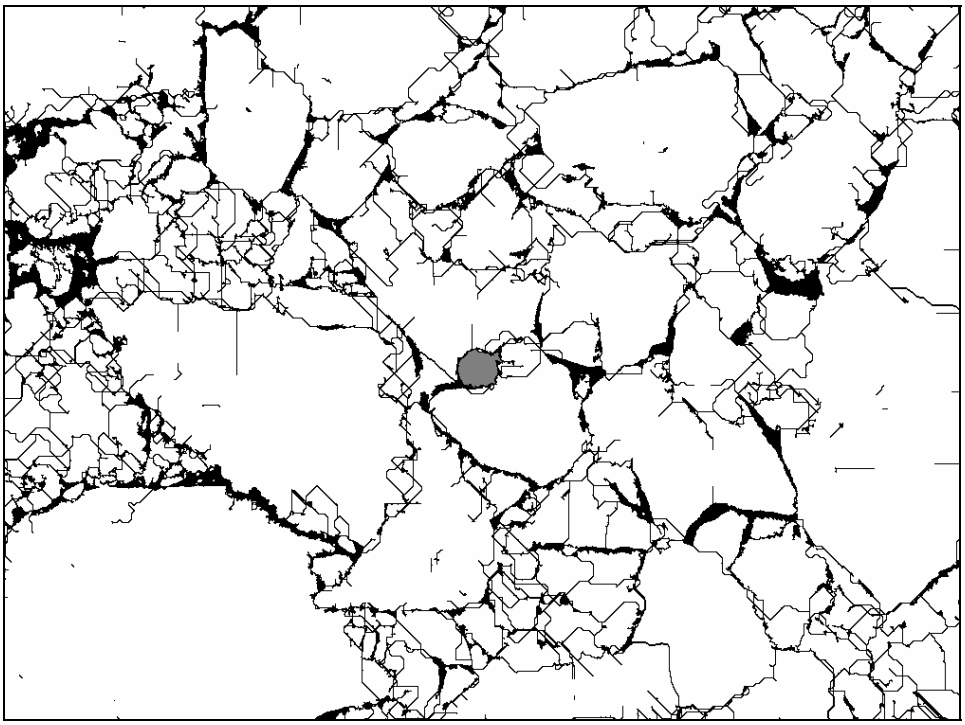

**Figure B.5 Bosung2, the analyzed image**

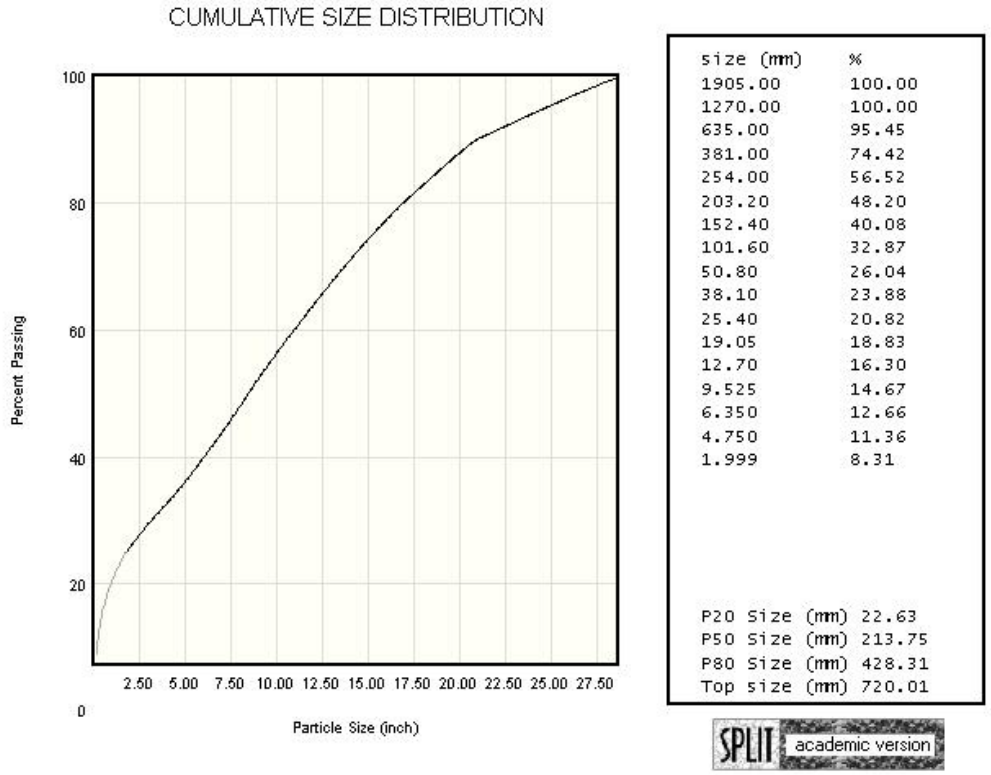


**Figure B.6 Bosung2, the size distribution of the muckpile**

**Figure B.7 Bosung3, the muckpile image**

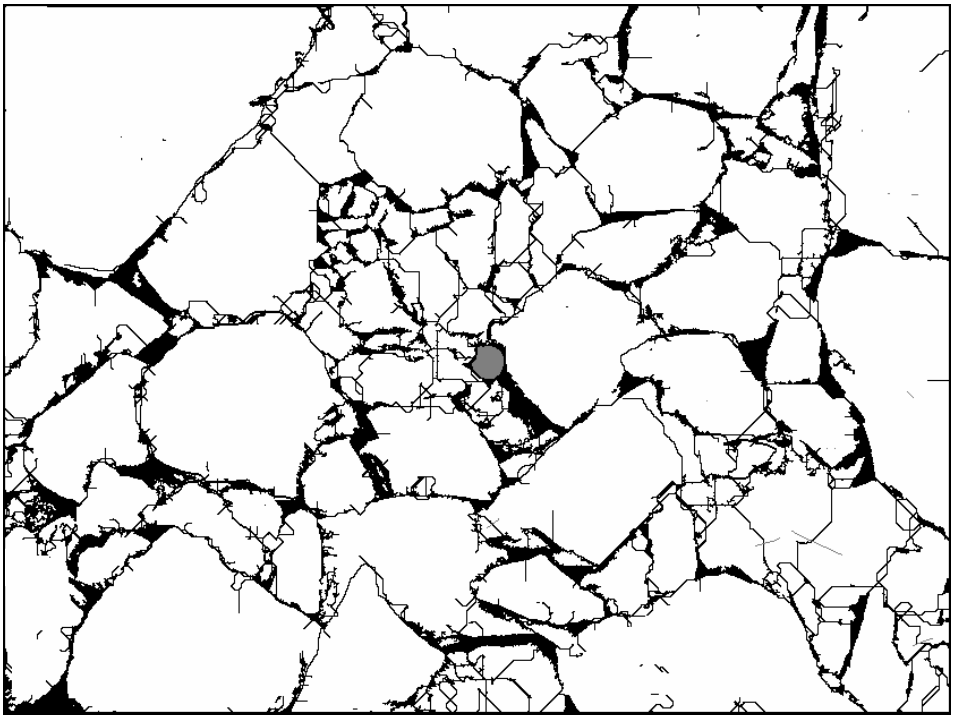

**Figure B.8 Bosung3, the analyzed image**

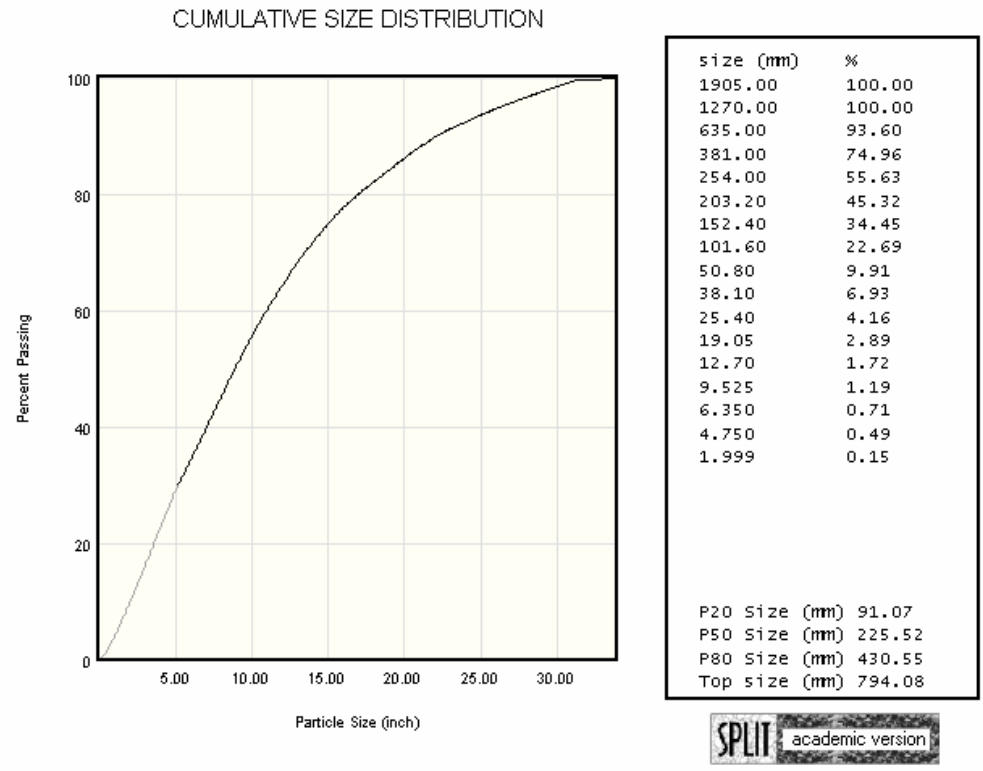


**Figure B.9 Bosung3, the size distribution of the muckpile**

**Figure B.10 Bosung4, the muckpile image**

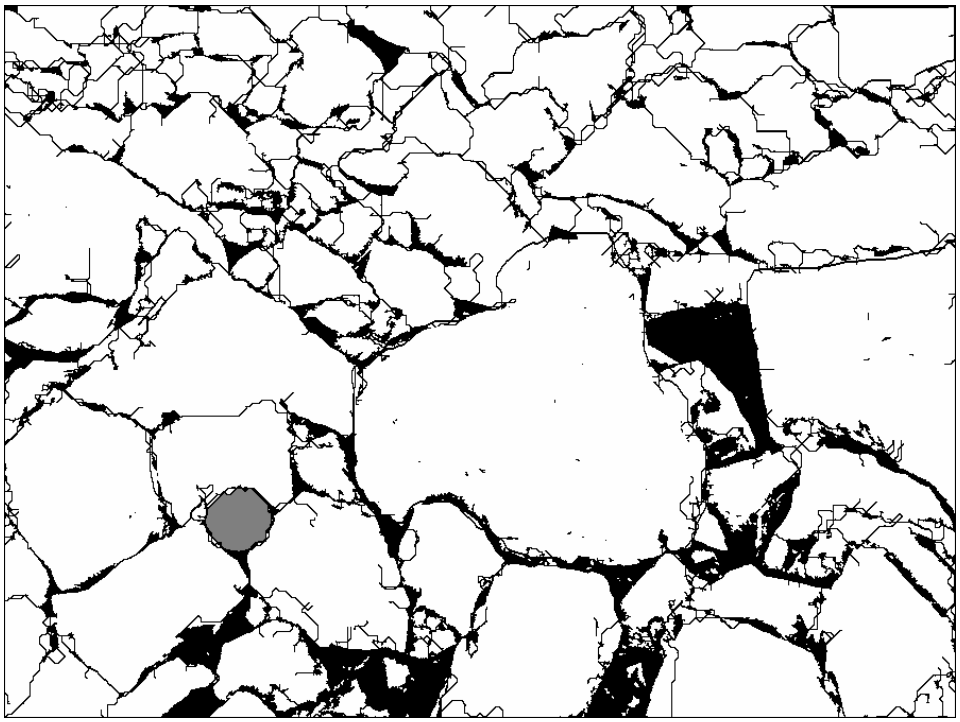

**Figure B.11 Bosung4, the analyzed image**

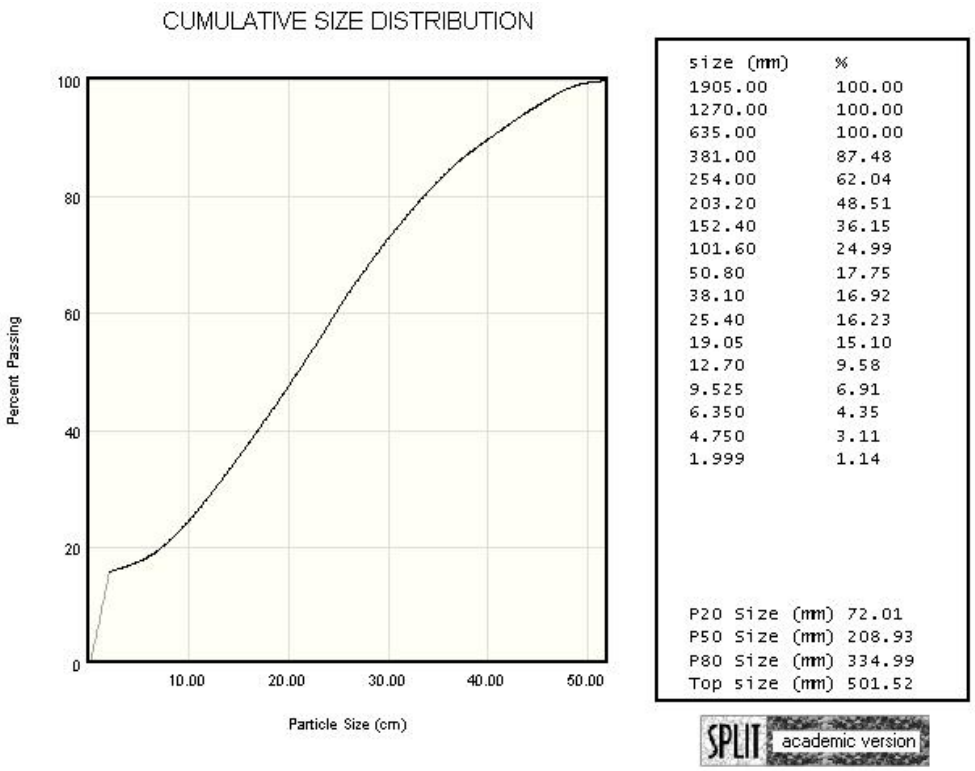


**Figure B.12 Bosung4, the size distribution of the muckpile**

**Figure B.13 Bosung5, the muckpile image**

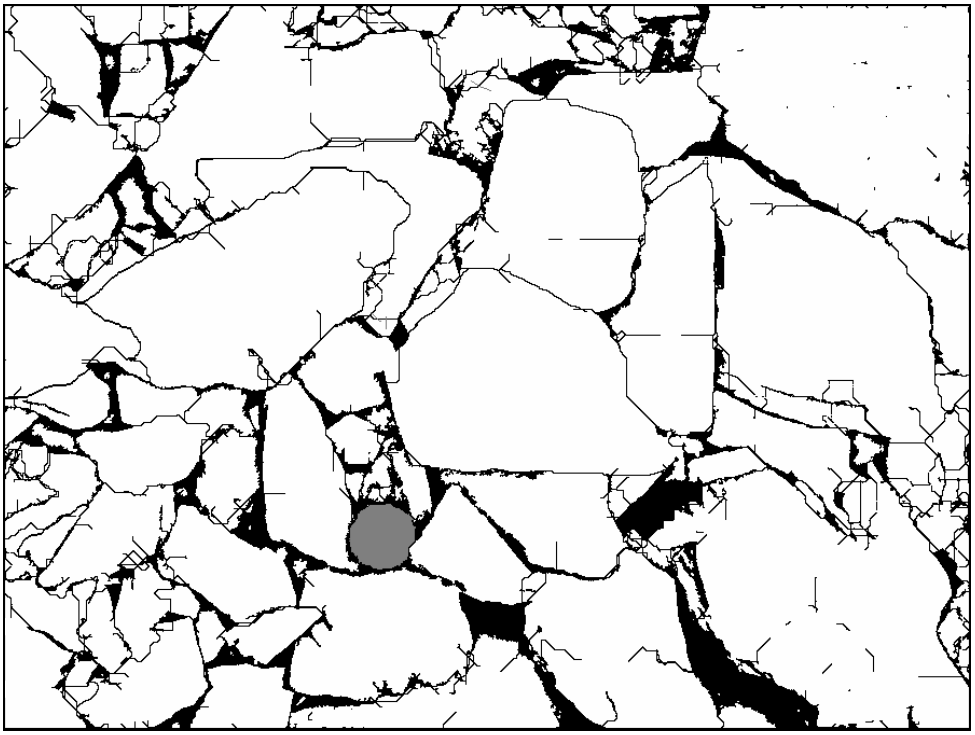

**Figure B.14 Bosung5, the analyzed image**

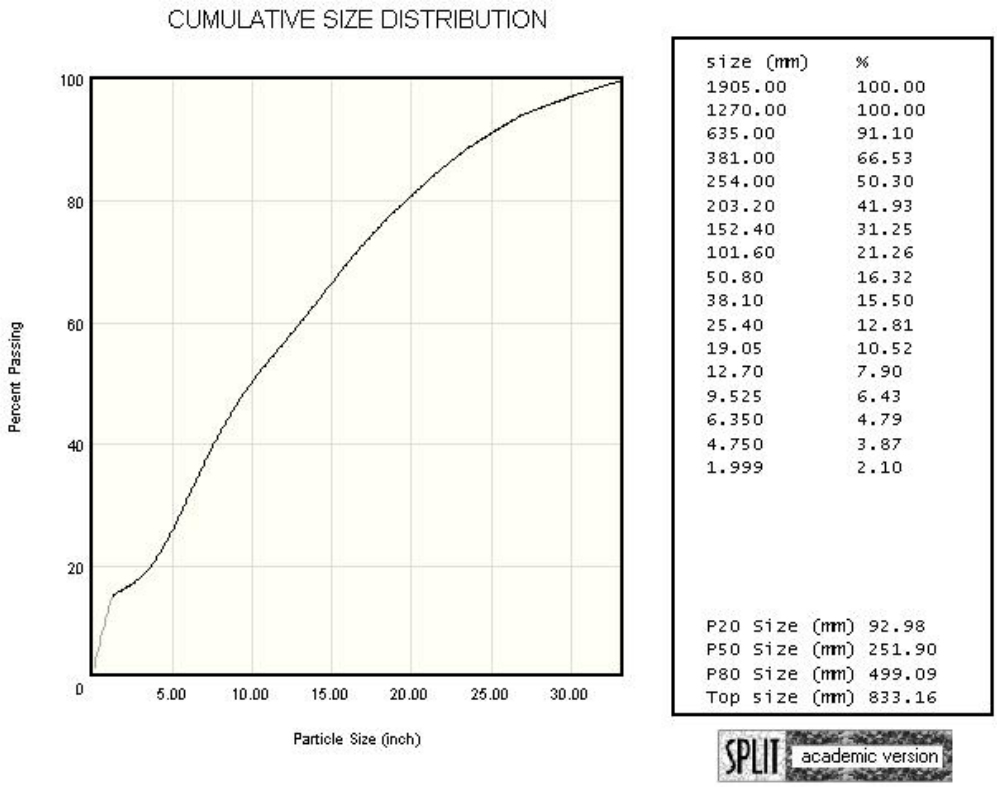


**Figure B.15 Bosung5, the size distribution of the muckpile**

**Figure B.16 Pittsboro, the muckpile image**

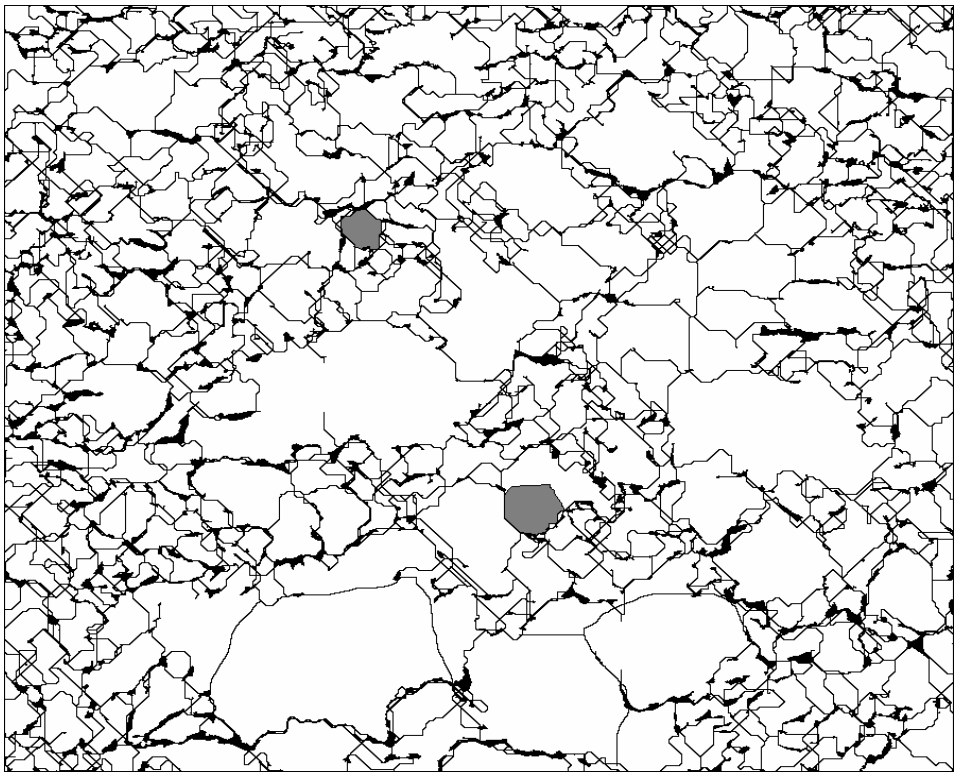

**Figure B.17 Pittsboro, the analyzed image**

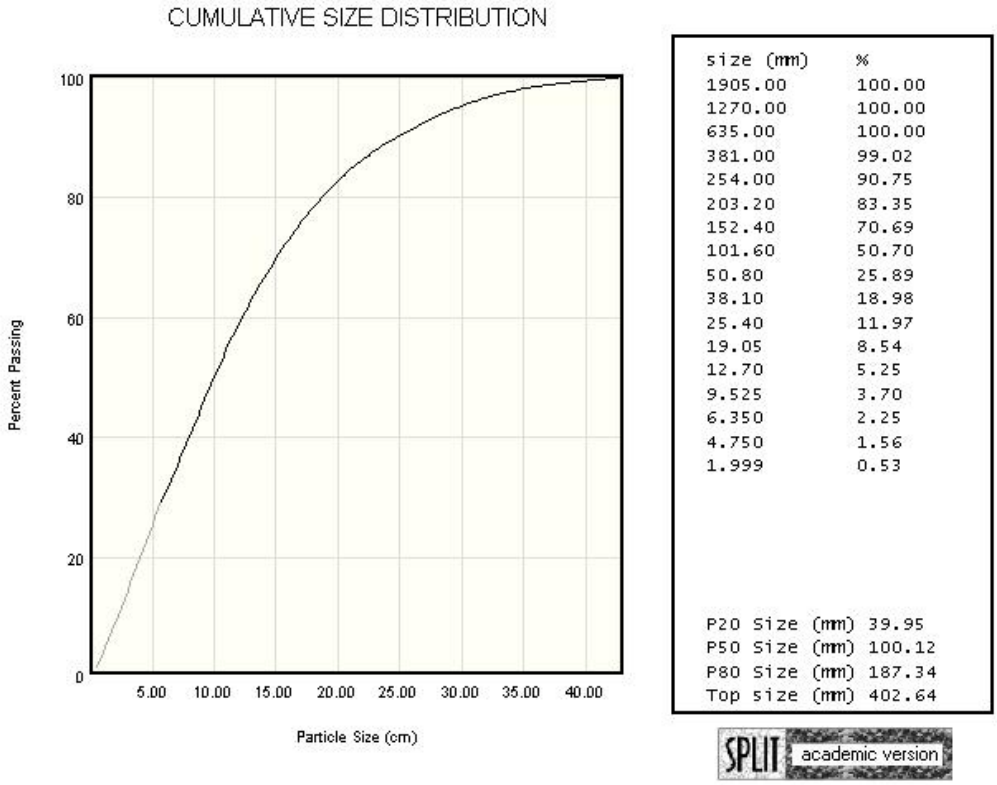


**Figure B.18 Pittsboro, the size distribution of the muckpile**

**Figure B.19 Boxley, the muckpile image**

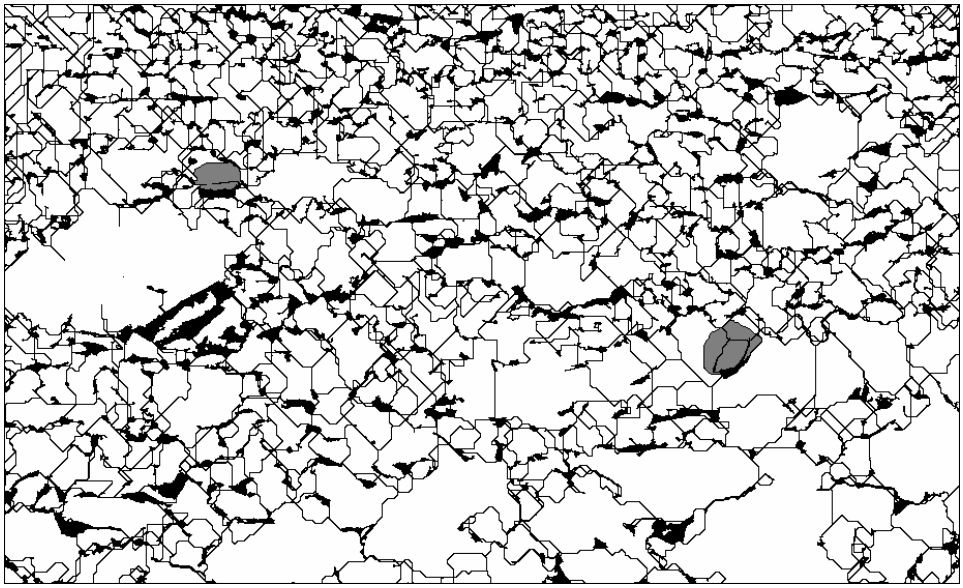

**Figure B.20 Boxley, the analyzed image**

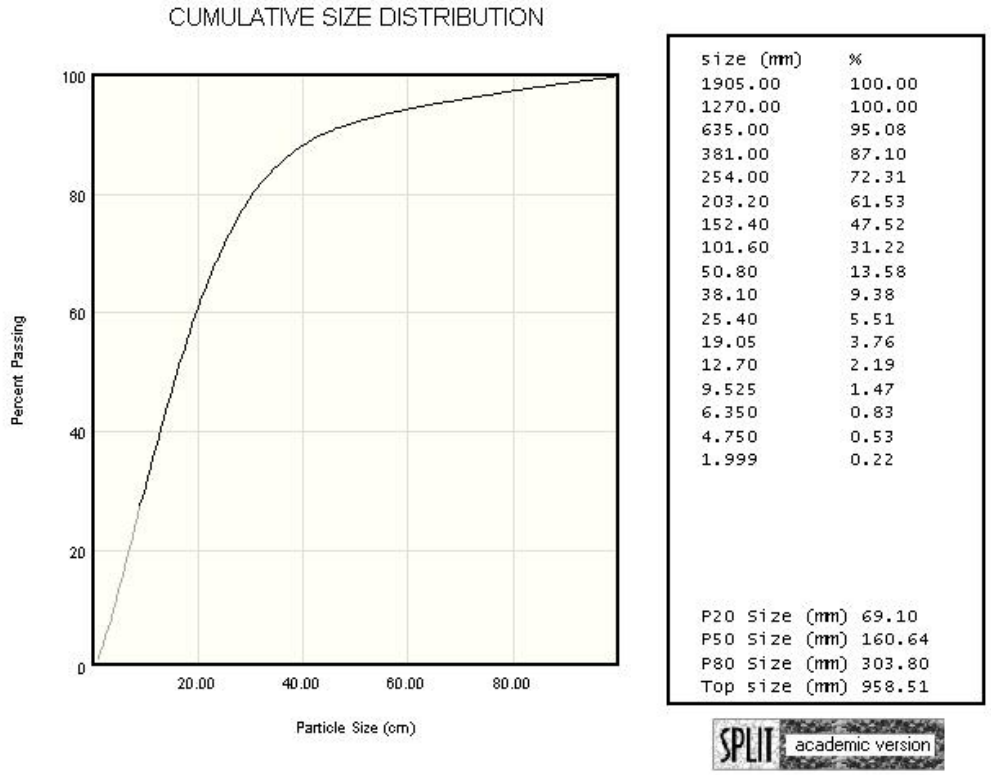


**Figure B.21 Boxley, the size distribution of the muckpile**

**Figure B.22 Sanyang1, the muckpile image**

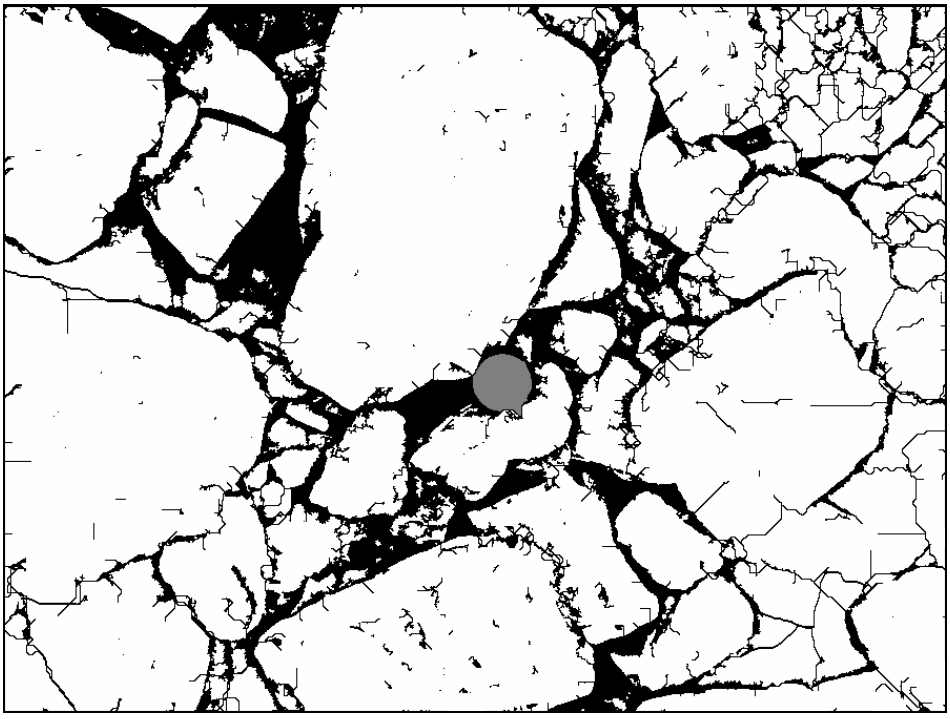

**Figure B.23 Sanyang1, the analyzed image**

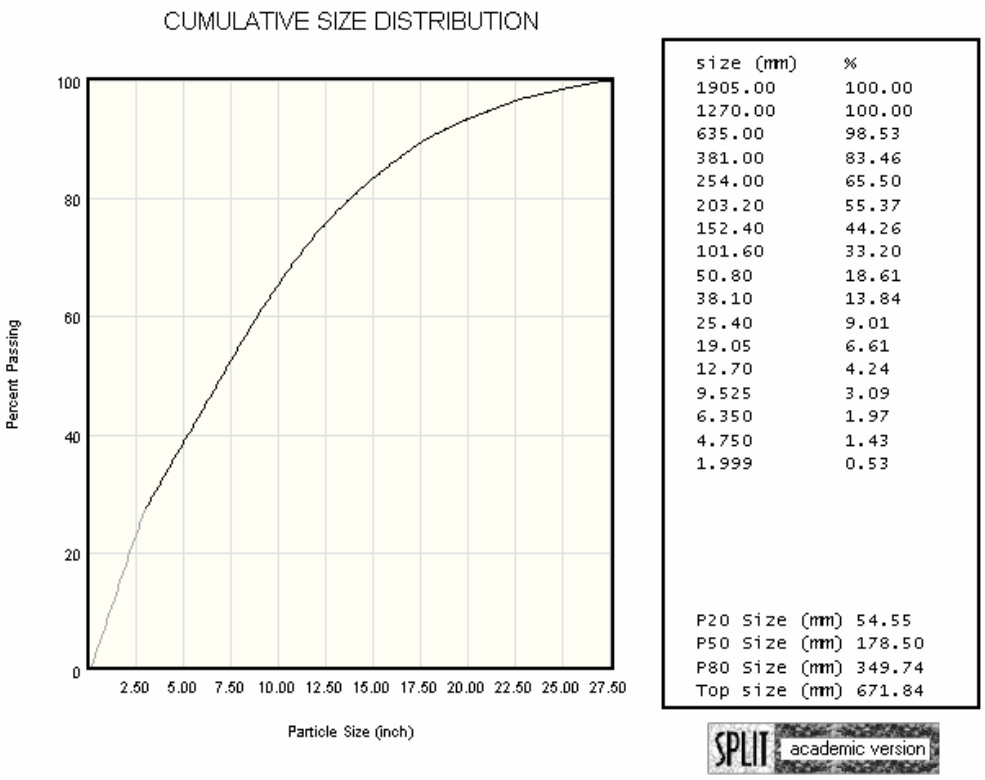


**Figure B.24 Sanyang1, the size distribution of the muckpile**

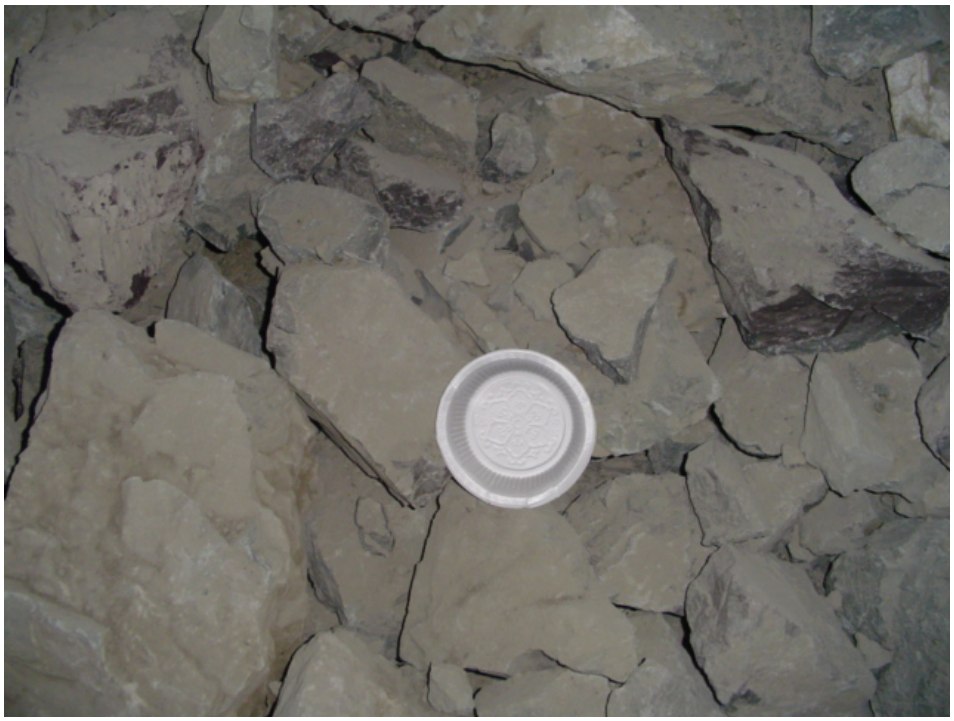

**Figure B.25 Sanyang2, the muckpile image**

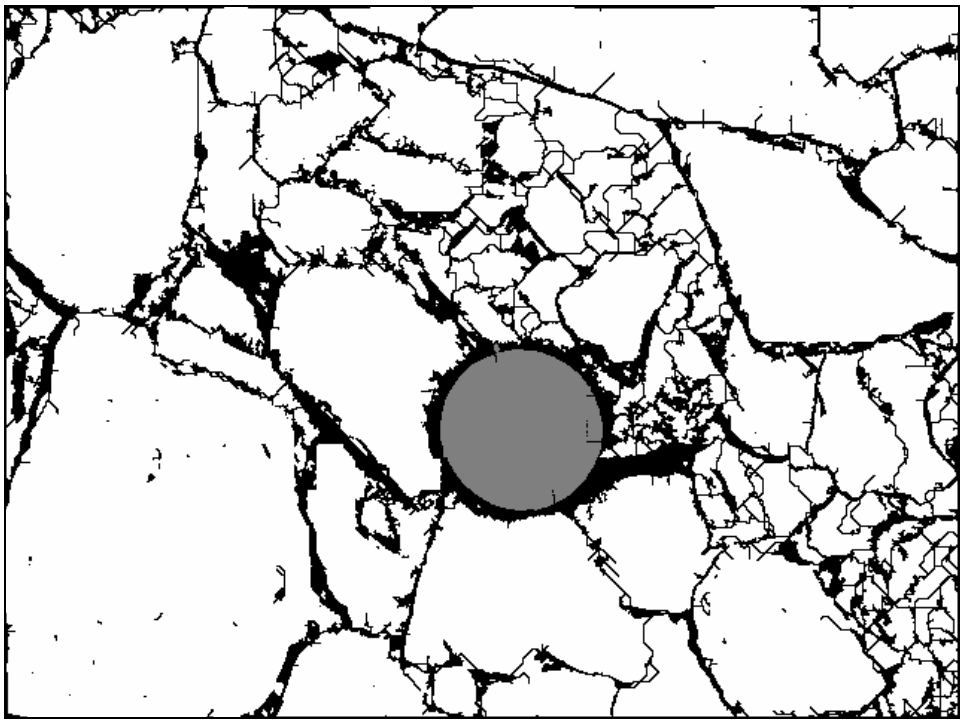

**Figure B.26 Sanyang2, the analyzed image**

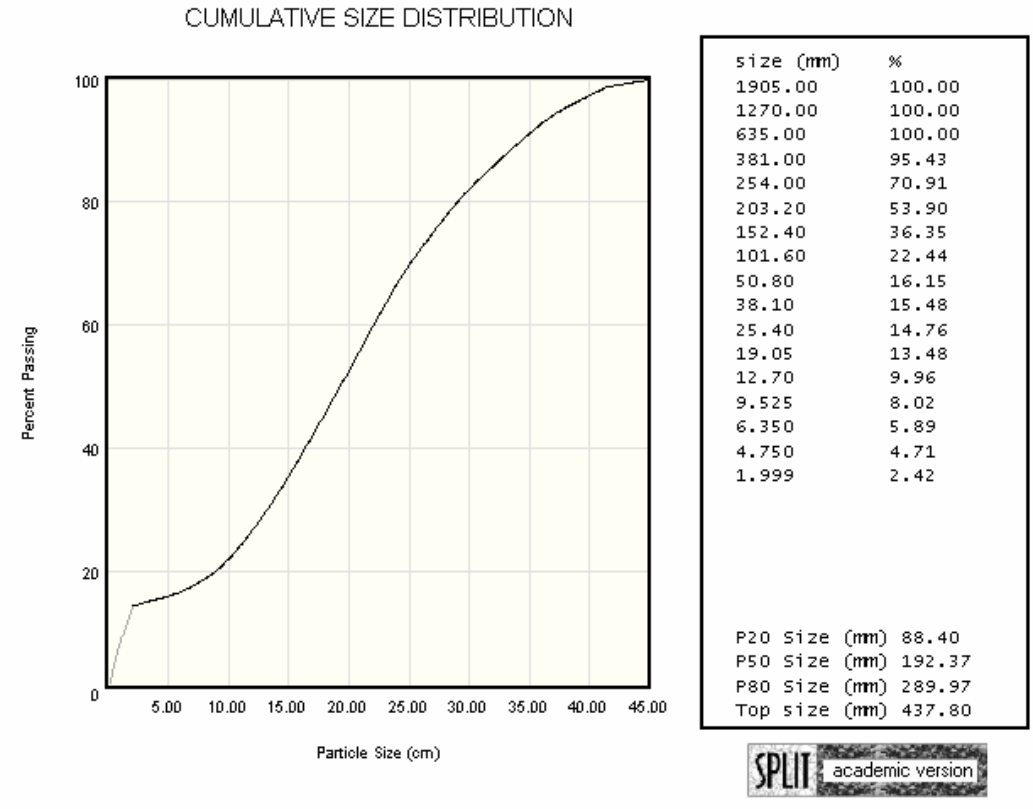


**Figure B.27 Sanyang2, the size distribution of the muckpile**

**Figure B.28 Sanyang3, the muckpile image**

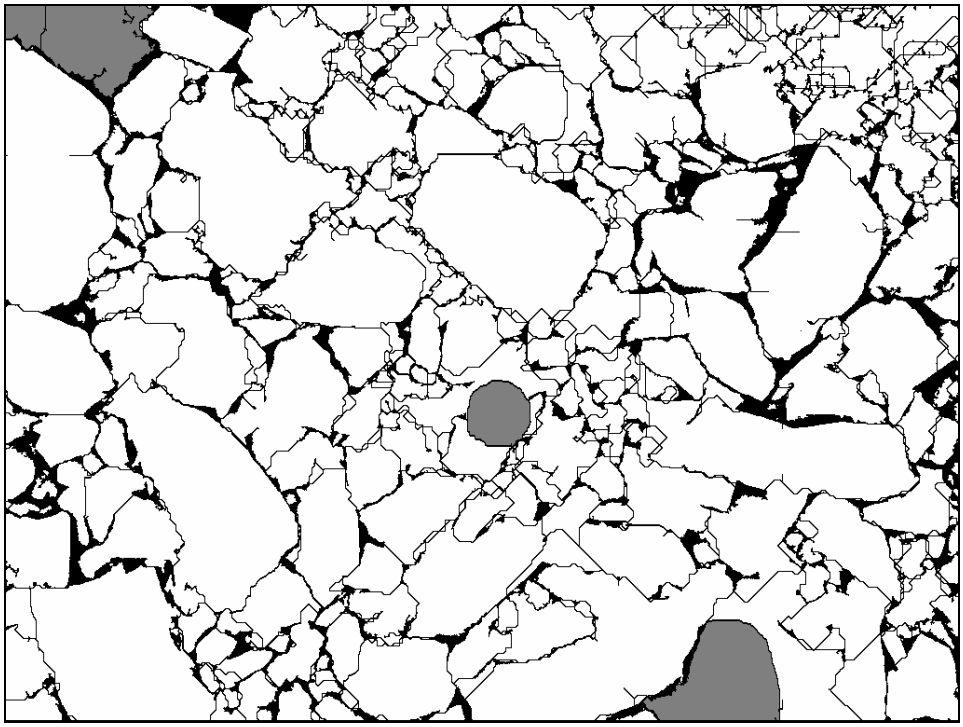

**Figure B.29 Sanyang3, the analyzed image**

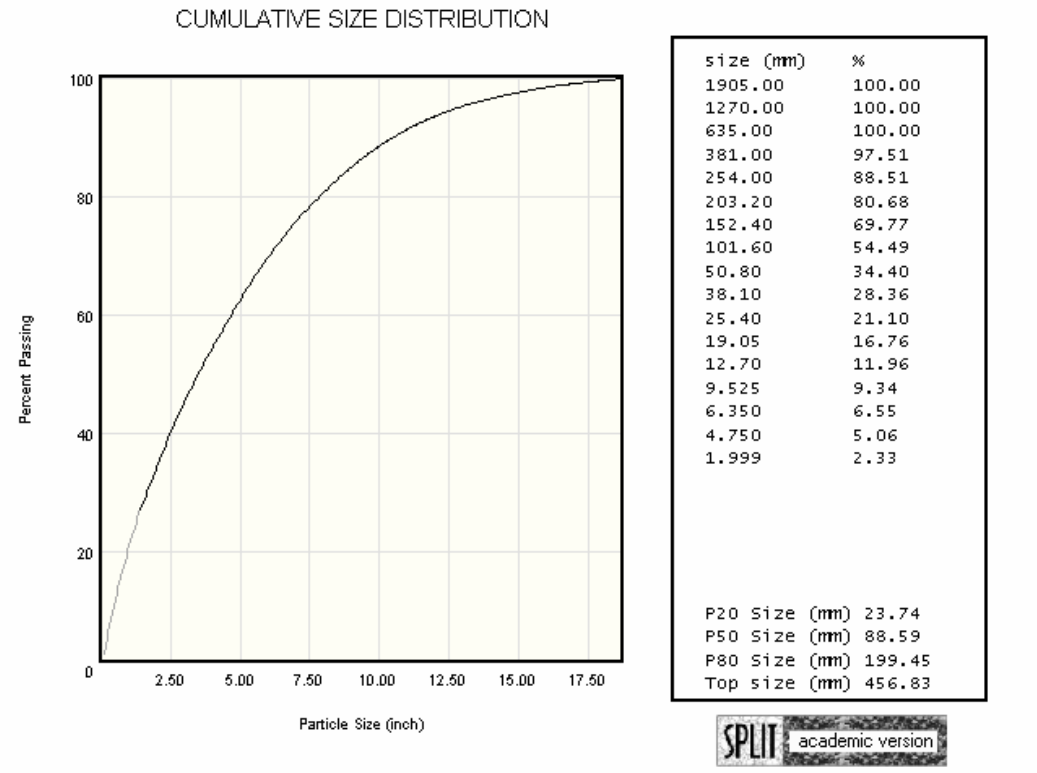


**Figure B.30 Sanyang3, the size distribution of the muckpile**

**Figure B.31 Sanyang4, the muckpile image**

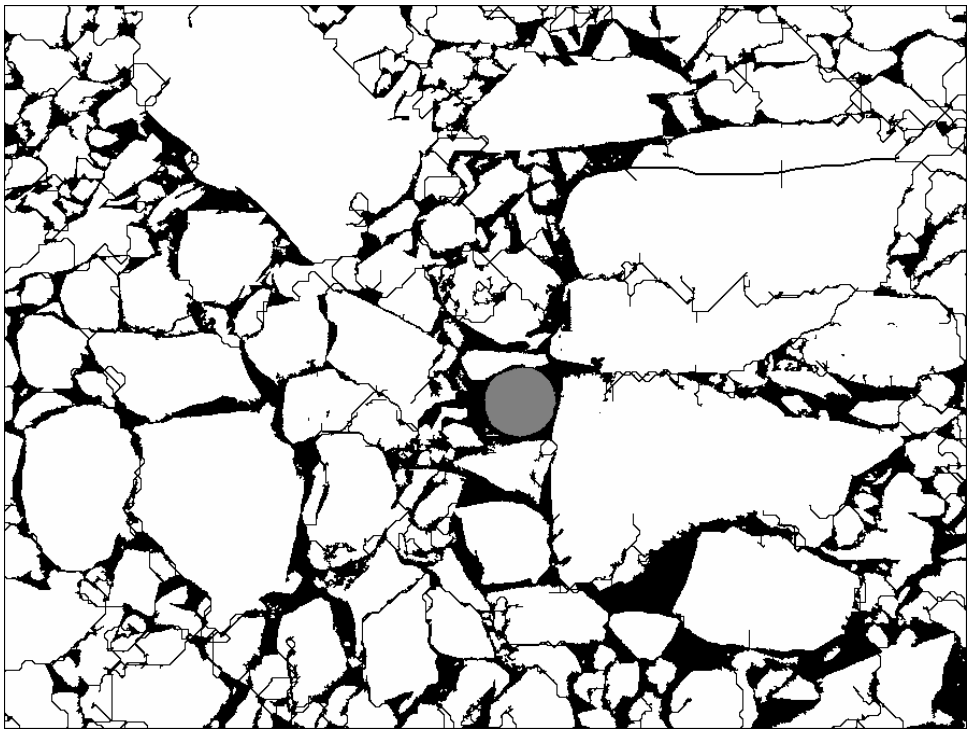

**Figure B.32 Sanyang4, the analyzed image**

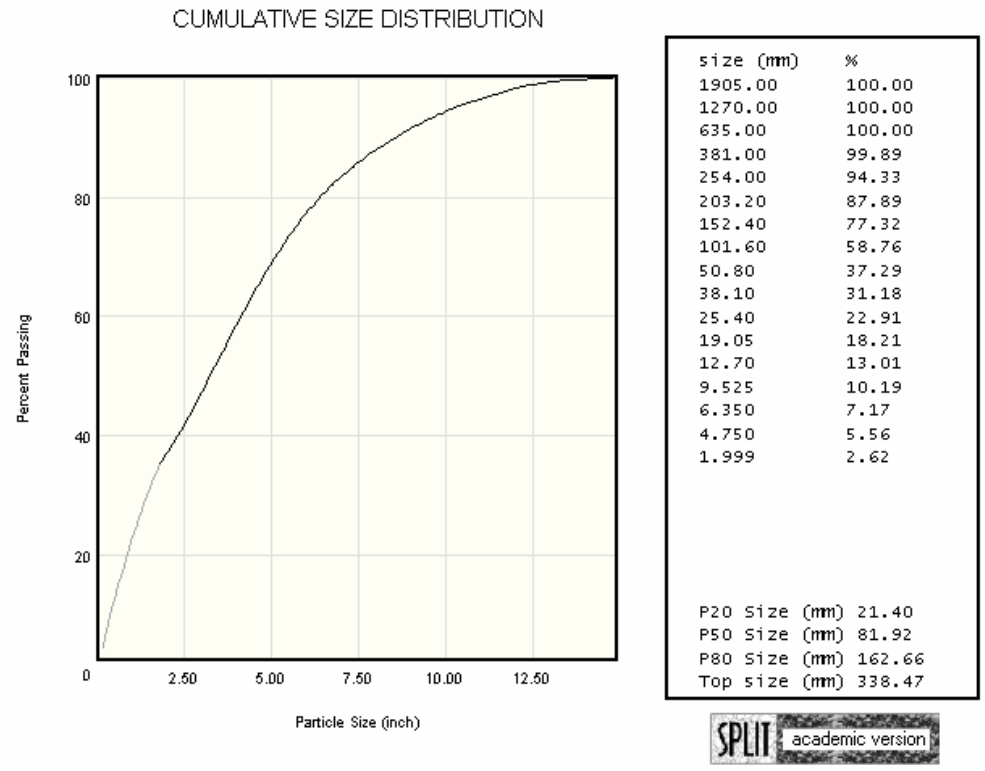


**Figure B.33 Sanyang4, the size distribution of the muckpile**

**Figure B.34 Sanyang5, the muckpile image**

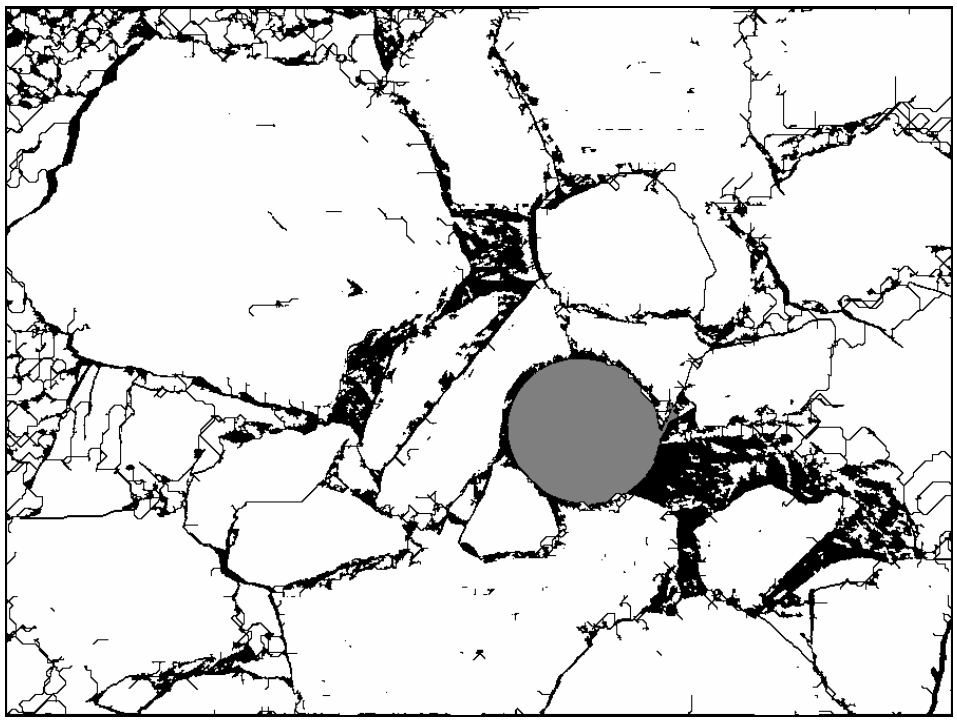

**Figure B.35 Sanyang5, the analyzed image**

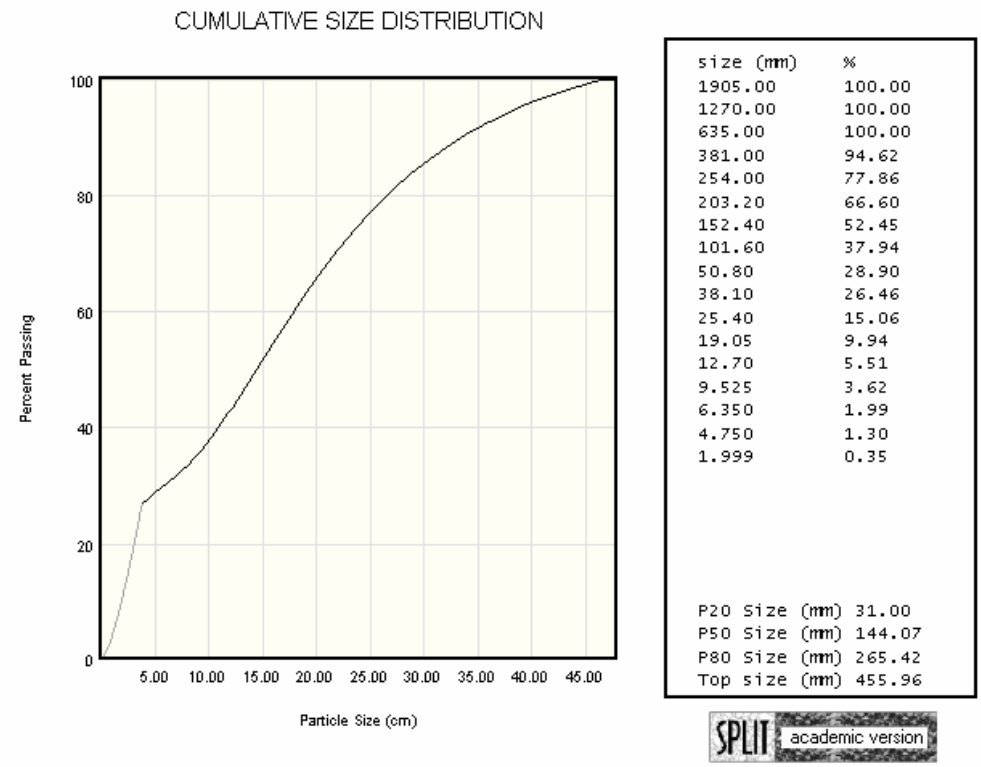


**Figure B.36 Sanyang5, the size distribution of the muckpile**

# APPENDIX C -

## Rock tests (Brazilian, Tilt, and $K_{IC}$ Test)

**Table C.1 Bosung, Mode I fracture toughness, $K_{IC}$**

| Sample # | Peak Load | Crack Length | Thickness | Diameter | P-splitting | F-Gregory | Kq |
|---|---|---|---|---|---|---|---|
| | Pv, N | a, m | t, m | D, m | Psp, N | m-1/2 | MPa(m1/2) |
| BS-2 | 1540.7 | 0.02263 | 0.02697 | 0.05423 | 1075.451 | 17.148 | 1.497 |
| BS-3 | 1597.7 | 0.02276 | 0.02586 | 0.05423 | 1115.247 | 17.292 | 1.628 |
| BS-4 | 1594.7 | 0.02253 | 0.02593 | 0.05423 | 1113.162 | 17.033 | 1.604 |
| BS-5 | 1874.6 | 0.02281 | 0.03048 | 0.05425 | 1308.544 | 17.334 | 1.623 |
| BS-6 | 1470.4 | 0.02258 | 0.02492 | 0.05428 | 1026.368 | 17.059 | 1.541 |
| BS-7 | 1756.5 | 0.02248 | 0.02944 | 0.05425 | 1226.106 | 16.961 | 1.552 |
| BS-8 | 1856.7 | 0.02281 | 0.03005 | 0.05423 | 1296.049 | 17.350 | 1.632 |
| BS-9 | 1551.5 | 0.02263 | 0.02858 | 0.05425 | 1083.008 | 17.132 | 1.422 |
| BS-10 | 1382.7 | 0.02271 | 0.02692 | 0.05425 | 965.179 | 17.218 | 1.349 |
| BS-11 | 1968.5 | 0.02309 | 0.02687 | 0.05423 | 1374.090 | 17.675 | 1.959 |

| | |
|---|---|
| Coefficient of Friction,μ | 0.580 |
| Wedge Angle, α | 0.19198622 |
| Tensile Strength, $\sigma_t$ | 18.85 Mpa |

| | |
|---|---|
| AVG | 1.539 |
| STDEV | 0.100 |

**Table C.2 Bosung, Size Check for $K_{IC}$ validity**

| Size Check | | | | | | | | | |
|---|---|---|---|---|---|---|---|---|---|
| Sample # | a | D-a | t | Value | Value | Validity | Validity | Validity | Validity |
| | m | m | m | D-a, a | t | a | D-a | t | Overall |
| BS-2 | 0.023 | 0.032 | 0.027 | 0.0158 | 0.0017 | OK | OK | OK | OK |
| BS-3 | 0.023 | 0.031 | 0.026 | 0.0187 | 0.0020 | OK | OK | OK | OK |
| BS-4 | 0.023 | 0.032 | 0.026 | 0.0181 | 0.0019 | OK | OK | OK | OK |
| BS-5 | 0.023 | 0.031 | 0.030 | 0.0185 | 0.0020 | OK | OK | OK | OK |
| BS-6 | 0.023 | 0.032 | 0.025 | 0.0167 | 0.0018 | OK | OK | OK | OK |
| BS-7 | 0.022 | 0.032 | 0.029 | 0.0169 | 0.0018 | OK | OK | OK | OK |
| BS-8 | 0.023 | 0.031 | 0.030 | 0.0187 | 0.0020 | OK | OK | OK | OK |
| BS-9 | 0.023 | 0.032 | 0.029 | 0.0142 | 0.0015 | OK | OK | OK | OK |
| BS-10 | 0.023 | 0.032 | 0.027 | 0.0128 | 0.0014 | OK | OK | OK | OK |
| BS-11 | 0.023 | 0.031 | 0.027 | 0.0270 | 0.0029 | NO | OK | OK | NO |
| Average | 0.023 | 0.032 | 0.028 | 0.0167 | 0.0018 | OK | OK | OK | OK |

**Table C.3 Bosung, Brazilian Test**

| Sample ID | Diameter(in) | Thickness(in) | Load(lbs) | Tensile Strength(Mpa) |
|---|---|---|---|---|
| BS-1 | 2.134 | 1.040 | 7566 | 14.96 |
| BS-2 | 2.132 | 1.008 | 7788 | 15.91 |
| BS-3 | 2.133 | 1.033 | 7550 | 15.04 |
| BS-4 | 2.139 | 1.076 | 9834 | 18.75 |
| BS-5 | 2.133 | 1.067 | 10354 | 19.97 |
| BS-7 | 2.130 | 1.035 | 8866 | 17.65 |
| BS-8 | 2.140 | 1.012 | 8024 | 16.26 |

| | |
|---|---|
| Average | 16.94 |
| S.D. | 1.92 |

**Table C.4 Bosung, Tilt test**

| Sample | angle | | | | | Ave.angle |
|---|---|---|---|---|---|---|
| B-1 | 31 | 33 | 32 | 32.5 | 33 | 32.3 |
| B-2 | 27 | 27 | 28 | 29 | 32 | 28.6 |
| B-3 | 30 | 31 | 32 | 32.5 | 35 | 32.1 |
| B-4 | 30 | 27 | 27 | 26 | 27 | 27.4 |
| B-5 | 27 | 32 | 30 | 27 | 34 | 30 |

| | |
|---|---|
| Average | 30.1 |
| Friction Coe. | 0.58 |

**Table C.5 Sanyang, Mode I fracture toughness, $K_{IC}$**

| Sample # | Peak Load | Crack Length | Thickness | Diameter | P-splitting | F-Gregory | Kq |
|---|---|---|---|---|---|---|---|
| | Pv, N | a, m | t, m | D, m | Psp, N | m-1/2 | MPa(m1/2) |
| S-1 | 1421.5 | 0.02248 | 0.02634 | 0.05436 | 1106.972 | 16.898 | 1.562 |
| S-2 | 1520.3 | 0.02283 | 0.02598 | 0.05428 | 1183.911 | 17.347 | 1.723 |
| S-3 | 1154.9 | 0.02248 | 0.02705 | 0.05425 | 899.362 | 16.961 | 1.239 |
| S-4 | 1964.7 | 0.02283 | 0.02687 | 0.05425 | 1529.982 | 17.363 | 2.155 |
| S-5 | 1597.1 | 0.02273 | 0.02604 | 0.05428 | 1243.718 | 17.231 | 1.799 |
| S-6 | 2311.4 | 0.02268 | 0.02576 | 0.05428 | 1799.969 | 17.173 | 2.626 |
| S-7 | 1419.9 | 0.02266 | 0.02708 | 0.05425 | 1105.726 | 17.161 | 1.534 |
| S-8 | 2112.7 | 0.02281 | 0.02662 | 0.05428 | 1645.234 | 17.318 | 2.335 |
| S-9 | 1874.6 | 0.02281 | 0.02738 | 0.05431 | 1459.817 | 17.301 | 2.013 |
| S-10 | 1433.7 | 0.02299 | 0.02710 | 0.05428 | 1116.473 | 17.523 | 1.569 |
| S-11 | 1889.2 | 0.02301 | 0.02637 | 0.05425 | 1471.187 | 17.569 | 2.129 |

| | |
|---|---|
| Coefficient of Friction,μ | 0.514 |
| Wedge Angle, α | 0.19198622 |
| Tensile Strength, $\sigma_t$ | 20.01 Mpa |

| | |
|---|---|
| AVG | 1.724 |
| STDEV | 0.193 |

**Table C.6 Sanyang, Size Check for $K_{IC}$ validity**

| Size Check | | | | | | | | | |
|---|---|---|---|---|---|---|---|---|---|
| Sample # | a | D-a | T | Value | Value | Validity | Validity | Validity | Validity |
| | m | m | M | D-a, a | t | a | D-a | t | Overall |
| S-1 | 0.022 | 0.032 | 0.026 | 0.0152 | 0.0016 | OK | OK | OK | OK |
| S-2 | 0.023 | 0.031 | 0.026 | 0.0185 | 0.0020 | OK | OK | OK | OK |
| S-3 | 0.022 | 0.032 | 0.027 | 0.0096 | 0.0010 | OK | OK | OK | OK |
| S-4 | 0.023 | 0.031 | 0.027 | 0.0290 | 0.0031 | NO | OK | OK | NO |
| S-5 | 0.023 | 0.032 | 0.026 | 0.0202 | 0.0022 | OK | OK | OK | OK |
| S-6 | 0.023 | 0.032 | 0.026 | 0.0430 | 0.0046 | NO | NO | OK | NO |
| S-7 | 0.023 | 0.032 | 0.027 | 0.0147 | 0.0016 | OK | OK | OK | OK |
| S-8 | 0.023 | 0.031 | 0.027 | 0.0340 | 0.0037 | NO | NO | OK | NO |
| S-9 | 0.023 | 0.031 | 0.027 | 0.0253 | 0.0027 | NO | OK | OK | NO |
| S-10 | 0.023 | 0.031 | 0.027 | 0.0154 | 0.0017 | OK | OK | OK | OK |
| S-11 | 0.023 | 0.031 | 0.026 | 0.0283 | 0.0030 | NO | OK | OK | NO |
| Average | 0.023 | 0.032 | 0.027 | 0.0186 | 0.0020 | OK | OK | OK | OK |

**Table C.7 Sanyang, Brazilian Test**

| Sample | Diameter(in) | Thickness(in) | Load(lbs) | Tensile strength(MPa) |
|---|---|---|---|---|
| S-1 | 2.133 | 1.022 | 7509 | 15.12 |
| S-2 | 2.137 | 0.805 | 8530 | 21.76 |
| S-3 | 2.129 | 1.000 | 7404 | 15.26 |
| S-4 | 2.131 | 1.021 | 8336 | 16.82 |
| S-5 | 2.131 | 1.010 | 8004 | 16.32 |
| S-6 | 2.133 | 1.064 | 8538 | 16.51 |
| S-7 | 2.135 | 1.054 | 10416 | 20.32 |

| | |
|---|---|
| Average | 17.45 |
| S.D. | 2.57 |

**Table C.8 Sanyang, Tilt test**

| Sample | angle | | | | | Ave.angle |
|---|---|---|---|---|---|---|
| S-1 | 25 | 24 | 25 | 28 | 27 | 25.8 |
| S-2 | 26 | 26 | 29 | 25 | 27 | 26.6 |
| S-3 | 30 | 28.5 | 30 | 31 | 31 | 30.1 |
| S-4 | 25 | 32 | 25 | 24 | 27 | 26.6 |
| S-5 | 26 | 28 | 26 | 26 | 29 | 27 |

| | |
|---|---|
| Average | 27.2 |
| Friction Coe. | 0.514 |

**Table C.9 Boxley, Mode I fracture toughness, $K_{IC}$**

| Sample # | Peak Load | Crack Length | Thickness | Diameter | P-splitting | F-Gregory | Kq |
|---|---|---|---|---|---|---|---|
| | Pv, N | a, m | t, m | D, m | Psp, N | m-1/2 | MPa(m1/2) |
| B-1-1 | 889.0 | 0.02032 | 0.02449 | 0.05022 | 760.764 | 17.035 | 1.177 |
| B-1-2 | 621.0 | 0.02123 | 0.02390 | 0.05024 | 531.422 | 18.158 | 0.878 |
| B-1-3 | 1103.6 | 0.02156 | 0.02682 | 0.05024 | 944.408 | 18.594 | 1.413 |
| B-2-1 | 1008.8 | 0.02149 | 0.02629 | 0.05024 | 863.283 | 18.492 | 1.313 |
| B-2-2 | 1556.8 | 0.02129 | 0.02573 | 0.05024 | 1332.235 | 18.224 | 2.050 |
| B-3-1 | 1111.2 | 0.02118 | 0.02741 | 0.05019 | 950.912 | 18.129 | 1.369 |
| B-3-2 | 1874.0 | 0.02136 | 0.02748 | 0.05022 | 1603.680 | 18.343 | 2.321 |
| B-4-1 | 1306.0 | 0.02139 | 0.02507 | 0.05022 | 1117.613 | 18.376 | 1.775 |
| B-4-2 | 1432.0 | 0.02149 | 0.02687 | 0.05019 | 1225.438 | 18.530 | 1.826 |

| | |
|---|---|
| Coefficient of Friction,μ | 0.462 |
| Wedge Angle, α | 0.19198622 |
| Tensile Strength, $\sigma_t$ | 15.95 Mpa |

| | |
|---|---|
| AVG | 1.230 |
| STDEV | 0.216 |

**Table C.10 Boxley, Size Check for $K_{IC}$ validity**

| Size Check | | | | | | | | | |
|---|---|---|---|---|---|---|---|---|---|
| Sample # | a | D-a | t | Value | Value | Validity | Validity | Validity | Validity |
| | m | m | m | D-a, a | t | a | D-a | t | Overall |
| B-1-1 | 0.020 | 0.030 | 0.024 | 0.0136 | 0.0015 | OK | OK | OK | OK |
| B-1-2 | 0.021 | 0.029 | 0.024 | 0.0076 | 0.0008 | OK | OK | OK | OK |
| B-1-3 | 0.022 | 0.029 | 0.027 | 0.0196 | 0.0021 | OK | OK | OK | OK |
| B-2-1 | 0.021 | 0.029 | 0.026 | 0.0169 | 0.0018 | OK | OK | OK | OK |
| B-2-2 | 0.021 | 0.029 | 0.026 | 0.0413 | 0.0044 | NO | NO | OK | NO |
| B-3-1 | 0.021 | 0.029 | 0.027 | 0.0184 | 0.0020 | OK | OK | OK | OK |
| B-3-2 | 0.021 | 0.029 | 0.027 | 0.0529 | 0.0057 | NO | NO | OK | NO |
| B-4-1 | 0.021 | 0.029 | 0.025 | 0.0310 | 0.0033 | NO | NO | OK | NO |
| B-4-2 | 0.021 | 0.029 | 0.027 | 0.0328 | 0.0035 | NO | NO | OK | NO |
| Average | 0.021 | 0.029 | 0.026 | 0.0149 | 0.0016 | OK | OK | OK | OK |

**Table C.11 Boxley, Brazilian Test**

| Sample | Diameter(in) | Thickness(in) | Load(lbs) | Tensile Strength(Mpa) |
|---|---|---|---|---|
| B-2-5 | 1.977 | 1.057 | 7990 | 16.78 |
| B-2-6 | 1.977 | 1.055 | 6034 | 12.70 |
| B-2-7 | 1.977 | 0.914 | 6316 | 15.34 |
| B-1-4 | 1.976 | 0.987 | 6638 | 14.94 |
| B-1-5 | 1.975 | 1.070 | 7142 | 14.83 |
| B-1-6 | 1.976 | 1.058 | 7257 | 15.24 |
| B-3-3 | 1.977 | 1.073 | 6354 | 13.15 |
| B-3-4 | 1.976 | 1.007 | 6750 | 14.89 |
| B-4-3 | 1.975 | 1.135 | 6964 | 13.64 |
| B-4-4 | 1.977 | 1.117 | 7898 | 15.70 |

| | |
|---|---|
| Average | 14.72 |
| S.D. | 1.23 |

**Table C.12 Boxley, Tilt test**

| Sample | angle | | | | | Ave.angle |
|---|---|---|---|---|---|---|
| B-1-7 | 28 | 27 | 26 | 24.5 | 25.5 | 26.2 |
| B-1-8 | 30.5 | 33 | 28.5 | 27.5 | 27.5 | 29.4 |
| B-3-5 | 23.5 | 21 | 25 | 21.5 | 22.5 | 22.7 |
| B-4-5 | 20 | 23.5 | 22.5 | 21.5 | 22 | 21.9 |
| B-2-8 | 24.5 | 21.5 | 24.5 | 25 | 24 | 23.9 |

| | |
|---|---|
| Average | 24.8 |
| Friction Coe. | 0.462 |

**Table C.13 Pittsboro, Mode I fracture toughness, $K_{IC}$**

| Sample # | Peak Load | Crack Length | Thickness | Diameter | P-splitting | F-Gregory | Kq |
|---|---|---|---|---|---|---|---|
| | Pv, N | a, m | t, m | D, m | Psp, N | m-1/2 | MPa(m1/2) |
| PB-3-10 | 1991.0 | 0.02108 | 0.02601 | 0.05004 | 1760.324 | 18.108 | 2.670 |
| PB-3-8 | 2083.0 | 0.02083 | 0.02596 | 0.05006 | 1841.665 | 17.764 | 2.763 |
| PB-2-7 | 1035.0 | 0.02096 | 0.02713 | 0.05001 | 915.086 | 17.963 | 1.324 |
| PB-2-8 | 1697.6 | 0.02070 | 0.02715 | 0.05001 | 1500.917 | 17.640 | 2.143 |
| PB-1-1 | 1357.0 | 0.02045 | 0.02494 | 0.04968 | 1199.779 | 17.550 | 1.861 |
| PB-1-2 | 1991.0 | 0.02118 | 0.02789 | 0.05022 | 1760.324 | 18.111 | 2.489 |
| PB-1-3 | 1389.0 | 0.02108 | 0.02616 | 0.05019 | 1228.071 | 17.998 | 1.844 |
| PB-1-4 | 2031.0 | 0.02126 | 0.02761 | 0.05006 | 1795.690 | 18.322 | 2.586 |
| PB-3-14 | 1570.0 | 0.02042 | 0.02553 | 0.05004 | 1388.101 | 17.276 | 2.080 |
| PB-3-11 | 1113.0 | 0.02007 | 0.02499 | 0.05004 | 984.049 | 16.848 | 1.481 |

| | |
|---|---|
| Coefficient of Friction,μ | 0.445 |
| Wedge Angle, α | 0.19198622 |
| Tensile Strength, $\sigma_t$ | 27.18 Mpa |

| | |
|---|---|
| AVG | 1.889 |
| STDEV | 0.398 |

**Table C.14 Pittsboro, Size Check for $K_{IC}$ validity**

| Size Check | | | | | | | | | |
|---|---|---|---|---|---|---|---|---|---|
| Sample # | a | D-a | t | Value | Value | Validity | Validity | Validity | Validity |
| | m | m | m | D-a, a | t | a | D-a | t | Overall |
| PB-3-10 | 0.021 | 0.029 | 0.026 | 0.0241 | 0.0026 | NO | OK | OK | NO |
| PB-3-8 | 0.021 | 0.029 | 0.026 | 0.0258 | 0.0028 | NO | OK | OK | NO |
| PB-2-7 | 0.021 | 0.029 | 0.027 | 0.0059 | 0.0006 | OK | OK | OK | OK |
| PB-2-8 | 0.021 | 0.029 | 0.027 | 0.0155 | 0.0017 | OK | OK | OK | OK |
| PB-1-1 | 0.020 | 0.029 | 0.025 | 0.0117 | 0.0013 | OK | OK | OK | OK |
| PB-1-2 | 0.021 | 0.029 | 0.028 | 0.0210 | 0.0023 | OK | OK | OK | OK |
| PB-1-3 | 0.021 | 0.029 | 0.026 | 0.0115 | 0.0012 | OK | OK | OK | OK |
| PB-1-4 | 0.021 | 0.029 | 0.028 | 0.0226 | 0.0024 | NO | OK | OK | NO |
| PB-3-14 | 0.020 | 0.030 | 0.026 | 0.0146 | 0.0016 | OK | OK | OK | OK |
| PB-3-11 | 0.020 | 0.030 | 0.025 | 0.0074 | 0.0008 | OK | OK | OK | OK |
| Average | 0.021 | 0.029 | 0.026 | 0.0121 | 0.0013 | OK | OK | OK | OK |

**Table C.15 Pittsboro, Brazilian Test**

| Sample ID | Diameter(in) | Thickness(in) | Load(lbs) | Tensile Strength(Mpa) |
|---|---|---|---|---|
| PB-3-21 | 1.970 | 1.069 | 11760 | 24.51 |
| PB-1-8 | 1.972 | 1.186 | 10580 | 19.86 |
| PB-1-9 | 1.978 | 1.062 | 6904 | 14.43 |
| PB-3-15 | 1.974 | 1.073 | 11052 | 22.90 |
| PB-3-16 | 1.974 | 1.057 | 12318 | 25.91 |
| PB-3-18 | 1.970 | 0.990 | 12110 | 27.25 |

| | |
|---|---|
| Average | 22.48 |
| S.D. | 4.7 |

**Table C.16 Pittsboro, Tilt test**

| Sample | angle | | | | | Ave angle |
|---|---|---|---|---|---|---|
| PB-1-6 | 24 | 29 | 26 | 16 | 27 | 24.4 |
| PB-3-12 | 23 | 26 | 24 | 24 | 22 | 23.8 |
| PB-2-9 | 22 | 22 | 22 | 21 | 24 | 22.2 |
| PB-3-13 | 25 | 22 | 22 | 26 | 24 | 23.8 |
| PB-1-7 | 25 | 24 | 26 | 30 | 23 | 25.6 |
| PB-2-10 | 25 | 24 | 24 | 24 | 25 | 24.4 |

| | |
|---|---|
| Average | 24.0 |
| Friction Coe. | 0.445 |

# APPENDIX D -

## Summarized Blasting pattern and $E_{SE}$

Table D.1 Summarized blasting pattern and Ese

| Blasting pattern | Pittsboro | Boxley | Bosung1 | Bosung2 | Bosung3 | Bosung4 | Bosung5 | Sanyang1 | Sanyang2 | Sanyang3 | Sanyang4 | Sanyang5 | Unit |
|---|---|---|---|---|---|---|---|---|---|---|---|---|---|
| Bench Height | 19.8 | 15.54 | 11.1 | 11.1 | 11.1 | 11.1 | 5.3 | 14.3 | 14.3 | 8.4 | 10.7 | 11.4 | m |
| Burden | 4.57 | 4.27 | 3 | 3 | 2.8 | 2.9 | 2.2 | 2.5 | 2.3 | 1.9 | 1.9 | 1.8 | m |
| Spacing | 4.57 | 5.49 | 2.9 | 2.9 | 3 | 2.9 | 2.2 | 2.3 | 2.1 | 1.9 | 2.0 | 1.8 | m |
| Rock Specific Gravity | 2.69 | 2.73 | 2.58 | 2.58 | 2.58 | 2.58 | 2.58 | 2.49 | 2.49 | 2.49 | 2.49 | 2.49 | t/m^3 |
| Hole diameter | 165 | 165 | 76 | 76 | 76 | 76 | 76 | 76 | 76 | 76 | 76 | 76 | mm |
| Explosives | Hydromite4400 | Heet30,Austinite | New mite plus II | | | | | Emulite 150, New ANFO | | | | | |
| Explosives amount per hole | 429 | 259.5(155.54,103.96) | 20 | 20 | 20 | 20 | 5.7 | 42 | 38 | 20 | 17 | 16 | kg |
| Explosives energy per gram | 863 | 863 and 912 | 1100 | 1100 | 1100 | 1100 | 1100 | 1100 | 1100 | 1100 | 1100 | 1100 | Kcal/Kg |
| Explosives energy per hole | 431 | 266 | 25.59 | 25.59 | 25.59 | 25.59 | 7.29 | 53.73 | 48.27 | 25.39 | 21.75 | 20.21 | Kwh |
| **Ese** | **387** | **268** | **103** | **103** | **107** | **107** | **110** | **268** | **292** | **336** | **222** | **210** | wh/tonne |